CIVIL ENGINEERING STUDIES
Illinois Center for Transportation Series No. 08-026
UILU-ENG-2008-2014
ISSN: 0197-9191

ADHESION TESTING PROCEDURE FOR HOT-POURED CRACK SEALANTS

Prepared By

Imad L. Al-Qadi
Eli H. Fini
University of Illinois at Urbana-Champaign

Hector D. Figueroa
Quality Engineering Solutions

Jean-François Masson
National Research Council of Canada

Kevin K. McGhee
Virginia Transportation Research Council

Research Report ICT-08-026

Illinois Center for Transportation

November 2008

Technical Report Documentation Page

1. Report No.	2. Government Accession No.	3. Recipient's Catalog No.
ICT-08-026		

4. Title and Subtitle
ADHESION TESTING PROCEDURE FOR HOT-POURED CRACK SEALANTS

5. Report Date
November 2008

6. Performing Organization Code

7. Author(s)
Imad Al-Qadi, Eli Fini, Hector Figueroa, and Jean-Francois Masson

8. Performing Organization Report No.
ICT-08-026
UILU-ENG-2008-2014

9. Performing Organization Name and Address

University of Illinois at Urbana Champaign
Department of Civil and Environmental Engineering
205 N. Mathews Ave, MC-250
Urbana, Illinois 61081

10. Work Unit (TRAIS)

11. Contract or Grant No.
VTRC Project # 67775
TPF-5(045)

13. Type of Report and Period Covered
Technical Report

12. Sponsoring Agency Name and Address

Federal Highway Administration
400 North 8th Street, Room 750
Richmond, VA 23219-4825

Virginia DOT – Lead State
1401 E. Broad St
Richmond, VA 23219

14. Sponsoring Agency Code

15. Supplementary Notes

16. Abstract
Crack sealing is a common pavement maintenance treatment because it extends pavement service life significantly. However, crack sealant often fails prematurely due to a loss of adhesion. Because current test methods are mostly empirical and only provide a qualitative measure of bond strength, they cannot predict sealant adhesive failure accurately. Hence, there is an urgent need for test methods based on bituminous sealant rheology that can better predict sealant field performance. This study introduces three laboratory tests aimed to assess the bond property of hot-poured crack sealant to pavement crack walls. The three tests are designed to serve the respective needs of producers, engineers, and researchers. The first test implements the principle of surface energy to measure the thermodynamic work of adhesion, which is the energy spent in separating the two materials at the interface. The work of adhesion is reported as a measure of material compatibility at an interface. The second test is a direct adhesion test, a mechanical test which is designed to closely resemble both the installation process and the crack expansion due to thermal loading. This test uses the Direct Tensile Test (DTT) machine. The principle of the test is to apply a tensile force to detach the sealant from its aggregate counterpart. The maximum load, Pmax, and the energy to separation, E, are calculated and reported to indicate interface bonding. The third test implements the principles of fracture mechanics in a pressurized circular blister test. The apparatus is specifically designed to conduct the test for bituminous crack sealant, asphalt binder, or other bitumen-based materials. In this test, a fluid is injected at a constant rate at the interface between the substrate (aggregate or a standard material) and the adhesive (crack sealant) to create a blister. The fluid pressure and blister height are measured as functions of time; the data is used to calculate Interfacial Fracture Energy (IFE), which is a fundamental property that can be used to predict adhesion. The stable interface debonding process makes this test attractive. This test may also provide a means to quantify other factors, such as the moisture susceptibility of a bond. In addition, the elastic modulus of the sealant and its residual stresses can be determined analytically. While the direct adhesion test is proposed as part of a newly developed performance-based guideline for the selection of hot-poured crack sealant, the blister test can be used to estimate the optimum annealing time and installation temperature.

17. Key Words	18. Distribution Statement
	No restrictions. This document is available to the public through the National Technical Information Service, Springfield, Virginia 22161.

19. Security Classif. (of this report)	20. Security Classif. (of this page)	21. No. of Pages	22. Price
Unclassified	Unclassified	103	

ACKNOWLEDGEMENT

The research on the Development of Performance-Based Guidelines for the Selection of Bituminous–Based Hot-Poured Pavement Crack Sealants is sponsored by the Federal Highway Administration “pooled-fund study TPF5 (045)” and the US-Canadian Crack Sealant Consortium. The contribution of the participating states, industry, and provinces is acknowledged. This report is part of a series of reports that resulted from this study. Four reports were published by the Illinois Center for Transportation:

Al-Qadi, I.L., E.H. Fini, H.D. Figueroa, J.-F Masson, and K.K. McGhee, Adhesion Testing Procedure for Hot-Poured Crack Sealants, Final Report, No. ICT-08-026, Illinois Center for Transportation, Rantoul, IL, Dec 2008, 103 p.

Al-Qadi, I.L., E.H. Fini, J.-F Masson, A. Loulizi, K.K. McGhee, M.A. Elseifi, Development of Apparent Viscosity Test for Hot-Poured Crack Sealants, Final Report, No. ICT-08-027, Illinois Center for Transportation, Rantoul, IL, Dec 2008, 41 p.

Al-Qadi, I.L., S.-H. Yang, J.-F. Masson, and K.K. McGhee, Characterization of Low Temperature Mechanical Properties of Crack Sealants Utilizing Direct Tension Test, Final Report, No. ICT-08-028, Illinois Center for Transportation, Rantoul, IL, Dec 2008, 70 p.

Al-Qadi, I.L., S.-H. Yang, M.A. Elseifi, S. Dessouky, A. Loulizi, J.-F. Masson, and K.K. McGhee, Characterization of Low Temperature Creep Properties of Crack Sealants Using Bending Beam Rheometry, Final Report, No. ICT-08-029, Illinois Center for Transportation, Rantoul, IL, Dec 2008, 81 p.

Two internal reports on aging and sealant characterization were published by the National Research Council of Canada and a summary can be found in the following papers):

Collins, P., Veitch, M., Masson, J-F., Al-Qadi, I. L., Deformation and Tracking of Bituminous Sealants in Summer Temperatures: Pseudo-field Behaviour, *International Journal of Pavement Engineering*, Vol. 9, No. 1, 2008, pp. 1-8.

Masson, J-F., Woods, J. R., Collins, P., Al-Qadi, I. L., Accelerated Aging of Bituminous Sealants: Small-kettle Aging, *International Journal of Pavement Engineering*, Vol. 9, No. 5, 2008, pp. 365-371.

In addition, an executive summary report of the study was published by the Virginia Transportation Research Council (the leading state of the study):

Al-Qadi, I. L. J-F. Masson, S-H. Yang, E. Fini, and K. K. McGhee, Development of Performance-Based Guidelines for Selection of Bituminous-Based Hot-Poured Pavement Crack Sealant: An Executive Summary Report, Final Report, No. VTRC 09-CR7, Virginia Department of Transportation, Charlottesville, VA, 2008, 40 p.

DISCLAIMER

The project that is the subject of this report was completed under contract with the Virginia Transportation Research Council, which served as lead-state coordinator and project monitor for the partner states of Connecticut, Georgia, Maine, Michigan, Minnesota, New Hampshire, New York, Rhode Island, Texas, and Virginia. The contents of this report reflect the views of the authors, who are responsible for the facts and the accuracy of the data presented herein. The contents do not necessarily reflect the official views or policies of the Virginia Transportation Research Council, the partnering states, the Illinois Center for Transportation, the Illinois Department of Transportation, the Federal Highway Administration, or the remaining members of the Crack Sealant Consortium. This report does not constitute a standard, specification, or regulation. Any inclusion of manufacturer names, trade names, or trademarks is for identification purposes only and is not to be considered an endorsement.

EXECUTIVE SUMMARY

Crack sealing is a common pavement maintenance treatment because it extends pavement service life significantly. However, crack sealant often fails prematurely due to a loss of adhesion. Because current test methods are mostly empirical and only provide a qualitative measure of bond strength, they cannot predict sealant adhesive failure accurately. Hence, there is an urgent need for test methods based on bituminous sealant rheology that can better predict sealant field performance. This study introduces three laboratory tests aimed to assess the bond property of hot-poured crack sealant to pavement crack walls. The three tests are designed to serve the respective needs of producers, engineers, and researchers. The first test implements the principle of surface energy to measure the thermodynamic work of adhesion, which is the energy spent in separating the two materials at the interface. The work of adhesion is reported as a measure of material compatibility at an interface. The second test is a direct adhesion test, a mechanical test which is designed to closely resemble both the installation process and the crack expansion due to thermal loading. This test uses the Direct Tensile Test (DTT) machine. The principle of the test is to apply a tensile force to detach the sealant from its aggregate counterpart. The maximum load, P_{max}, and the energy to separation, E, are calculated and reported to indicate interface bonding. The third test implements the principles of fracture mechanics in a pressurized circular blister test. The apparatus is specifically designed to conduct the test for bituminous crack sealant, asphalt binder, or other bitumen-based materials. In this test, a fluid is injected at a constant rate at the interface between the substrate (aggregate or a standard material) and the adhesive (crack sealant) to create a blister. The fluid pressure and blister height are measured as functions of time; the data is used to calculate Interfacial Fracture Energy (IFE), which is a fundamental property that can be used to predict adhesion. The stable interface debonding process makes this test attractive. This test may also provide a means to quantify other factors, such as the moisture susceptibility of a bond. In addition, the elastic modulus of the sealant and its residual stresses can be determined analytically. While the direct adhesion test is proposed as part of a newly developed performance-based guideline for the selection of hot-poured crack sealant, the blister test can be used to estimate the optimum annealing time and installation temperature.

TABLE OF CONTENTS

FINAL CONTRACT REPORT

ADHESION TESTING PROCEDURE FOR HOT-POURED CRACK SEALANTS

Imad L. Al-Qadi
Founder Professor of Engineering
Illinois Center for Transportation, Director
University of Illinois at Urbana-Champaign

Jean-François Masson
Senior Research Officer
Institute for Research in Construction
National Research Council of Canada

INTRODUCTION

Approximately 60 percent of the nation's annual transportation budget is spent on pavement maintenance. Crack sealing is one of the most common pavement maintenance treatments because it can significantly extend the pavement service life if the appropriate sealant is used and properly installed. Hot-poured, bituminous-based crack sealant failure can be divided into two general classifications: (i) the separation of the sealant from itself (cohesive fracture) and (ii) the separation of a sealant from the crack walls at the bond line between the two materials (adhesive fracture). Cohesive failure of bituminous crack sealants, which relates to bulk properties of the material, has long been characterized by manufacturers and, therefore, this type of failure rarely occurs in cold weather conditions. However, adhesive failure, which relates to debonding near the sealant and hot-mix asphalt (HMA) interface, has not been well researched though it has been recognized as the major failure mode for bituminous crack sealants (Masson et al., 2000). Unfortunately, sealant field performance cannot be predicted because current available testing methods (ASTM D6690) are mostly empirical. The available tests generally provide a qualitative measure of the bonding based on a geometric parameter. Hence testing methods are needed that are based on the sealant's rheology and surface characteristics, which are capable of predicting field performance. The objective of this project is to develop a laboratory testing approach to predict the adhesion of crack sealant to aggregate at service temperatures ranging from -4ºC to -40ºC.

Adhesion is a fundamental property which directly depends on interatomic and intermolecular forces between the adhesive (sealant) and HMA. It has also been shown that sealant adhesion depends on aggregate composition, with adhesion to siliceous aggregates half that obtained for limestone (Masson et al., 2000). In addition, factors such as temperature, sealant geometry, and sealant bulk properties have all been reported to influence adhesion characteristics. In this project, all tests were conducted at a temperature ranging from -4ºC to -40ºC. To conduct a test at such low temperatures, alcohol was selected as a fluid medium. Alcohol was selected because it has a relatively low freezing temperature, is nearly incompressible, and does not react with sealant specimens during testing or limited conditioning period

Several research studies have investigated the effect of surface energy on sealant-aggregate adhesion. Cheng et al. (2001) measured the thermodynamic surface-free energy

of aggregates using the universal sorption device. They used a surface energy approach to evaluate adhesive fracture and moisture damage characteristics within the asphalt-aggregate system and argued that knowing the surface energy of the asphalt and aggregates would lead to the selection of the most compatible asphalt-aggregate combination with the best ability to resist adhesion failure. Bhasin et al. (2006) used the same approach to quantify the adhesive bond energy between the aggregate and asphalt. They observed significant differences in the bond energies developed between various aggregates and a given binder. This study showed that the bonding in reality is generally several orders of magnitude higher than the bond energy derived through this approach; this difference is attributed to dissipative contributions (Galerie et al., 2004). While the measured work of adhesion does not measure the real bonding, it can serve to define compatible pairs among different combinations of sealant-aggregate.

Many mechanical testing methodologies have been used to measure adhesion. Masson and Lacasse (1999) used both a small-scale and a full-scale adhesion test to measure the level of sealant adhesion to heat-treated substrates. Using a direct tension tester (DTT) to bring an assembly of adhesive/substrate to failure is very common in the adhesive industry (e.g., pull out test, butt joint test). This method has received attention because it resembles crack/joint opening and contraction. Masson and Lacasse (1999) and Zanzotto (1996) independently measured the bonding of sealants to concrete by bringing sealant-concrete assemblies to tensile failure. In both studies, bonding was defined as the energy that is required to bring the assemblies to failure. Masson and Lacasse (1999) measured energies of 200-500J/m^2 at -37ºC, whereas Zanzotto (1996) obtained values of 500-1000J/m^2 at -30ºC. Traditional adhesive joint strength tests (e.g., butt tensile test, pull out test, and lap shear test) continue to be used. However, due to their dependence on geometry and other drawbacks, current usage is mostly restricted to studies of a single adhesive-substrate system using a single specimen size and geometry (Jiang and Penn, 1990). Because traditional tests result in unknown stress distributions and mode-mixities at the interface, data from different geometries cannot be compared. In addition, because of the role of elastic moduli, comparison of two substrates is also uncertain. Even if it were possible to compare the aforementioned results from Masson and Lacasse (1999) and Zanzotto (1996), the comparison would not show that adhesion was greater at -30ºC than at -37ºC. Such a comparison may indicate only that the sealants extended farther at higher temperatures and that more energy was spent to stretch the sealant.

Another test, the blister test, is commonly used in the thin-film coating, polymer, microelectronics device, packaging, and polymer industries. This test is used to measure the interfacial fracture energy, which is a fundamental property of the interface, of a thin film deposited on or attached to a substrate. The blister test configuration has been widely used to predict adhesion in a variety of interlaminated structures, such as dental cements and teeth (Despain et al., 1970), thin film coatings (Dannenberg, 1961), polymer composite and microelectronic devices (Shirani and Liechti, 1998; Chu and Durning, 1992).

A major milestone of this project was the development of laboratory tests which can assess sealant-HMA adhesion in a setting that closely resembles field conditions. In this study, three tests were developed to be used by sealant producers, engineers and contractors, and researchers. The first test uses a surface energy approach and is expected to be used by sealant producers to check the compatibility of sealants with local materials. Even a quality sealant may fail if installed at a site that has incompatible materials. The second approach is a test setup that uses the direct tension test (DTT) machine. This method is more of a qualitative approach to assess the bond between sealant and crack walls and is expected to be used by departments of transportation and consulting agencies for quality control projects. The selected parameters relate the sealant-HMA interfacial bonding to the wetting phenomenon, which is governed by sealant viscosity, filler content,

aggregate type, and surface roughness. The third test uses the concept of fracture mechanics. This test is more suited for profound studies and research projects than the other tests are. However, as equipment and training become available, it can also be used for quality control projects.

PURPOSE AND SCOPE

Hot-poured bituminous sealants are typically selected based on standard tests of an empirical nature, such as penetration, resilience, flow, and bond to cement concrete briquettes (ASTM D3405). There is, however, no indication that the results of these standard tests pertain to field performance. In an effort to bridge the gap between a sealant's fundamental properties and its field performance, this study developed performance-based guidelines for selection of hot-poured crack sealants. One section of these guidelines addresses the adhesion of hot-poured crack sealant to aggregate. The goal is to develop a method that can assess sealant adhesion under conditions that closely simulate those in the field.

METHODS

To measure the adhesion of crack sealant to aggregate at service temperatures ranging from -4ºC to -40ºC (24.8ºF to -40ºF), three laboratory testing approaches were developed. The first laboratory approach examined the sealant-substrate compatibility, assessed by measuring the free energy of the bond. The second approach uses the DTT machine to predict the adhesion at the interface. The third approach uses the fracture mechanics concepts. The three approaches are presented below.

Surface Energy Method

One of the theories used to explain the adhesion phenomenon effectively is adsorption theory (Masson and Lacasse, 2000). Adsorption theory describes wettability and is based on the measured contact angle between a liquid and a solid on a horizontal surface under thermal equilibrium. A schematic of the contact angle experiment is presented in Figure 1, where θ is the contact angle between the solid-liquid interface and the tangent of the liquid-vapor interface. When a drop of liquid is placed onto a solid surface such as an aggregate, the drop remains stationary (contact angle > 90º) or it spreads (contact angle <90º). If it spreads, the surface of the solid is wetted, and adhesion between the liquid and the solid is likely to be strong. If the drop does not spread, then adhesion is weak. The contact angle is an indicator of the affinity of a liquid for a solid. The shape of a liquid drop on a solid surface is related to the molecular interaction among the surface, the liquid, and the air surrounding them (Van Oss et al., 1988). To be at stationary status, the forces between the three materials should be in equilibrium (Figure 1), which leads to Young's equation as follows:

$$\gamma_{sa} = \gamma_{sl} + \gamma_{la}\cos\theta \qquad (1)$$

where,
γ_{sl} is the solid-liquid interfacial free energy (mJ/m^2);
γ_{sa} is the surface energy of the substrate (mJ/m^2);
γ_{la} is the surface energy of the liquid (mJ/m^2); and
θ is the contact angle (^{o}).

When two dissimilar materials form an interface by being in intimate contact, a tensile force can be applied to split the materials into dissimilar parts. For a completely brittle interface, the energy expended (or work of adhesion) can be obtained using the Young-Dupré equation:

$$W_a = \gamma_l(1+\cos\theta) \quad \textbf{(2)}$$

The Young-Dupré equation is basically the sum of the individual surface energies for the two materials involved. Surface energy is composed of a polar and a non-polar component (Fowkes, 1964):

$$\gamma_l = \gamma^{LW} + \gamma^{AB} \quad \textbf{(3)}$$

where,
γ_l is the liquid surface energy (mJ/m^2);
γ^{LW} denotes the Lifshitz-van der Waals component; and
γ^{AB} is the acid-base component.

Van Oss et al. (1988) presented the full version of the Young-Dupré equation as follows:

$$(1+\cos\theta)\gamma_l = 2[(\gamma_s^{LW}\gamma_l^{LW})^{\frac{1}{2}} + (\gamma_s^{+}\gamma_l^{-})^{\frac{1}{2}} + (\gamma_s^{-}\gamma_l^{+})^{\frac{1}{2}}] \quad (4)$$

$$\gamma_s^{total} = \gamma_s^{LW} + 2[(\gamma_s^{+})(\gamma_s^{-})]^{\frac{1}{2}} \quad (5)$$

where,
γ_s^{LW} is the Lifshitz van der Waals (non-polar) component;
γ_s^{+} is the acid (electron accepting);
γ_s^{-} is the base (electron donating);
γ_s^{LW}.,γ_s^{+}, and γ_s^{-} are the solid surface energy components;
θ is the contact angle; and
γ_l^{LW}.,γ_l^{+}, and γ_l^{-} are the liquid surface energy components.

Using the above equations, one can predict the work of adhesion, W_a, between two materials. The condition of components at the time of wetting is very important. For example, when asphalt binder is applied to hot aggregate, it has a stronger bond than when it is applied to cold aggregate (Thelen, 1958).

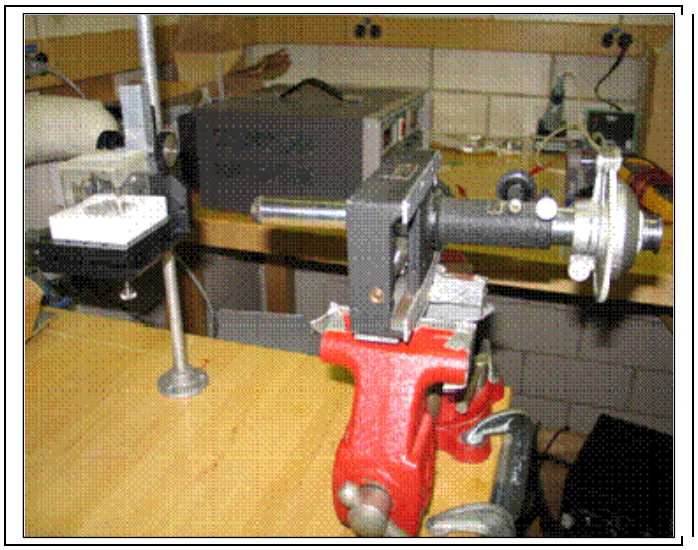

Figure 1-a. Sessile drop equipment and microscope

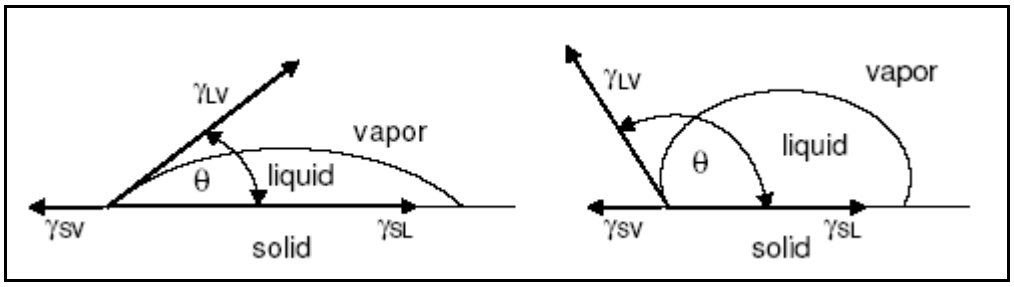

Figure 1-b. Contact angle of a drop of liquid on a solid

Experimental Program

The sessile drop method was used to determine both the surface energy of the hot-poured crack sealant and its wettability (contact angle) with respect to a specific substrate. The surface energy components of 13 different sealants were measured using this method. Each sealant was heated and mixed at the manufacturer's recommended installation temperature and poured onto an aluminum sheet to form a thin, smooth surface. The sealants were cooled at room temperature to solidify and make thin plates. A five-micrometer pipette was used to manually apply liquid drops from three probe liquids (water, formamide, and glycerol) onto the sealant plate. The image of each drop was captured by microscope within 15sec after it was applied. Knowing the surface energy components of the three probe liquids: water, formamide, and glycerol (Table 1), and their respective contact angles with a specific sealant, the Young-Dupré Equation was used to calculate the surface energy component of the sealant (Equation 4). Substituting the calculated surface energy components of the sealant in Equation 5, one can calculate total surface energy of the sealant (Table 2).

The next step was to measure the contact angle between sealant and a specific substrate. The aggregate types: quartzite, granite, and limestone, were freshly cut to 50x50x5mm plates, cleaned with acetone and distilled water, and oven dried. The sessile drop method was used to place a drop of each sealant on the aggregate surface. The contact angle between each individual pair of sealant and aggregate was captured by the microscope (Table 3). In addition, to establish aluminum as a replacement for aggregate,

the contact angle between the same sealants and an aluminum plate, made out of 6061-aluminum, was measured separately, (Table 3). Finally, using surface energy of the sealant and its contact angle to a specific substrate, the work of adhesion, W_a, was calculated using equation 2; the results are presented in Figures 2a and 2b.

Table 1. Surface Energy Characteristics of Probe Liquids at 20ºC, mJ/m^2(after Van Oss et al., (1988)

Probe Liquid	γ_l	γ_l^{LW}	γ_l^+	γ_l^-
Water	72.8	21.8	25.5	25.5
Glycerol	64	34	3.92	57.4
Formamide	58	39	2.28	39.6

Table 2. Surface Energy (mJ/m^2) and Its Components for Various Crack Sealants

Sealant	□^{LW}	□̃	□$^+$	□^{total}
AD	34.49	5.68	1.84	40.96
AE	43.99	5.21	4.36	53.53
BB	9.97	40.01	0.94	22.25
DD	18.28	4.38	0.29	20.52
EE	0.1	4.88	18.72	19.22
UU	2.39	6.32	4.75	13.35
VV	32.45	2.18	0.84	35.15
MM	45.15	12.01	4.93	60.54
NN	6.63	19.99	0.37	12.06
PP	13.98	4.4	0.6	17.22
QQ	0.01	5.39	11.6	15.83
WW	9.03	18.8	1.2	18.54
YY	2.89	10.03	2.4	12.7
ZZ	10.03	5.17	0.39	12.89

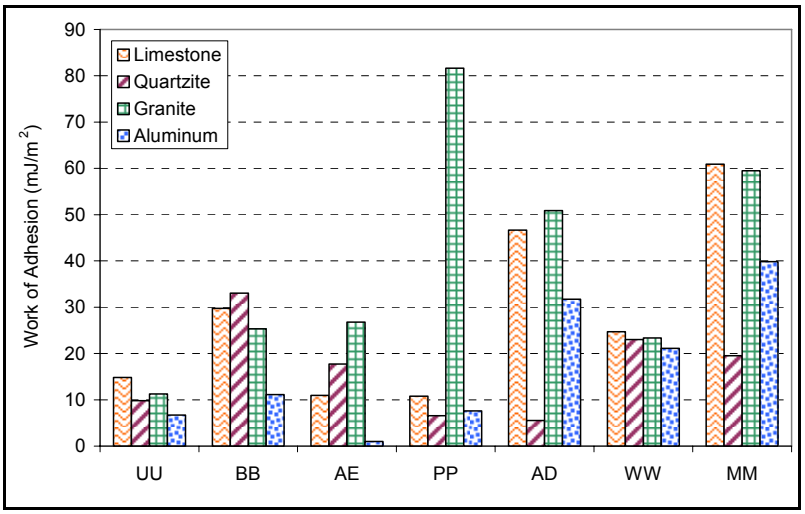

Figure 2-a. Work of adhesion between sealants and limestone, quartzite, granite, and aluminum

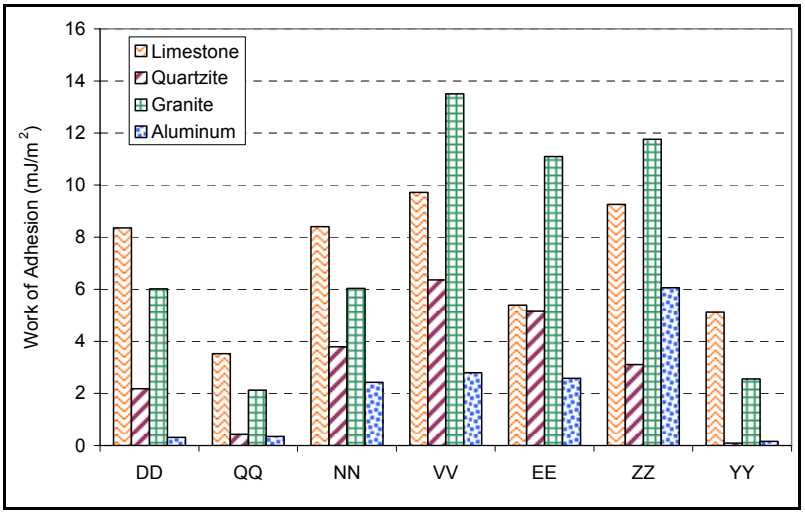

Figure 2-b. Work of adhesion between sealants and limestone, quartzite, granite, and aluminum

Summary of the Surface Energy Method

The study found that work of adhesion for each pair of adhesive-substrate can be the first step to evaluate the bond. Each material possesses a unique surface energy. The compatibility of two materials can be studied using the energy they release once in contact. Knowing the surface energy of the sealant, one can approximately predict if it would be compatible with a specific HMA composition. Some sealants are more appropriate to be used with aggregates which are high in silica while some others are more suited for HMA in which calcium carbonate is the dominant component.

Table 3. Contact Angle between Various Sealants and Substrates

Sealant/Substrate	Limestone	Quartzite	Granite	Aluminum
AD	82	150	76	103
AE	143	132	120	169
BB	70	61	82	120
DD	126	153	135	170
EE	136	137	115	150
UU	84	105	99	120
VV	136	145	128	157
MM	90	133	91	110
NN	108	133	120	143
PP	112	128	115	124
QQ	141	167	150	168
WW	71	76	75	82
YY	127	173	143	171
ZZ	106	139	95	122

Direct Adhesion Test Method (DAT)

The second approach is a test using a newly developed setup incorporated in the DTT device. Since aggregate composes more than 80 percent of the HMA, it was assumed that a strong correlation exists between the adhesion at the sealant-HMA interface and the adhesion at the sealant-aggregate interface. Based on this assumption, the proposed test evaluates the adhesion at the sealant-aggregate interface. Various testing specimens were examined.

Because of the difficulty in preparing an adequate butt joint, it was suggested that the sealant be poured onto one aggregate/HMA piece and the other end be anchored to it (Figure 3). However, this approach was not appropriate, since the forces at the anchor are not well-defined. Therefore, it is not clear what mechanism is resisting failure in this case.

Figure 3. Anchorage used in adhesion test

The second specimen type was similar to the first one; but to avoid using an anchor, two cylindrical aggregates were used as end pieces. A split mold was used to pour the hot sealant between the two cylindrical HMA/aggregate blocks with hot-poured sealant sandwiched in between. To allow for this modification in the setup, it was essential to increase the size of the specimen to account for the HMA maximum aggregate size.

However, because of the sealant's high viscosity, the mold could not be filled appropriately, and the sealant failed to completely cover the end pieces (Figure 4). In the next trial, the mold was replaced with an insulated mold, and a vacuum was applied to fill it. At first, the mold was opaque and the sealant flow could not be tracked; so a transparent material was used in an attempt to address this difficulty. But again the sealant was too viscous (and its viscosity increased as its temperature decreased to room temperature), which caused the sealant to clog the hose (Figure 5). Due to high variability in the design of HMA, later trials use aggregate with high calcium carbonate or silica content.

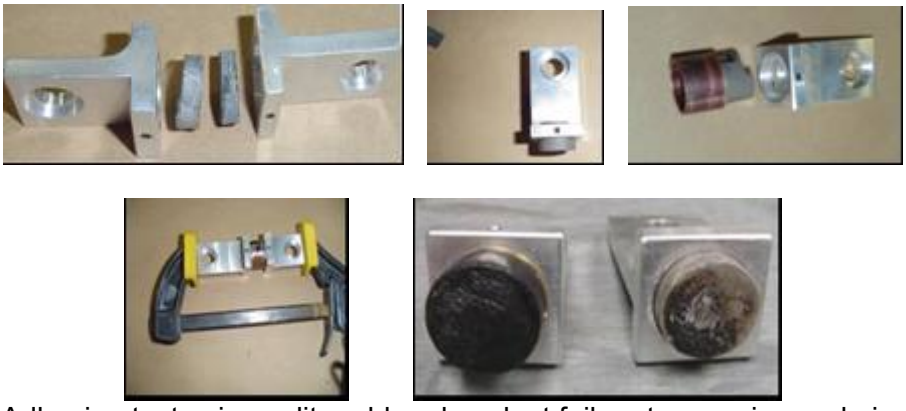

Figure 4. Adhesion test using split-mold and sealant failure to covering end pieces (lower right)

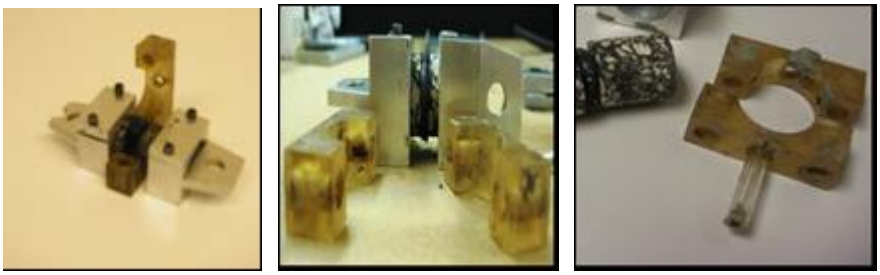

Figure 5. Transparent mold and clogged hose

To address the difficulty of sealant pouring, another testing fixture was developed. The briquette assembly consists of two half-cylinder aggregates of 25-mm-in-diameter and 12-mm-long. Each aggregate is confined within an aluminum grip designed to work with the DTT sitting posts. The assembly has a half cylinder mold, open at the upper part. The mold is placed between the two aggregates on a level surface; so that sealant poured into the mold will be confined between the two end pieces. In order to ensure that adhesive failure occurs, and to define the failure's location, a pre-debonded area is made in the form of a crack at one side of the sealant-aggregate interface. To make the crack, a 25x2mm shim is placed on the upper edge of the aggregate piece that will sit on the fixed side of the DTT. After the sealant is poured into the mold and cooled, removing this shim leaves a notch 2mm deep at the aggregate-sealant interface that will be the initial failure location.

To prepare a specimen, two specified half cylinder substrates are assembled, and the mold and the notch are sprayed with a silicon-based release agent. The assembly is wrapped with a rubber band and placed on a base plate. The heated sealant is poured into the half cylinder mold. Sealant should be poured from one corner of the mold, until the mold is full. This helps avoid the formation of air bubbles. After one hour of annealing at room temperature, the specimen is trimmed and placed in a cooling bath for 15min. The specimen

is then removed from the bath, demolded, and placed back in the bath for another 45min before testing. Using the DT device, the end pieces are pulled apart by moving one of the end pieces at a speed of 0.05mm/s (strain rate of 0.005mm/mm/s), as shown in Figures 6 and 7. Test Builder software is used to record both load and displacement of the end pieces. Maximum load, P_{max}, and bond energy, E, are calculated for each pair of sealant-substrate. Energy is defined as the area under the load-displacement curve divided by the contact cross section. The resulted P_{max} and E can be regarded as indications of adhesion.

No energy is dissipated in crack initiation because of the already debonded area created by the edge notch. In addition, the failure path is defined. This approach resulted in consistent results compared to those conducted on un-notched specimens. Preliminary tests were conducted on 10 sealants using quartzite aggregate (Table 4). Tests were conducted at the lowest application temperature (-4ºC to -34ºC ±1, depending on sealant type). Each sealant-aggregate pair was brought to failure utilizing direct adhesion tester (DAT) at sealants' recommended application temperature. Material properties of these sealants, including their surface energy, glass transition temperature, viscosity, and test temperature along with their energy to separation, are reported in Table 4. A plot of the calculated energy versus the surface energy of the sealant for each pair of sealant-aggregate shows that a sealant with lower surface energy produced higher adhesion (Figure 8). This could be due to the fact that a sealant with lower surface energy can spread and wet the surface better.

Feasibility Studies

Using the setup described above, and as shown in Figure 6, several sealant-aluminum pairs were tested at temperatures ranging from -4ºC to -40ºC. Aluminum was selected as an appropriate replacement for aggregate because of its compatibility with sealant, low diffusion, controllable roughness, high resistance to extreme temperatures, and availability. It also has a similar thermal coefficient to that of aggregates. Further details on the selection of aluminum and comparison to other aggregates are presented under the third testing method. The load versus displacement of the end pieces was recorded. The P_{max} and E were calculated for each pair (Figure 7). The calculated area was then divided by the cross-section of the end piece in which failure occurred. P_{max} and E are plotted in Figures 9 and 10. The test results show both candidate parameters can differentiate among sealants and temperatures.

Figure 6. Pulling end pieces apart at a constant displacement rate, using tensile force in the DT machine

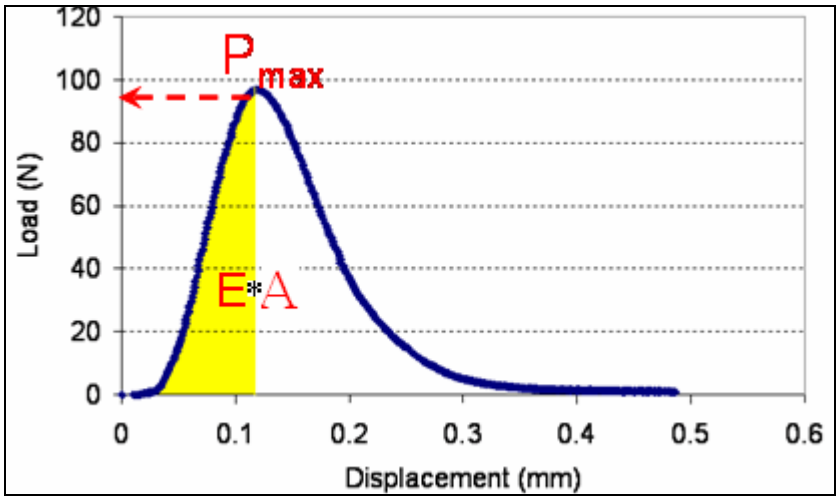

Figure 7. Maximum load and area under the load-displacement curve before the peak

Table 4. Measured Parameters for 10 Crack Sealants on Quartzite (without notch)

Sealant	Surface energy (mJ/m^2)	Viscosity (Pa.s)	T_g (°C)	Testing Temp. (°C)	Energy (J/m^2)
MM	60.54	1.66	-54.54	-34	3.31
VV	35.15	0.99	-30.65	-34	4.85
AD	40.96	0.35	-45.54	-34	7.29
AE	53.53	1.64	-67.69	-34	8.01
QQ	15.83	5.11	-53.45	-4	9.15
WW	18.54	2.58	-62.83	-34	12.33
PP	17.22	3	-77.91	-34	22.44
YY	12.7	1.75	-38.11	-10	25.01
NN	12.06	6.1	-59.59	-34	25.59
UU	13.35	2.53	-30.16	-10	45.44

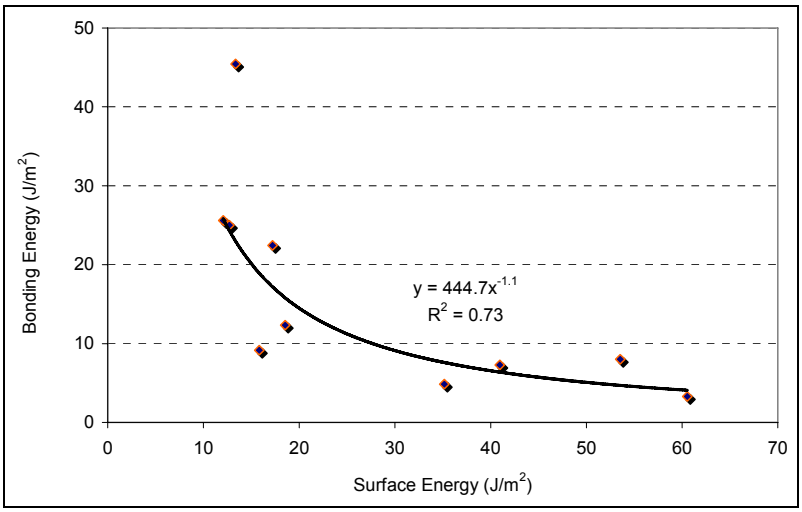

Figure 8. Bonding energy versus surface energy of the crack sealant for sealant-quartzite pairs

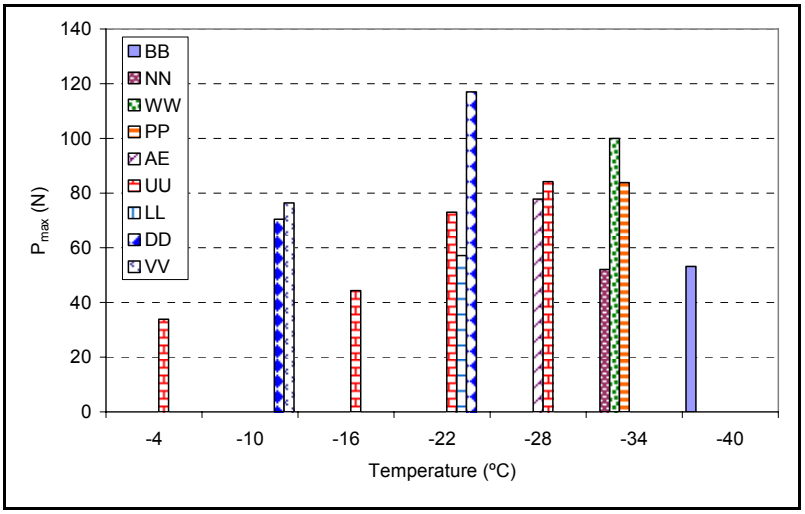

Figure 9. Required load to separate sealant from its aluminum counterpart at various temperatures

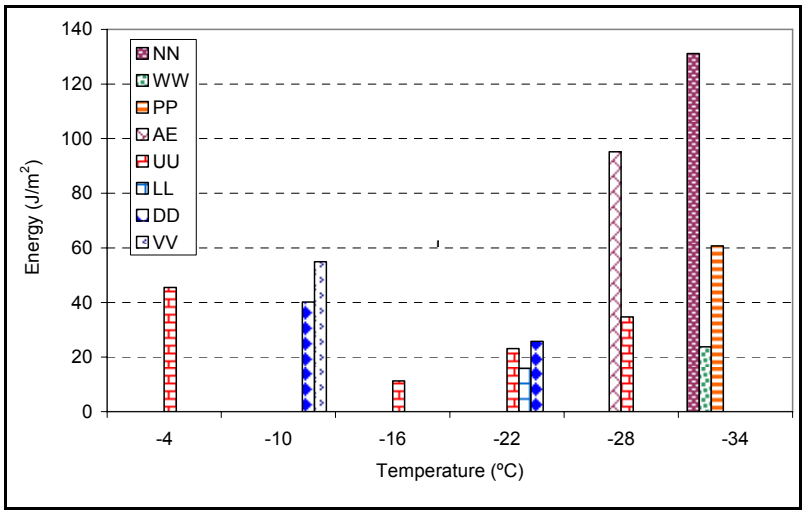

Figure 10. Energy spent to separate sealant from its aluminum counterpart at various temperatures

Selecting the End Pieces

To examine the effect of aggregate composition and topography, the study used aggregates from five states with very different geological conditions: Oklahoma, Illinois, Ohio, Wisconsin, and Pennsylvania. These states provide good representations of the variation in geological conditions in the United States.

Each aggregate was tested using X-ray diffraction (XRD) analysis (conducted at the State Geological Survey, Illinois) to determine its mineral composition (Table 5a). X-ray diffraction is a powerful, non-destructive technique for characterizing crystalline materials. While this method is quite reliable for determining carbonates (limestone, $CaCO_3$ and dolomite, $CaMg(CO_3)_2$), it cannot provide the total amount of SiO_2 accurately because SiO_2 can be in a number of minerals such as quartz, feldspar, and clay. To measure the total amount of SiO_2, X-ray fluorescence (XRF) was used to measure the chemical composition

(Table 5b) of each aggregate (conducted at Actlabs, Canada). Sandstone from Pennsylvania shows the highest percentage of silica (98%).

Table 5-a. Mineral Composition of the Five Tested Aggregates (%)

Component	Granite [1]	Limestone [2]	Limestone [3]	Sandstone [4]	Quartzite [5]
Quartz	28.71	1.60	1.94	98.44	89.69
Potassium Feldspar	26.15	0.00	0.00	0.10	0.00
Plagioclase	33.18	0.00	0.00	0.10	0.25
Calcite	0.00	24.37	94.27	0.00	0.16
Dolomite	1.47	72.88	1.67	0.03	0.35
Hornblend	0.00	0.00	0.00	0.05	0.15
Pyrite	0.00	0.00	0.60	0.02	0.17
Illite	0.34	0.00	1.35	0.45	8.90
Kaolinite	0.00	0.00	0.00	0.54	0.04
Cholorite	0.00	0.00	0.18	0.10	0.09

1) Oklahoma; 2) Ohio; 3) Illinois; 4) Pennsylvania; 5) Wisconsin

Table 5-b. Chemical Composition of the Five Tested Aggregates (%)

Element	Granite [1]	Limestone [2]	Limestone [3]	Sandstone [4]	Quartzite [5]
SiO2	75.16	1.89	1.24	97.94	82.42
Al2O3	12.14	0.24	2.47	1.06	8.97
Fe2O3	2.37	0.23	0.53	0.06	3.36
MnO	0.042	0.02	0.119	0.003	0.006
MgO	0.31	11.67	0.5	0.05	0.34
CaO	0.53	27.5	53.14	0.02	0.43
Na2O	3.79%	0.01	< 0.01	0.02	0.08
K2O	4.85%	0.03	0.02	0.12	1.49
TiO2	0.2%	0.01	0.02	0.04	0.37
P2O5	0.01	0.02	0.03	0.01	0.06
Cr2O3	< 0.01	< 0.01	< 0.01	< 0.01	< 0.01
LOI	0.523	44.63	41.97	0.333	2.43
Total	99.93	86.24	100	99.65	99.95

1) Oklahoma; 2) Ohio; 3) Illinois; 4) Pennsylvania; 5) Wisconsin

The highest amount of calcium carbonate was found in the Illinois limestone at 94.3 percent. To calculate the amount of this component from the XRF method, the amount of CaO in Table 5b should be multiplied by a factor of 1.78, which is the ratio of the molecular weight of $CaCO_3$ (100g) to CaO (56g). Using this factor, Illinois limestone having 53.14 percent CaO consists of 95 percent calcium carbonate, which is close to the result from the XRD method.

Experimental Program

All aforementioned tests were performed on non-aged sealant; however, it was shown that short-term sealant aging occurs mainly during heating in the kettle (Masson and Al-Qadi, 2004). Therefore, sealant is already aged even before exiting the wand and entering the crack. Aging affects sealant chemistry; therefore, it is expected that sealants'

rheological behavior changes after aging. Depending on its composition and percentage of polymer, ground rubber, and/or mineral filler, the sealant may become stiffer or softer after aging. If the polymer chains are degraded during aging, sealant becomes softer, while if chains coalesce sealant becomes stiffer after aging. Considering the effect of aging on the bonding, and the fact that the main part of aging occurs in the kettle, sealant adhesion should be measured for aged sealant. Hence, an adhesion threshold should be recommended based on the test results from aged sealants. To study if an aging process affects the bonding significantly, first, an aging method able to resemble short-term aging needs to be developed, and second, bonding between aluminum and several aged sealants need to be determined and compared to unaged sealants.

As part of this project, a method and procedure for aging was developed to simulate aging and weathering of crack sealants (Masson and Al-Qadi, 2004). In this method, the homogenized sealant is cut into pieces and placed in a stainless steel pan in a heated oven until it melts and creates a 2-mm-thick film. Then it is cooled down to room temperature and placed in a vacuum oven aging (VOA) device, heated to 115ºC for 16hrs at a vacuum of 760mm of mercury. The sealant is then transferred to a regular oven, heated at 180°C to melt and stored in containers (Masson and Al-Qadi, 2004). Comparison of the chemical composition of the aged and un-aged sealants to those of field specimens proved this method is a suitable approach for aging bituminous crack sealants (Masson and Al-Qadi 2004).

To examine the effect of aging on bonding, six sealants were aged following the aforementioned aging procedure. Bonding potential of these sealants to aluminum end pieces was measured using DAT. The bonding of the same sealants, but unaged, were also measured and compared, Figures 11 and 12. As can be seen, P_{max} and E values vary with aging. In addition, both parameters show the same pattern. For example, both parameters show lower bonding for aged sealant NN at -34ºC, and both parameters show higher bonding for aged sealant UU at -16ºC. This variation among sealants can be attributed to variation in the chemical composition of the sealant, which is highly affected by the type and content of the polymer used.

To fine-tune the test method and check the test variation, eight sealants, which are widely used in various regions in North America, were selected for final testing. These sealants have various rheological characteristics and are used in regions with low temperatures between -4 to -40ºC. Each sealant was aged in accordance with the procedure by Masson and Al-Qadi (2004). Adhesion of the aged sealants with aluminum was estimated using the adhesion test setup. Maximum load and energy to failure was calculated for each pair. Figures 13 and 14 show the test results for aged sealants at temperatures ranging from +2 to -34ºC.

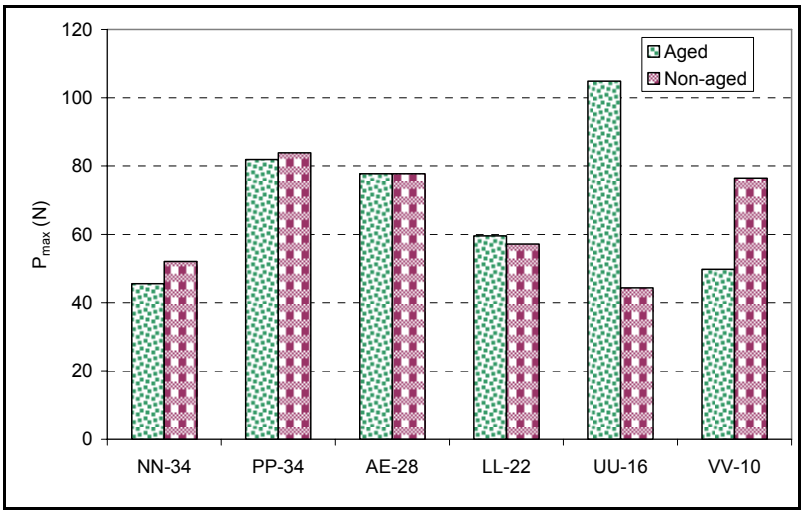

Figure 11. Required load to break the bond between aluminum and aged/ non-aged sealants

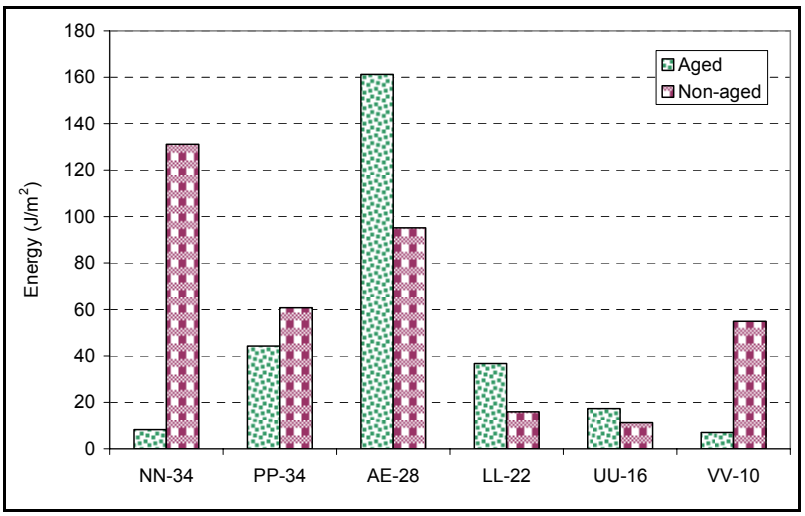

Figure 12. Required energy to break the bond between aluminum and aged/ non-aged sealants

Variation within Laboratories

A statistical analysis was conducted to estimate variation within laboratories. The repeatability of the adhesion test results was acceptable, with an average coefficient of variation of 19.3 percent. However, to ensure consistent test results, the steps presented under specimen preparation should be followed. In addition, pouring temperature, and consequently, viscosity of the sealant should be controlled. As discussed later in this report, sealant viscosity may significantly affect bonding. It is recommended to control temperature within ±1°C. In addition, it is preferred to pour sealant in a mold in a closed environment to minimize temperature variations while casting specimens. Another concern is the homogeneity of the sealants; especially with products containing a high percentage of rubber and/or filler. To ensure homogeneity of the sealants, sealant preparation using ASTM D5167 is recommended. In accordance with the ASTM C670 standard, the acceptable variation should be established using precision of individual measurements. The maximum acceptable range for individual measurements is obtained by multiplying the standard

deviation of the measurements by a factor reflecting the number of replicates. For three and four replicates, this factor is 3.3 and 3.6, respectively.

To evaluate data variability between operators, two operators tested sealants LL, MM, NN, UU, VV, and AE individually. A standard analysis of variance (ANOVA) was conducted to check whether the results of the two sets of tests were statistically different. The results showed no statistical evidence that the measured P_{max} was different at a level of significance of 5 percent (Table 6). In addition, another setup, built using different manufacturer was tested to check for variation among various test setups. Statistical analysis showed no significant difference among test setups (Tables 6 and 7)

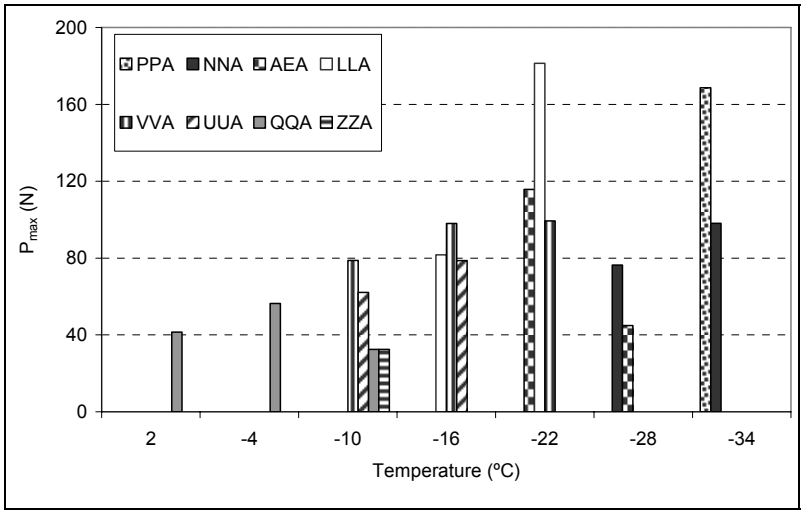

Figure 13. Measured maximum load for eight aged sealant-aluminum pairs

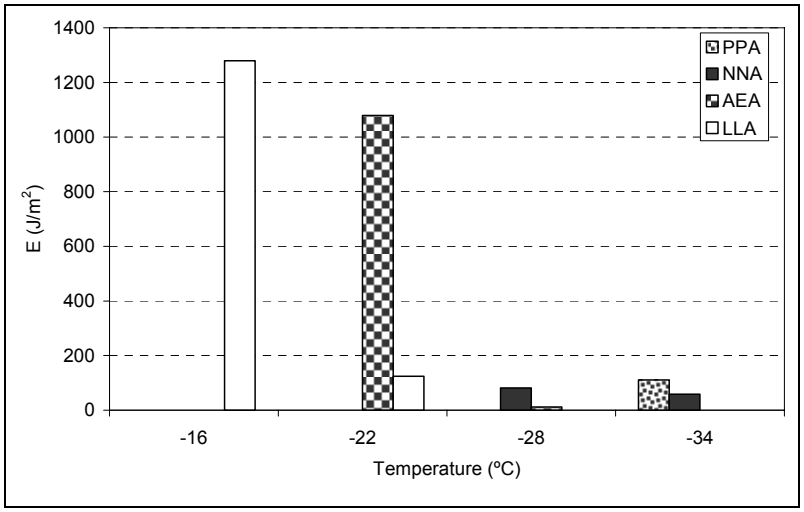

Figure 14-a. Measured energy measured for four aged sealant-aluminum pairs

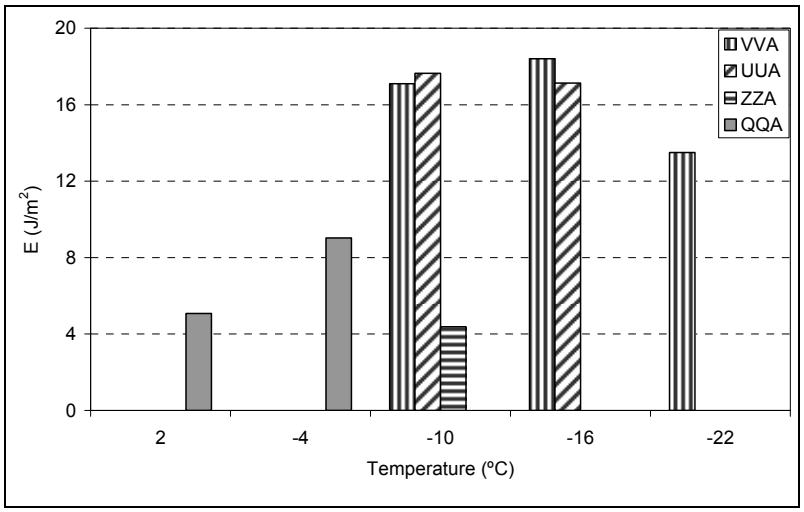

Figure 14-b. Measured energy for four aged sealant-aluminum pairs

Table 6. Analysis of Variance between Two Operators

Sealant	Testing Temp.(ºC)	SS	df	MS	F	P-value	F critical
AE	-28	15.84	1	15.84	0.057	0.82	7.71
LL	-16	191.49	1	191.49	5.024	0.09	7.71
MM	-28	414.09	1	414.09	2.488	0.19	7.71
NN	-28	0.12	1	0.12	0.001	0.97	7.71
UU	-10	207.89	1	207.89	0.919	0.39	7.71
VV	-10	1.54	1	1.54	0.046	0.84	7.71

Table 7. Analysis of Variance between Two Setups

Sealant	Testing Temp. (ºC)	SS	df	MS	F	P-value	F critical
QQ@+2	2	3.3	1	3.3	0.07	0.8	7.71
NN@-28	-28	392.06	1	392.06	1.542	0.28	7.71
LL@-16	-16	191.49	1	191.49	5.024	0.09	7.71
PP@-34	-34	95.32	1	95.32	0.972	0.38	7.71

Variation between Sealants

In the next step, a statistical analysis was conducted to examine the adequacy of determined parameters to distinguish among sealants tested at the same temperature. Characteristics of the tested materials are reported in Table 8.

The t test was used, when two sealants were compared at a specific temperature. The F test appeared to be an appropriate statistical method for multiple comparisons (more than two groups). Analysis of variances and multiple data comparison were conducted at temperatures ranging from +2ºC to -34ºC at 6ºC intervals. Analysis of variance procedures required the following assumptions:

- Each group is an independent random sample from a normal population.
- The variances of the groups are equal.

Table 8. Characteristics of Seven Sealants Selected for Testing

Sealant	Pouring Temp. (ºC)	Viscosity (Pa.s) @ application temperature	Molecular weight (g/Mol)	
			Mode I	Mode II
AE	189	1.639	1420	186100
VV	149	0.961	1470	184000
ZZ	193	4.156	1480	---
NN	188	6.356	1360	257700
QQ	193	4.725	1480	353700
PP	193	2.997	1440	137300
UU	193	2.533	1410	176900

To check the second assumption in which the null hypothesis is that the groups come from populations with the same variance, the Levene test at significance level of 0.05 was used. The observed significance level at all temperatures is greater than 0.05 (Table 9). Therefore, the null hypothesis would not be rejected and variances of the groups are equal.

Table 9. Levene Test Result to Examine the Equality of the Variances of the Groups

Groups	Levene Statistic	Sig.
@T-34	2.132	0.200
@T-28	0.017	0.903
@T-22	0.274	0.628
@T-16	4.737	0.058
@T-10	3.361	0.105
@T-4	4.664	0.097

Significant differences among the sealants tested at the same temperature was examined. The null hypothesis is that all groups have the same mean values at a 0.05 significance level. The statistical test for this null hypothesis is based on the F ratio. A significant F-value indicates that not all population means are equal. For this part, the best three out of four replicates were used in the analysis. As indicated in Table 10, the significant values for all groups with the exception of group T-22 are below 0.05, which means F is significant and the null hypothesis is rejected (Table 10). For cases in which two sealants are compared, i.e groups T-28, T-4, results show that test parameter can distinguish between sealants in these groups. However, for cases in which more than two sealants are compared, a significant F ratio only means there is at least one group which is different from the rest. In those cases, multiple comparisons followed by a Tukey's HSD (honestly significant difference) test are conducted to examine the ability of test parameters to differentiate between all sealants adequately. To study how much of the variation occurs between sealants, the sum of square between groups was divided by the total sum of square (Equation 6). Table 11 presents the percentage difference among sealants tested at each temperature.

$$DS = \frac{SS_b}{SS_t} \tag{6}$$

where,

DS is the variation among sealants at each temperature;
SS_b is the sum of squares between groups; and
SS_t is the total sum of square, (i.e. $SS_b + SS_w$).

Multiple comparisons were then conducted to determine which means are significantly different from the others. Tukey's HSD procedure allows for a comparison of the possible pairs of means. For example, if there are four sealants, six possible paired comparisons (comparisons between individual means) can be performed. Table 12 shows the homogeneous subset at -34, -16, and -10ºC.

Table 10. ANOVA Results Comparing Sealant Mean Values Using P_{max}

Temperature (ºC)		Sum of Squares	df	Mean Square	F	Sig.
-34	Between Groups	10,589.583	2	5,294.791	131.037	0.0000
	Within Groups	242.440	6	40.407		
	Total	10,832.023	8			
-28	Between Groups	2,273.629	1	2,273.629	14.497	0.0190
	Within Groups	627.330	4	156.832		
	Total	2,900.958	5			
-22	Between Groups	12.801	1	12.801	0.022	0.8894
	Within Groups	2,331.242	4	582.810		
	Total	2,344.043	5			
-16	Between Groups	7,031.484	2	3,515.742	30.077	0.0007
	Within Groups	701.341	6	116.890		
	Total	7,732.825	8			
-10	Between Groups	2,607.818	2	1,303.909	14.045	0.0055
	Within Groups	557.032	6	92.839		
	Total	3,164.850	8			
-4	Between Groups	2,325.271	1	2,325.271	89.707	0.0007
	Within Groups	103.682	4	25.921		
	Total	2,428.953	5			

Table 11. Sealant Variation Ratio at Each Temperature for P_{max}

Temperature (ºC)	DS (%)
-34	97.76
-28	78.38
-16	90.93
-10	82.40
-4	95.73

Table 12-a. Homogenous Subsets at -34ºC for P_{max}

Sealant	N	Subset for alpha = 0.05		
		1	2	3
NN	3	45.537667		
PP	3		84.490667	
AE	3			129.487333
Sig.		1.000	1.000	1.000

Table 12-b. Homogenous Subsets at -16ºC for P_{max}

Sealant	N	Subset for alpha = 0.05		
		1	2	3
UU	3	36.722667		
LL	3		65.289333	
VV	3			104.892000
Sig.		1.000	1.000	1.000

Table 12-c. Homogenous Subsets at -10ºC for P_{max}

Sealant	N	Subset for alpha = 0.05	
		1	2
VV	3	23.8077	
UU	3		49.7580
ZZ	3		65.0467
Sig.		1.000	0.207

At -34 and -16ºC, three sealants are categorized in three separate subsets, which means all three sealants are different. However, at -10ºC, sealants UU and ZZ at confidence level of 0.05 do not show significant difference. In further examination, the number of replicates was increased, and statistical analysis was repeated. Table 13 shows the test of homogeneity of variances, in which the observed significance level is 0.245 which is greater than 0.05; hence, the groups' variances are equal. The ANOVA results in Table 14 show that the F ratio is significant, which suggests the groups have different mean values. Finally, Table 15 shows the homogenous subsets at -10ºC. As can be seen at significance level 0.05, the three sealants are different; hence, the test parameter can adequately differentiate among sealants at each temperature. With the exception of sealants tested at -22ºC, significant differences were found among sealants.

Table 13. Levene Test Result to Examine Sealant Equality of Variances at -10ºC

Levene Statistic	df1	df2	Sig.
1.516	2	19	0.245

The fact that no significant difference was observed between the sealants tested at -22ºC can be attributed to the inherent similarity of the two sealants tested at this temperature.

Statistical analysis conducted for the second parameter, energy, led to the ANOVA table and homogenous subsets in Tables 16 and 17, respectively. As can be seen, energy can also distinguish among sealants tested at each temperature with the exception of -10ºC. It should be noted though; this parameter could not differentiate among sealants as clearly

as P_{max} did. For instance at -34 and -16ºC, it only categorizes the sealants into two subsets, and fails to distinguish between sealants NN and PP at -34ºC and sealants LL and VV at -16ºC.

In general, statistical analysis showed both parameters can distinguish between sealants to some extent; however, P_{max} was found to be a more sensitive parameter to sealant variation and able to clearly differentiate among sealants.

Table 14. ANOVA Results Comparing Sealants Tested at -10ºC Using P_{max}

	Sum of Squares	df	Mean Square	F	Sig.
Between Groups	8,930.900	2	4,465.450	26.464	0.000
Within Groups	3,205.992	19	168.736		
Total	12,136.892	21			

Table 15. Homogenous Subsets at -10ºC for P_{max}

Sealant	N	Subset for alpha = 0.05		
		1	2	3
VV	6		51.6967	
UU	13			79.6402
ZZ	3	23.8077		
Sig.		1.000	1.000	1.000

Variation of P_{max} with Substrates

The same eight sealants were tested with four different substrates: limestone, granite, quartzite, and aluminum. Figure 15 shows that substrate composition and surface property affect the interfacial bonding significantly. While sealant PP adheres best to quartzite; sealants NN, AE, UU, LL, and VV adhere better to granite; and sealants QQ and ZZ adhere better to limestone.

Summary of the Direct Adhesion Tester

This study concluded that the Direct Adhesion Tester (DAT) is an appropriate qualitative method to evaluate interfacial bonding at the application temperature. The test setup and specimen preparation are developed to simulate the load applied at the interface during crack contraction. Although, the selected displacement rate, 0.05 mm/s, may not resemble field conditions, it can provide a uniform test method and consistent test results provided the test method and specifications are followed. Two parameters, maximum load (P_{max}) and energy (E) were considered as a measure to predict adhesion. To check test repeatability, a statistical analysis was conducted. No difference was found between operators, nor between test setups. Further, statistical analysis showed both parameters can distinguish between sealants adequately. As a follow up to this study, round robin testing needs to be performed to establish precision and bias for this test method. This test may be used to qualitatively evaluate the effect of other factors such as annealing time, surface roughness, crack surface treatment, sealant viscosity, short and long-term aging, and water exposure.

Table 16. ANOVA Results Comparing Energy Values

Temperature (ºC)		Sum of Squares	df	Mean Square	F	Sig.
-34	Between Groups	5,003,440.996	2	2,501,720.498	100.705	0.000
	Within Groups	149,052.427	6	24,842.071		
	Total	5,152,493.423	8			
-28	Between Groups	29,744.001	1	29,744.001	5.008	0.089
	Within Groups	23,757.383	4	5,939.346		
	Total	53,501.384	5			
-22	Between Groups	936,090.588	1	936,090.588	6.267	0.067
	Within Groups	597,518.335	4	149,379.584		
	Total	1,533,608.923	5			
-16	Between Groups	235.152	2	117.576	18.394	0.003
	Within Groups	38.353	6	6.392		
	Total	273.504	8			
-10	Between Groups	575.232	2	287.616	2.755	0.142
	Within Groups	626.364	6	104.394		
	Total	1,201.597	8			
-4	Between Groups	44.442	1	44.442	31.106	0.005
	Within Groups	5.715	4	1.429		
	Total	50.157	5			

Table 17-a. Homogenous Subsets at -34ºC for the Bond Energy

Sealants	N	Subset for alpha = .05	
		1	2
NN	3	8.281458	
PP	3	49.039113	
AE	3		1,609.949193
Sig.		0.947	1.000

Table 17-b. Homogenous Subsets at -16ºC for the Bond Energy

Sealants	N	Subset for alpha = .05	
		1	2
LL	3	5.246706	
VV	3	8.301916	
UU	3		17.289782
Sig.		0.364	1.000

Table 17-c. Homogenous Subsets at -10ºC for Energy

Sealants	N	Subset for alpha = .05
		1
ZZ	3	1.3192
VV	6	8.4578
UU	13	109.8665
Sig.		0.134

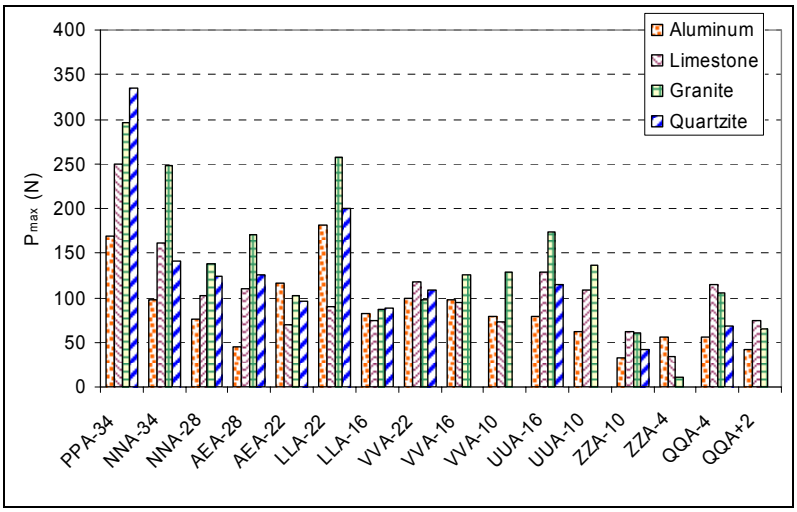

Figure 15. Measured load for various substrate pairs

Fracture Mechanics Approach

A weak bond results in cracks or delamination under loading; hence, a natural approach for assessing the resistance to delamination is to use fracture mechanics. Therefore, the third approach used the concept of fracture mechanics. Since fracture tests take into account both the specimen geometry and the elastic properties of the two adhering materials; the interfacial fracture energy (IFE) can be derived independent of the geometry.

Until now, many mechanical testing methodologies have been designed to evaluate IFE. Among these, the peel test, the double cantilever beam test, the indentation test, and the blister test appeared to have the most potential for application to a sealant-aggregate system. The conventional peel test is one of the well-received methods. However, the peel test has many drawbacks, which have been discussed in detail by Kim and Kim (1988). The main drawback is that most of the energy is dissipated or stored in deformation of the test specimen, and little energy contributes to fracture. Moreover, extracting IFE from a peel test is not very straightforward (Chu and Durning, 1992). Another limitation of the peel test is its

high bending angle and consequently the large amount of energy dissipated in plastic deformation (Wan and Mai, 1995). Also, because of the direct mechanical contact via a clamp, this test is not appropriate for viscoelastic adhesives such as bituminous material which is loading-history dependent. In addition, using a peel test on a rubber-glass system, Gent and Lewandowski (1987) showed that apparent IFE is very sensitive to peel rate. They observed that increasing the peel rate by tenfold led to an order of magnitude increase in IFE. They also observed that IFE measurements from blister tests are consistently lower than those from peel tests. They attributed that to the high energy dissipated when adhesive is bent sharply away from the substrate at 90º. After examining the feasibility of different methods to experimentally evaluate the IFE, the blister test was found to be promising.

Peel Test

The peel test is a common test in the polymer, paint, and microelectronics industries. Due to its relative simplicity, the peel test is a well-received method to measure adhesion of mainly deformable adhering layers. In the test, a thin flexible strip bonded to substrate is peeled away from the substrate at some angle to the substrate. The force applied to separate the adhesive from the substrate is called peel force. If there is no plastic deformation or residual stress involved, adhesion can be calculated as follows:

$$\gamma_a = (1 - \cos\theta)P \qquad \textbf{(7)}$$

where,
γ_a is adhesion;
θ is peel angle; and
P is peel force per unit width of the film.

However, in order to extract the intrinsic adhesion in the presence of plastic deformation, one needs to consider the energy dissipated during peeling. The aforementioned Equation 5 is unable to define a unique geometry-independent value, which can represent the adhesion, from the experimental data. The dominant component of many peel tests is energy dissipated in plastic bending of the peeling arm, and only a small portion is used to break the bond (Gent and Lewandowski, 1987). Later studies implemented a detailed elastoplastic analysis of steady state peeling. The film was modeled as a beam on a rigid substrate (Kim and Kim, 1988). An energy balance along with beam theory was used to extract the interfacial fracture energy from the experimental data (Kim and Kim, 1988). Later, finite element analysis of the peel test showed the singularity is limited to the crack tip and the dominant mode of deformation is bending. Several researchers tried to correlate the peel force and IFE; however, all specimens mentioned in their studies suffered a large yielding not only around the crack tip but also within the film thickness. Also, the plastic dissipation energy masked the component of IFE.

Blister Test

The blister test appears to be self-contained, practical, and repeatable. Interfacial fracture energy, which is a geometry-independent engineering term, can be extracted easily through this test. Having IFE as a system parameter and Young's modulus of the adhesive material, one can predict adhesive failure in complex adhesive joints by stress analysis and energy balance of the geometry. This test was first developed by Williams (1969) and later modified by Burton et al. (1971) by incorporating aspects of a test first suggested by

Dannenberg (1961). The test method starts with a torus-shaped disk of substrate covered with a layer of adhesive on top. When a liquid or gas is injected from below into the center of the annular disk, the adhesive lifts off the disk or substrate. A blister forms and its radius stays fixed until a critical pressure is reached. At this critical pressure value, the radius of the blister increases in size, signifying the initiation of the debonding process at the interface.

The intrinsically stable interface debonding process makes this test attractive and allows calculation of a fundamental property of the interface: the IFE. This parameter is defined as the energy required to separate a unit area of the interface (Bennett et al., 1974), which is found to be an inherent property of the interface and independent of the geometry (Penn and Defex, 2002). However, it is also important to note that it may depend on surface preparation (Bennett et al., 1974). Therefore, the surface preparation needs to remain constant if IFE is to be used to predict adhesion for various geometries. In addition to providing the IFE, the blister test also can provide the elastic modulus and residual stress of the adhesive layer. These features are unique to this test and make the test even more useful.

Theoretical Background

Fracture mechanics have already been used in the failure analysis of many materials, including HMA. Interfacial fracture energy (or bonding) depends on the thermodynamic work of adhesion, fracture mechanics, and rheology (Masson and Lacasse, 2000). In 1921, Griffith proposed an energy criterion of failure which serves as the basis of classical linear elastic fracture mechanics (LEFM) and of the more general elastic fracture mechanics (EFM, in which linearity is not required). This criterion is a statement of the principle of energy balance: a crack will propagate if the energy available is greater than or equal to the energy required to extend the crack by a unit surface area. Griffith showed that this energy for one material is the sum of the surface energies of each of the newly developed surfaces.

Williams (1969) explained that IFE is the difference between the surface energy of the bond and the sum of the surface energies of the newly developed surfaces. However, in reality, because the crack in most materials is rough and tortuous, and micro-cracking, frictional slip, and plasticity are involved in a sizable zone around the fracture tip, the energy required for unit crack propagation is much more than this value. This crack propagation energy is the sum of energy dissipated through a reversible component (thermodynamic work of adhesion) and a deformation component including viscous and plastic deformation which depends on the deformation rate. Williams applied fracture mechanics in the analysis of both thin plates with small deflections and very thick disks. Later, using a Winkler elastic foundation, he analyzed the adhesive layer to calculate the energy stored in the adhesive layer (Williams and Kelley, 1971) and showed that the IFE could be expressed in terms of the critical pressure and height of the dome. Gent and Lewandowski (1987) compared two different adhesives, elastic and elasto-plastic, and reported that the elastic adhesive exhibited a closer relationship to theoretically calculated IFE. However, very thin adhesive films (even ductile adhesive) should behave nearly elastically, because a thinner adhesive film has less material to dissipate energy (Hbaieb and Zhang, 2005).

Malyshev and Salganik (1965) conducted experiments using a point loaded blister test. They observed that the force applied to debond the film remained constant, while the height of the dome increased in proportion to the square of the radius of the orifice. Later, Jones (1969) used uniform pressure as the driving force through a pressurized blister test to improve the sensitivity of the test. During the experimental test, he observed that the same total force induced a smaller dome. Williams (1969) conducted some experiments using a pressurized blister test and observed that a bigger orifice resulted in lower failure pressure. In 1983, Hinkley examined the case of very thin films behaving like membranes; he found that IFE could be extracted from the critical pressure and the corresponding height of the

dome. A solution for IFE, accounting for residual tensile stress, is given by Allen and Senturia (1988). Their elastic model for thin flexible films was experimentally verified by Lin and Senturia (1990). Allen et al. (1987) also observed experimentally that with a larger orifice, the blister can rise more before debonding happens. Thouless et al. (1992) analyzed the blister test for both tensile and compressive residual stresses for both a small linear displacement limit (pure bending) and a large nonlinear membrane-type limit (pure stretching). Later, Cotterell and Chen (1992) studied the transition geometry of a blister from bending to stretching using Hencky's series solution. They produced a polynomial expression for the IFE and also discussed the mode-mixity of interfacial fracture in the blister test. They explained that the thinner adhesive film will result in greater IFE, and that the behavior of a blister is likely more akin to a plate than to a membrane. In 1998, Sheplak and Dugundji analyzed the transition from bending to stretching during a blister test; they showed that the tensile residual stress delayed the transition from bending to stretching. The mode-mixity at the interface can be important because the fracture energy usually increases considerably when the mode II component becomes significant (Evans et al., 1989).

In 1994, Anderson and coworkers in the Strategic Highway Research Program (SHRP) attempted to use the blister test to measure asphalt-aggregate bonding. They used a blister test to measure the adhesion of eight core asphalts with two different aggregates. They conducted a pressure control test using gas pressure as the driving force. They selected the failure pressure as a measure of adhesion. This simplistic approach investigated by SHRP led the researchers to conclude that their results did not reflect experience in the field and could not differentiate between various aggregates. Peak pressure alone, as used in the aforementioned study, neither serves as a measure of adhesion nor is a fundamental property. In order to have a unique measure of adhesion, the blister profile's evolvement along with the blister pressure should have been recorded, and fracture mechanics concepts should have been used to extract IFE.

In this study, a volume-controlled blister test was used to allow for stable crack propagation in contrast to the pressure-controlled test in which failure is catastrophic. This test can measure IFE, which is the sum of energy expended in reversible and irreversible processes.

Apparatus and Experimental Method

In the first trial, an annular aluminum plate with threaded orifice was attached to the piston through a plastic hose. The moving piston pushed the alcohol through the orifice forcing the sealant layer away from the annular plate. A blister was developed and kept growing. The pressure of the alcohol inside the blister was measured as a function of time. Pressure continued increasing until it reached its maximum level at which sealant started debonding from the aluminum plate and pressure dropped. The peak pressure was recorded and reported as the interfacial adhesion between the sealant and the aluminum (Figure 15). To make the setup more stable and reduce the test variation, a base setup was designed and connected to the piston. The base setup could accept annular plates of 50mm in outer diameter and 12.5mm inner diameter. To prepare the specimen, the orifice was closed with an aluminum plug which was designed to be incorporated in the Dynamic Shear Rheometer (DSR) water bath, the DSR spindle was replaced by a spindle of 37.5mm in diameter which was used as a press machine to control the sealant thickness. Sealant was poured on the annular plate and pressed to a 2-mm-thick film by lowering the spindle (Figure 16). The extra sealant was trimmed away, and the specimen was deplugged and placed in the base setup.

The test was conducted, and as before, the peak pressure was reported as the interface bonding. The test was conducted for both quartzite and aluminum plate (Figure 17). It clearly shows that the test not only differentiates between sealants at one temperature, but

it is also sensitive to substrate variation and temperature changes. In this setup, the orifice was quite small; therefore, even the lowest injected volume rate (within the piston capacity) was quite high, and failure was very quick and in some cases cohesive failure was observed. In addition, the edge effect was thought to be effective and capable of causing erroneous results. To deal with this problem, the specimen size was increased. In addition, as mentioned earlier, peak pressure, although differentiating between sealants and substrates, is geometry dependent. To come up with a geometry independent parameter, blister height needed to be measured as a function of time. The final modification of the test overcame these two issues.

Figure 15. The first trial of the blister test: annular plate covered with sealant and the connector hose

Figure 16. The second blister test setup: sample preparation, base setup, and supporting plate

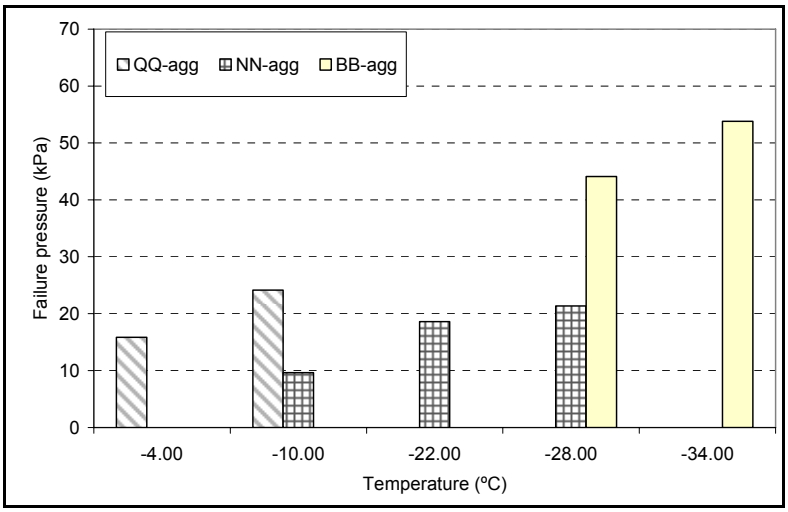

Figure 17-a. Failure pressure for three sealant-quartzite pairs at various temperatures

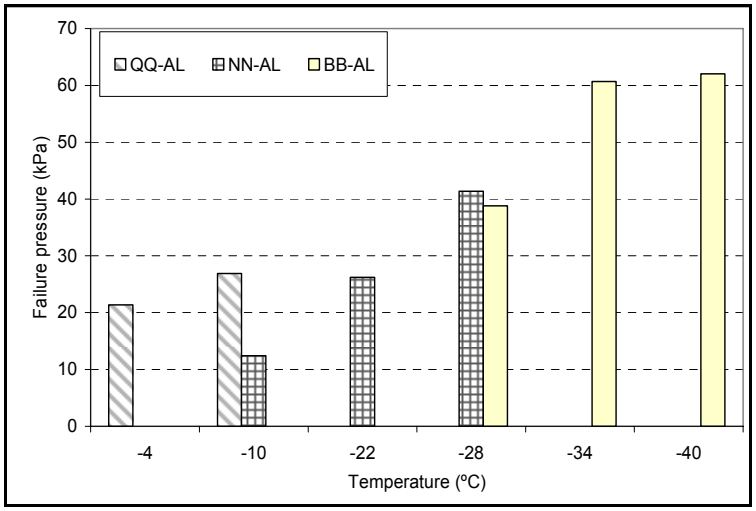

Figure 17-b. Failure pressure for three sealant-aluminum pairs at various temperatures

Figure 18 depicts a schematic of the current setup and specimen. In this setup, a fluid is injected at a constant rate at the interface between the substrate (a standard material or aggregate) and the adhesive (crack sealant) to create a blister. Pressure, p, and blister height, d, are recorded as a function of time. A servo-hydraulic pump was used to control the volume flow rate of alcohol at 0.1L/h. The induced pressure inside the blister was measured with a Viatran pressure transducer. The transducer resolution is 0.25 percent of full range and its maximum capacity is 3.5MPa (500psi). The height of the evolving blister is recorded through a linear variable displacement transducer of ±12mm.

To prepare an aggregate sample, a heavy duty masonry saw and coring machine were used. The irregularly shaped stone is cut on three sides, so that the stone can be held in the saw machine. With the stone confined in place in the saw machine, the center hole (25mm diameter) is cut through the chunk of stone, and then the core bit is changed to cut the outer perimeter (125mm diameter). The stone is then cut in slices of 10mm to achieve the annular disks (Figure 19). In addition to aggregate, aluminum substrates was tested. Annular-shaped aluminum substrates are prepared from 6061-aluminum. The inner and outer diameters are respectively 25mm and 125mm, and the aluminum substrate thickness is 6.3mm. The aluminum substrates are mechanically polished to a 63□m finish to attain

uniform surface roughness and cleaning conditions. To prepare samples, each aluminum substrate is washed with water and cleaning solvent and then air-dried. To improve the repeatability of the test, several cleaning approaches were tried, and the aforementioned one was found acceptable.

The orifice in the aluminum or aggregate substrate is sealed using a close-fitted aluminum plug flush with the substrate surface. Even though the plug is closely fitted in the orifice, sealants with very low viscosity could enter the tiny clearance between the plug and orifice edge, causing inconsistent test results. To solve this problem, and to create a debonding area which represents an initial crack in the interface between sealant and substrate (aluminum or aggregate), a piece of 0.09-mm-thick transparent fluoropolymer (FEP) film is cut in a circular shape having a diameter of 27mm and placed on top of the plug. This film is transparent and has adhesive backing. It can stick to the plug and be removed from the sample, leaving a crack at the interface (Figure 20). With an operating temperature of -100ºC to 400ºC, fluoropolymers can resist both extreme pouring (193ºC) and testing (-40ºC) temperatures.

To align the film with the center of the plug, a circle was drawn on the FEP film using compasses; a small pin was positioned on the center of the circle and the plug was placed on the pin (each plug has a center hole to let the pin pass through). Because the film is backed with adhesive, it sticks to the plug. After placing the film, a silicon-based release agent is sprayed on top of the film so the film will not stick to the sealant which will be cast on top of it. This approach improves the test repeatability substantially. The thin film will not only cover the tiny gap between the plug and the annular disk; it will also create an initial debonded area, representing a crack at the interface.

To prepare the specimen, hot-poured crack sealant is heated to its suggested application temperature, stirred thoroughly, and then poured onto the substrate. During preliminary tests, a press machine was used to press the sealant into a 4mm-thick flat disk. Replacing the press with cutter blade, the specimen was trimmed to the required diameter (Figure 21-a). This setup, however, was dropped due to the shearing effect of the press machine, which exposes the sealant to an unrealistic condition. In addition, the pressing action may force some sealants into the existing gap between the disk and the plug. In the current setup, sealant is poured into a 4.7-mm-thick mold that is made out of four arc-shaped aluminum pieces. The mold is assembled directly on top of the substrate surface (Figure 21-b). The molds are made so that they can be stacked on top of each other to allow for casting double and triple film thicknesses as needed. After one hour of annealing at room temperature, the extra sealant is trimmed with a heated potty knife. Then the sample is placed in a cooling bath for 15min, demolded, and placed back in the bath for another 20min prior to testing. The specimen is then placed on the blister test machine and confined with the support ring. Then the outlet valve is closed and the test is conducted. Pressure and blister height will then be collected as functions of time. Figure 22 shows a pressure-blister height curve for three typical sealants.

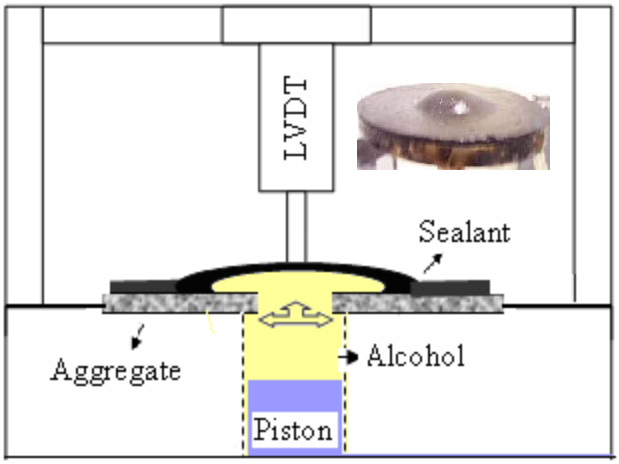

Figure 18. A schematic of blister apparatus before and after blister bulging


Figure 19. Preparation of aggregate disks


Figure 20. Aligning the FEP film on the plug and installing the plug in the orifice


Figure 21-a. Using the press/ cutter machine to prepare the specimen


Figure 21-b. Using the four piece mold to prepare the specimen

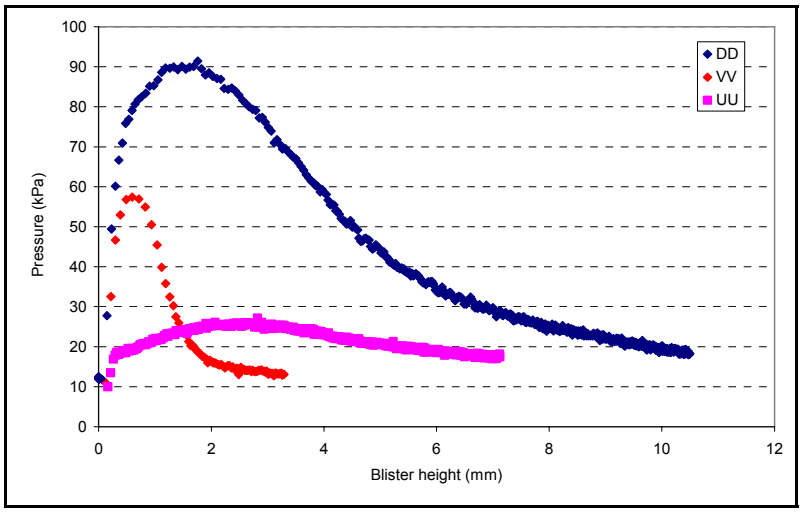

Figure 22. Pressure versus blister height for three different sealants

Analysis Approach and Discussion

Adhesive fracture mechanics is used to determine the IFE of interface system by means of the blister test (Bennett et al., 1974). The general form for all debonding problems is expressed by Equation 8 (Williams and Kelley, 1971), based on the balance between the potential energy provided by the externally applied pressure and the elastic strain energy stored in the adhesive (Wan and Mai, 1995):

$$IFE = \varphi p.d \quad \textbf{(8)}$$

where,
IFE is the interfacial fracture energy;
φ is a force factor;
d is the blister height;
p is the liquid pressure.

The value for φ can be defined based on the behavior of the adhesive film, if adhesive behaves like a plate, using fracture mechanics approach φ is 0.5. However, if the adhesive behaves like a membrane φ may vary depending on the assumed bubble shape (Cotterell and Chen, 1997). A value of 0.5 is generally accepted for small deformations of plate-like adhesives (Fernando and Kinloch, 1990). A perspective of the values for φ from various authors is provided in Table 18.

As previously mentioned, the blister test shows either plate or membrane behavior depending on the orifice size, film thickness, and adhesion. It was shown that for adhesion 100J/m^2, if the ratio of the orifice radius to the adhesive thickness is below 10, the blister exhibits a plate-like behavior, and the deviation from plate theory occurs when the ratio is over 10 (Bennett et al., 1974).

Table 18. Force Factors for Equation 8 as Suggested by Various Authors

Authors	Plate behavior	Membrane behavior
William (1997)	0.5	0.6456
Cotterell and Chen (1997)	0.5	$0.645.[1-\exp(-1.35.d_c^{0.36})]$
Allen (1988)	0.5	0.625
Gent and Lewandowski (1987)	N/A	0.6495
Shirani and Liechti (1998)	N/A	0.619
Fernando and Kinloch (1990)	0.5	N/A

Another approach to confirm the blister behaves as a plate is through examining the relation between pressure and blister height before the peak pressure. The data before the peak is related to the adhesive behavior before any debonding begins. This part of the data can be used to study the properties of the adhesive layer independently of the data after the peak, which is related to the interface (Dannenberg, 1961). For data before the peak, it was shown that if pressure is a cubic function of the blister height, the blister's behavior can be analyzed as a membrane (Allen, 1988). However, if there is a linear relationship between pressure and blister height, which is the case in this study, the blister exhibits plate behavior (Fernando and Kinloch, 1990). After the behavior of the blister is defined, the coefficient of proportionality φ can then be found (Table 18).

As can be seen in Figure 23, data before the peak pressure fits well to a linear function (R^2=95%). This implies that in this range of deformation, plate behavior is dominant (Allen, 1988). The deviation of the data from the straight line is due to both softening and viscoelastic behavior of the sealant near the peak pressure, this feature is even clearer at high temperature. In other words, due to stress relaxation which occurs during bulging (data before peak pressure), the slope of the pressure-blister height curve, which is related to the sealant's modulus, also decreases. Considering that the sealant shows plate behavior, the value φ = 0.5 was selected and plugged into Equation 8 to calculate the IFE. The IFE, in this method, appeared to be insensitive to material behavior and extent of deformation (William, 1997), which adds considerable practical advantages in simplifying the experiment.

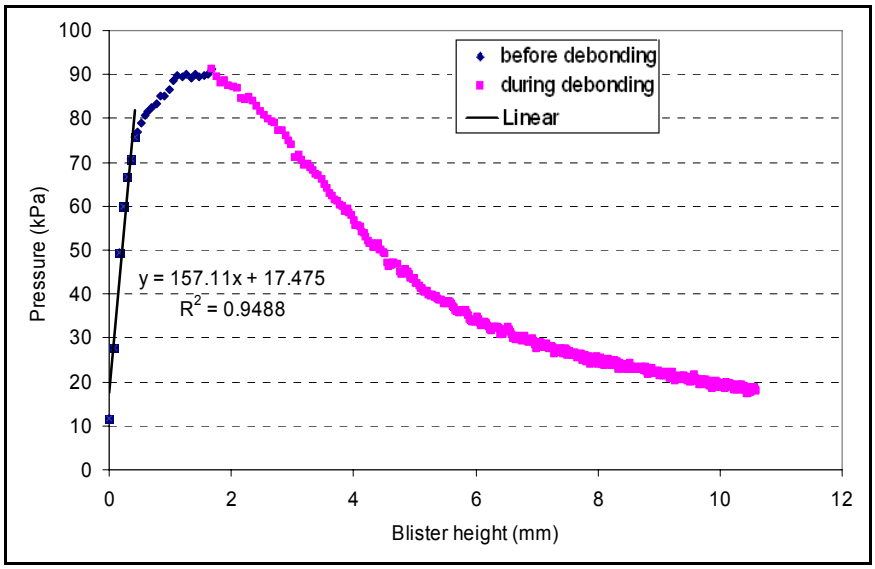

Figure 23. Pressure versus blister height, before and during delamination, for sealant bonded to aluminum

Equation 8 neglects a small membrane (tensile) force developed in the sealant. To account for the membrane force in the adhesive layer, one would need the elastic modulus of the adhesive layer. One way to obtain the adhesive's elastic modulus is to use a supplemental test such as a uniaxial test (Chu and Durning, 1992). However, for rate dependent materials, that may not be the best approach. As depicted in Figure 24, the modulus changes with the loading rate. In addition, the loading mode in the uniaxial test is not the same as that in the blister test.

Determining sealant modulus from the blister test is another aspect which makes this test attractive (Beams, 1959). The correspondence principle can be used to calculate the modulus; the boundary condition is constant until the crack initiates just before the peak pressure (Equation 9). The modulus calculated at the peak pressure can be used to calculate the IFE using Equation 10 (Allen, 1988).

$$E(t) = p[2.77(\frac{h}{a})^4(\frac{d}{h})^3 + \frac{5.3}{(1-\upsilon^2)}(\frac{h}{a})^4(\frac{d}{h})]^{-1} \quad \textbf{(9)}$$

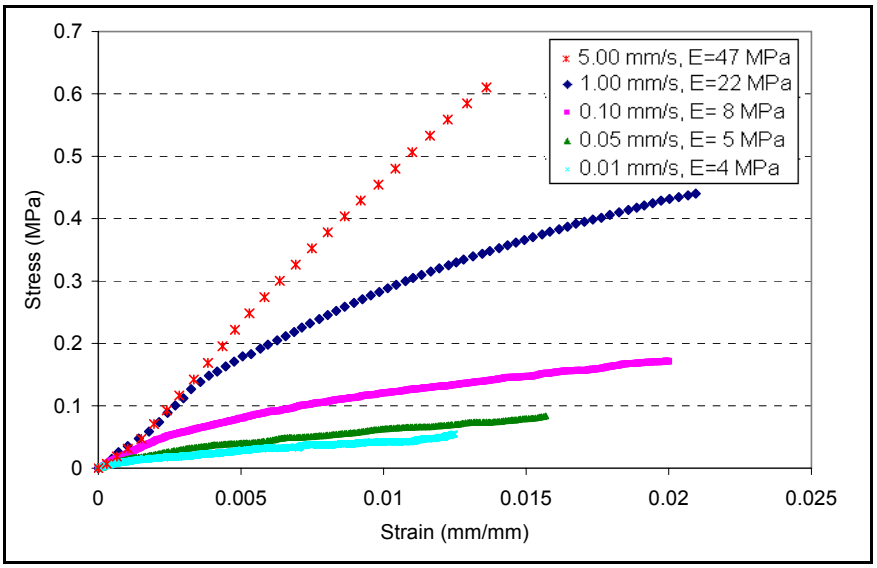

Figure 24. Stress versus strain from uniaxial test at various loading rates

$$IFE = 0.012E(t_c)h\left(\frac{d_c}{a}\right)^4 + \frac{2.67E(t_c)h^3}{(1-\upsilon^2)}\frac{d_c^2}{a^4} \quad \textbf{(10)}$$

where,
IFE is interfacial fracture energy;
P is pressure of the liquid inside the blister;
D is height of the blister;
p_c is critical pressure of the liquid inside the blister;
d_c is critical height of the blister;
a is orifice diameter;
$E(t_c)$ is relaxation modulus of the sealant at peak point;
v is Poisson's ratio;
$t=t_c$is critical time (corresponding to peak pressure); and
h is thickness of the adhesive layer.

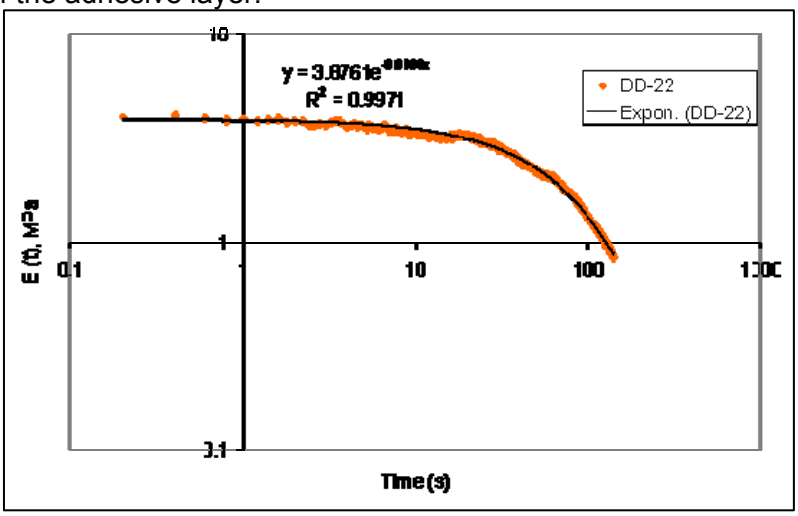

Figure 25. Modulus versus time during bulging (before debonding starts)

Using Equations 8 and 10, IFE was found to be 80.31 and 74.4 J/m^2, respectively. An 8 percent overestimation results when the membrane effect is ignored. Considering that test variation is within 10 percent, such error may be acceptable. Hence, Equation 8 is considered acceptable for the aforementioned specimen geometry.

It should be noted that although the blister test is conducted at a constant fluid injection rate, the debonding rate may not be constant because of the specimen's geometry and the axisymmetric debonding process. After completion of the crack front, IFE has very little variation and becomes independent of the delamination length and initial crack length (Bennett et al., 1974).

During the debonding phase, the crack radius increases, while the thickness of the sealant is constant. Therefore, the aspect ratio $\frac{a}{h}$ increases. As would be expected, the IFE is nearly the same during the debonding period because it is independent of geometry.

The above equation, which is based on pure bending, is satisfactory for relatively thin adhesive layers; however, in cases where the adhesive needs to be cast in a relatively large thickness (very soft sealants), the shear forces along with those of bending need to be considered. While shear forces in thin films are negligible, shear forces in thick films can be quite significant.

It has been shown if the orifice radius is over 10 times the adhesive thickness, the analysis can be satisfactorily conducted using classical plate theory (CPT), which neglects the shear effect and is more appropriate for relatively thin plates (Reddy, 1998). However, in this study, a relatively thick layer of sealant was placed on the aluminum plate, so the shear effect may not be neglected.

Using the relationship between the bending solution of CPT and Mindlin first order shear deformable theory (FSDT), the above equation can be expanded to account for the shear effect, built-in boundary condition used for the adhesive (Wang et al., 2000). Using the relation between CPT and FSDT, transversal displacement of a circular plate under axis-symmetric uniform pressure is presented in Equation 11 (Wang et al., 2000), in which the first and second terms are respectively due to bending and shear forces.

$$d(r) = \frac{3pa^4(1-v^2)}{16Eh^3}\left(1-\frac{r^2}{a^2}\right)^2 + \frac{pa^2}{4k_sGh}\left(1-\frac{r^2}{a^2}\right) \qquad (11)$$

where,
p is pressure;
r is distance from the center of the circular film;
a is radius of the orifice;
h is sealant thickness;
d(r) is displacement at distance r from the center of the circular film;
E is sealant modulus;
v is Poisson ratio;
k_s is shear correction factor (5/6 for a circular plate);
G is shear modulus, $G = \frac{E}{2(1+v)}$

For further investigation, a numerical study was conducted to examine the shear effect in both deformation and stress analysis of the blister. Axisymmetric numerical analysis was conducted using finite element (FE) code written in MATLAB. Two degrees of freedom per node and Hermitian shape functions were used to calculate the stiffness matrix and load

vector (Reddy, 1998). Figure 26 shows the normalized blister deflection, $\bar{d}$, versus the value of a/h (radius of the orifice divided by thickness of the adhesive). Neglecting the shear effect in CPT leads to underestimating the transversal deformation. This error increases significantly as the value of a/h decreases. As can be seen, for a small value of a/h, the error is substantial. In this study, the radius of the orifice is 12.5mm, and the thickness of the adhesive is 4.7mm, so the value of a/h is 2.66. In addition, Figure 26 shows a significant difference in normalized center deflection between FSDT and CPT. Figure 27 compares the deformation versus radial distance for CPT and FSDT for both analytical and numerical results. To normalize the center deflection (height of the blister in the center, d_0), Equation 11 was written at r = 0 and multiplied by the normalizing factor (Equation 12).

$$\bar{d} = d_0 \frac{Eh^3}{pa^4} \tag{12}$$

$$\bar{d} = \frac{3(1-\nu^2)}{16} + \frac{3(1+\nu)h^2}{5a^2} \tag{13}$$

where,

$\bar{d}$ is the normalized center transverse deflection, and

d_0 is the height of the blister in the center of the disk.

Determining IFE as a Bonding Index

To calculate the bonding, an energy balance analysis should be conducted. Energy available for crack propagation in a specimen is generated by two sources. The first one is due to deflection of the specimen; the second is due to stress concentration around the orifice. If the specimen is infinitely thick ($h \to \infty$), the first source approaches zero because the plate is too thick to bend or deflect. Hence, in that case, a Griffith type analysis can be used (Griffith, 1921). The concept of Griffith theory is that the bonding surfaces of any solid have a surface energy; when a crack propagates, the decrease in the strain energy is balanced by the increase in the potential energy due to this surface energy (Griffith, 1921).

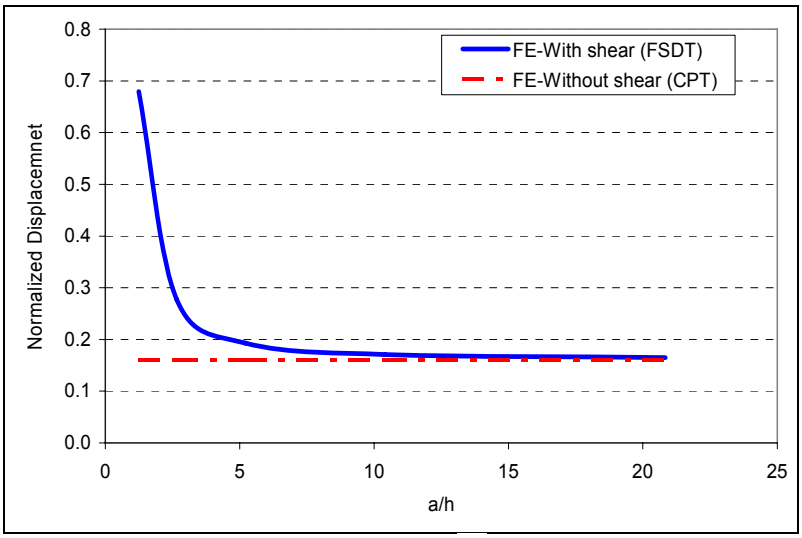

Figure 26. Normalized displacement in the center, $\bar{d}$ versus radius divided by thickness (a/h)

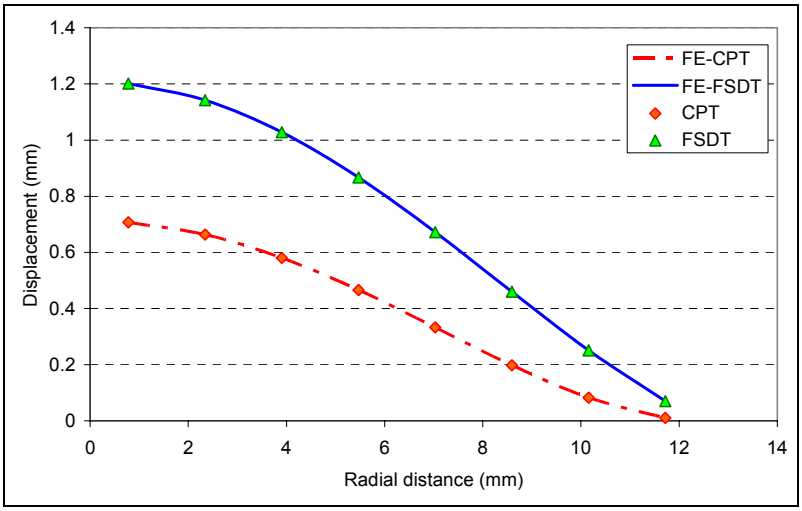

Figure 27. Center deflection versus radial distance for both analytical and numerical solutions

Collecting both sources, one can derive the following equation for IFE (Sneddon, 1946 and Griffith, 1921).

$$IFE = \frac{p_c^{\,2} a}{E(t)}\left[\frac{3a^3(1-\nu^2)}{32h^3} + \frac{3a(1+\nu)}{10h} + \frac{2(1-\nu^2)}{\pi}\right] \quad \textbf{(14)}$$

$$f(h,a) = \left[\frac{3a^3(1-\nu^2)}{32h^3} + \frac{3a(1+\nu)}{10h} + \frac{2(1-\nu^2)}{\pi}\right]^{-1} \quad \textbf{(15)}$$

If h<<a, the last two terms can be neglected, and the equation used by Williams (1969) for pure bending can be applied. If h>>a, the first two terms can be neglected, and the equation by Sneddon can be applied (Sneddon 1946), Figure 28. However, the adhesive

layer in this study is neither of the two extremes. Therefore, Equation 14 is best suited for calculating IFE for this specific test geometry.

Knowing the relation between pressure and blister height, the modulus, E (t) can be calculated during bulging (before reaching the peak pressure) as explained earlier. However, for more precise measurement of the modulus, one may confine the adhesive film to ensure no debonding occurs during the bulging period. Since sealants are viscoelastic materials, their time dependent modulus can be calculated as a function of time and used in Equation 14. This allows the calculation of IFE at the start of debonding. Using Equations 8 and 14, IFE = 80.31 and IFE = 60.12 J/m^2, respectively.

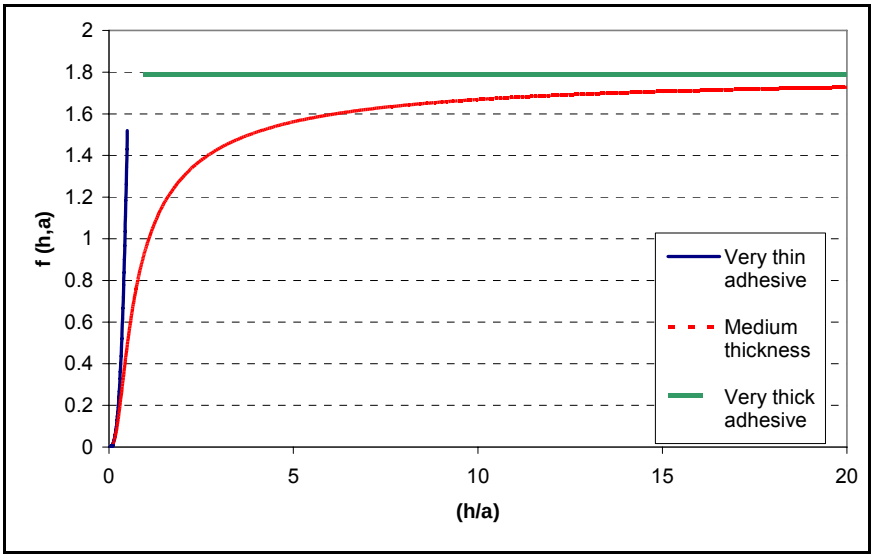

Figure 28. The function f(h, a) for various sealant thicknesses

Since IFE is a geometry independent value, it remains nearly the same as the debonding continues. Therefore, the average of IFE values during debonding (tail of the curve P-d in Figure 23) can be a better representative of the interface properties than the single value calculated at the peak pressure (Figure 29). However, it should be noted that the modulus can only be defined up to the peak pressure because after that, the boundary condition starts changing as debonding continues. To calculate the IFE average, Equation 6 was applied along the tail of the curve P-d in Figure 23. Another option is to fit a hyperbolic equation (p=C/d) to the tail of the P-d curve; defining the constant C, using the Equation 6, the IFE value can be calculated as the constant C divided by two, which would be 100.14 J/m^2 (Figure 30). IFE_{avg} calculated from arithmetic average and the curve fitting approach found to be nearly the same (i.e. 101.91 and 100.14 J/m^2, respectively). However, for some sealants, crack fronts deviate from symmetric growth after some propagation, and the tail of the curve is not smooth enough. Therefore, calculating the IFE_{avg} from 40sec of the debonding period instead of the whole tail is more appropriate. As a feasibility study and to fine-tune the test procedure, IFE at peak pressure was used. However, for the experiments conducted after finalizing the test procedure, both parameters are reported: IFE_{avg} refers to the average of the IFE values during 40sec of debonding and IFE_{peak} refers to IFE calculated at the peak pressure.

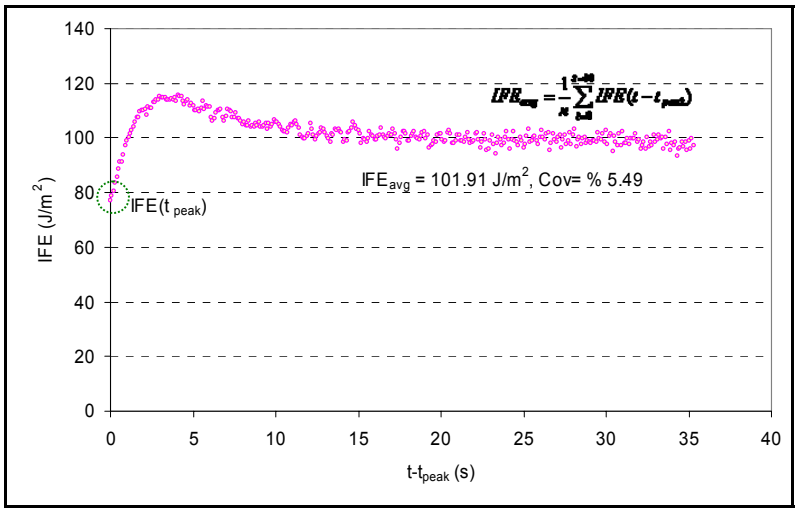

Figure 29. IFE_{peak} and IFE_{avg} during the debonding

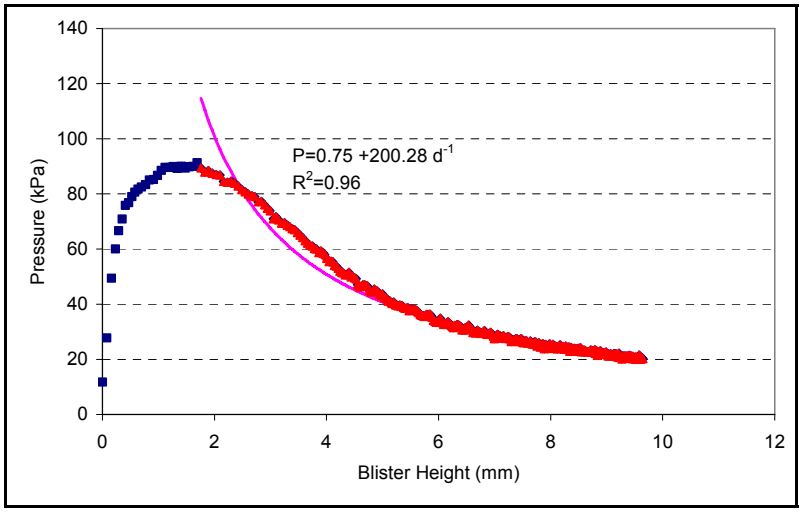

Figure 30. IFE_{avg} using a hyperbolic curve fit to the tail of the curve

Feasibility Study

To determine if the test can properly distinguish between sealants, five sealants were tested using aluminum substrate at -22°C. Figure 31 shows the values of IFE calculated for six pairs of sealant-aluminum. The sealants were purported to meet ASTM D6690 standards. The next step was to check if the test can differentiate between various substrates. The blister test was conducted for combinations of three sealants with aluminum, limestone, quartzite, and granite, and the IFE was measured for each pair (Figure 32). The results show that the new blister test not only can differentiate between different adhesive/substrate systems, it can also capture the variation due to test temperature.

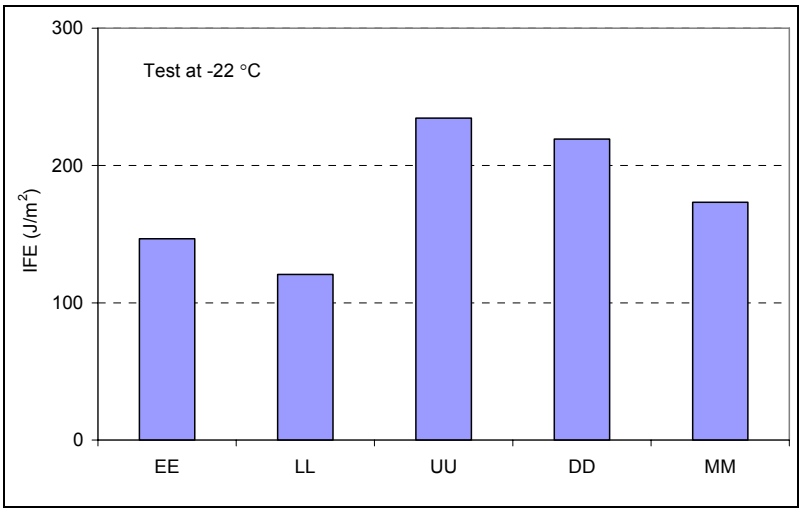

Figure 31. IFE for five sealant-aluminum pairs at -22°C


Figure 32-a. Specimens and stone annular plates used as substrates (from right, Limestone, Granite, Quartzite)

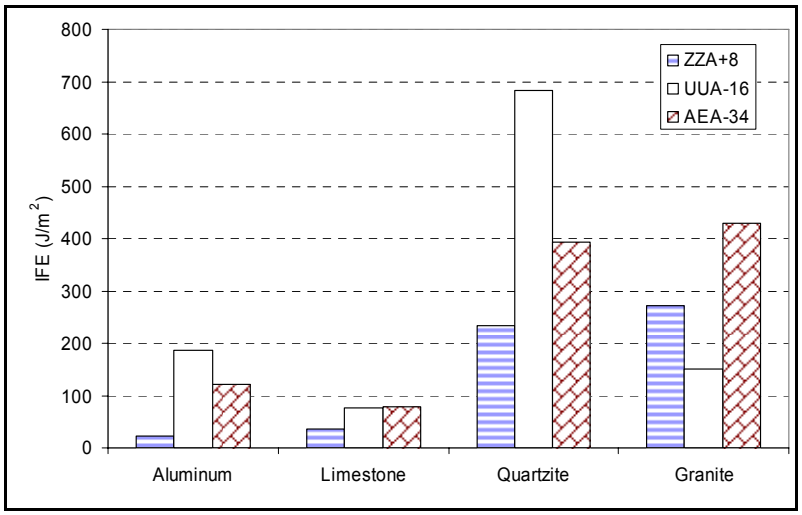

Figure 32-b. IFE for combinations of three sealants and four substrates

Substrate Selection

The current specifications for hot-poured bituminous sealants, ASTM D6690, require the use of concrete block as the substrate. Consequently, the specifications do not account for the variation in aggregate composition in the field. Aggregate composition plays a key role in sealant-aggregate adhesion (Masson and Lacasse, 2002). However, due to much variation between aggregates, even from the same quarry, using local aggregate as the substrate is impractical and would lead to poor reproducibility. In an effort to find an appropriate substitute for aggregate, four substrates were examined: stainless steel, glass, polycarbonate, and aluminum. These materials were ranked based on the similarities in their adhesion mechanism with that of aggregate: wettability, roughness, coefficient of thermal expansion, diffusion, and chemical bonding. In terms of wettability, the parameter of surface energy was found to be an appropriate indication. The surface energy of candidate materials is given in Table 19. Because the surface of aluminum is always oxidized, the surface energy of oxidized aluminum (rather than aluminum) is used in Table 19. Figure 33 illustrates the importance of surface energies as shown by the contact angle of one sealant with various aggregates. High-energy surfaces (e.g., granite) lead to low contact angles and good adhesion, whereas low energy surfaces (e.g., basalt) lead to high angles and lower adhesion (Masson and Lacasse, 2000). Standard materials were selected to have low surface energy to simulate worst case aggregates in terms of surface energy.

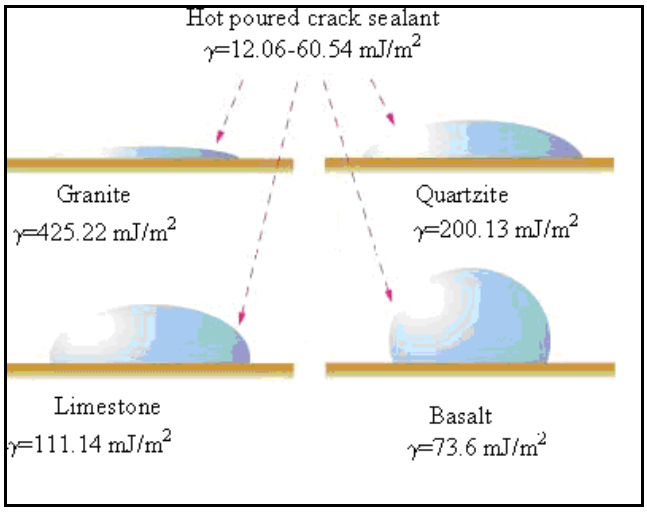

Figure 33. Schematic of surface energy values for adhesive (hot-poured crack sealant) and substrates (aggregates)

During cooling of the hot-poured crack sealant on the substrate, stresses develop at the interface due to the difference in the respective coefficients of thermal expansion. Hence, to be selected as replacement for aggregates, standard materials were selected to have thermal expansion comparable to those of aggregates. Among the pool of materials, glass was too brittle at very low temperature; it broke before testing when used as a substrate at -40°C. The surface of plates made from polycarbonate wore out after a couple of tests. Therefore, stainless steel and aluminum were selected and compared in terms of surface roughness. Atomic force microscopy was used to take images of these two materials along with several aggregates (Figure 34). Using this approach, the limestone found to have the roughest surface followed by sandstone, quartzite, granite, steel, and aluminum. Because aluminum had the smoothest surface among all, it was selected as the standard substrate to represent worst scenario in the field.

Due to its rapid oxidation, aluminum develops a surface layer of aluminum oxide groups, Al-OH. These groups are similar in chemistry to the silicon oxide groups, Si-OH. Both groups are found in aluminum silicate minerals (aggregates). Hence, an aluminum substrate has chemical surface similar to granites, quartzite, and sandstone; aggregates that have OH groups on their surface. In addition, since most bituminous sealants are acidic, compatibility between an aluminum oxide surface and sealant is likely. Given the aforementioned characteristics of aluminum oxide, aluminum was selected as a potential standard substrate.

Hot-poured bituminous sealant diffusion into aggregate (adsorption) is another factor that may need to be considered. Aggregate adsorption (of binders) can vary significantly (Curtis, 1992). However, due to the relatively high viscosity of bituminous sealants at pouring temperature, the diffusion is expected to be relatively low. However, it still needs to be explored. The pore size of sandstone and quartzite was measured using gas absorption method, and compared with those of aluminum. Adsorption of crack sealants into aggregates is expected to be very low, for two reasons: To have a good adsorption, a liquid should make a low contact angle with the substrate; and the diffusion distance must be significant. As reported in Table 19, the contact angles of sealants with corresponding aggregates are quite large; correspondingly, their diffusion distance calculated using Einstein's diffusion equations (Equations 16 and 17), is very small (Einstein, 1956). The pore size of sandstone and quartzite was found to be 7.7 and 6.2nm using the gas adsorption method. As can be seen in Figure 35, the diffusion length for three substrates is quite comparable.

$$D = \frac{KT}{6\pi\eta r} \tag{16}$$

where,
D is the diffusion;
K is 1.380 x 10E-23J/K (Joule/Kelvin);
T is temperature (K, Kelvin); and
r is the relative size of sealant molecules to average pore diameter.

$$L = \sqrt{2Dt} \tag{17}$$

where,
L is the diffusion distance (m); and
t is the diffusion time (s).

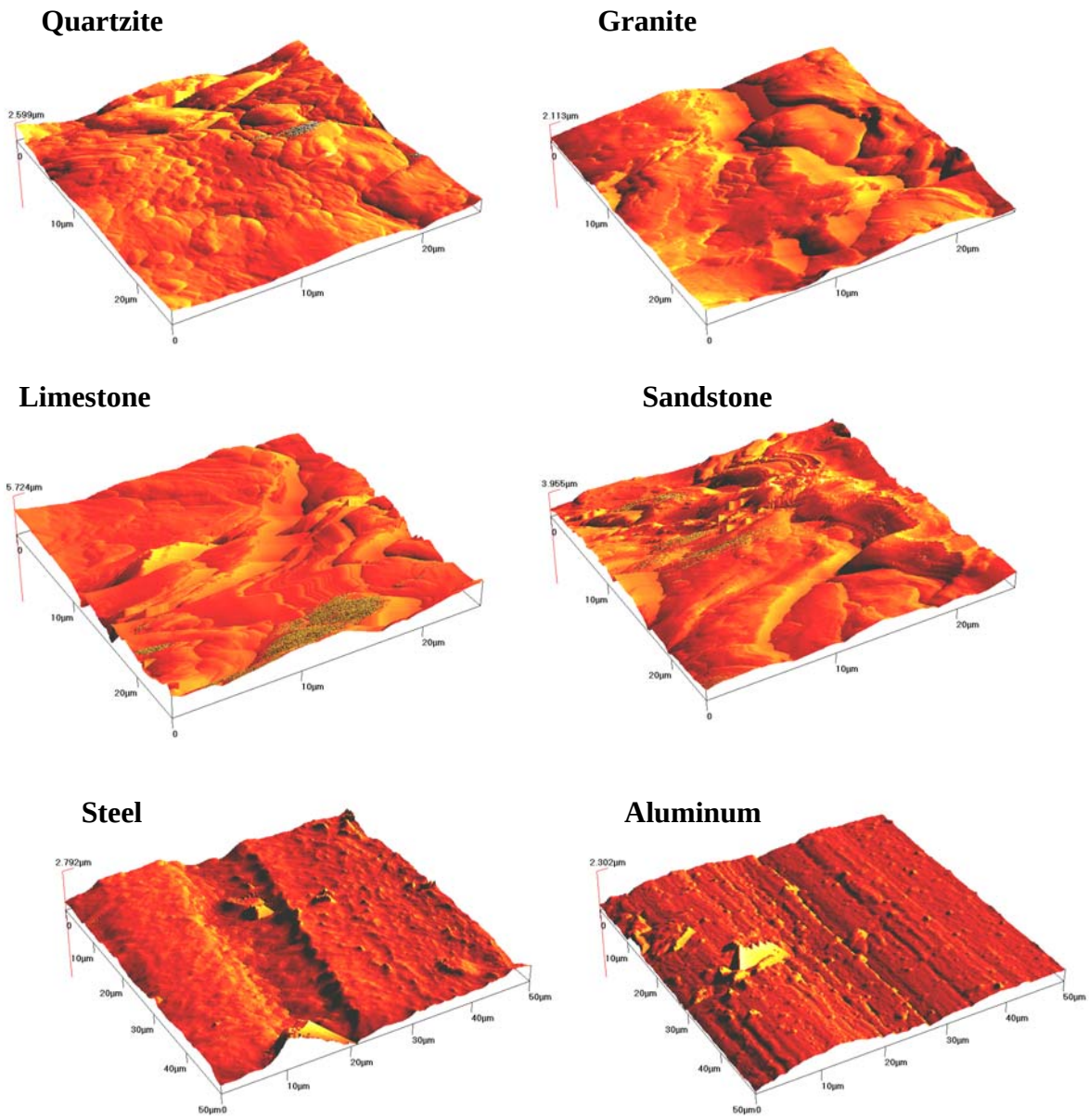

Figure 34. Atomic Force Microscopy to compare surface roughness of substrates

The viscosity of sealant varies approximately between 1Pa.s and 3.5Pa.s at pouring temperature; sometimes it can reach 7Pa.s. However, sealant temperature at the time of contact with a crack's sides should be considered. In reality, a sealant's temperature can drop over 50ºC after the sealant is pumped out of the nozzle and before the sealant contacts the crack's sides (Collins et al., 2006). As can be seen in Figure 35, sealants with very low viscosity can diffuse farther into aggregates with higher porosity (smaller bead size). Sealant viscosity increases with cooling as time passes, so this calculation, which is based on initial contact temperature, will overestimate the diffusion distance. In addition, sealant cools quickly; it takes about 7min for the sealant to cool to gel temperature, at which point the sealant has lost a substantial part of its fluidity and cannot diffuse farther into the aggregate (Collins et al., 2006). Therefore, the diffusion length is expected to be even less in reality. Knowing the sealant viscosity, pore size, temperature, and time, the diffusion length can be

calculated. Figure 35 shows that the diffusion lengths for three substrates are quite comparable. This conclusion supports the use of oxidized aluminum, which has a very low pore size (5.8nm), as an aggregate replacement. Therefore, aluminum was conservatively selected as the substrate and used to develop the three test methods.

Table 19. Surface Energy and Coefficient of Thermal Contraction for Candidate Materials (Cheng et al., 2001)

Material	Coefficient of Thermal Contraction, cm/cm/°C x 10^{-6}	Surface Energy, mJ/m^2
Aluminum oxide	23	70
Soda Lime Glass	8	72
Polycarbonate	22	46
Stainless Steel	9.9–17.3	57
Granite	7–9	425
Limestone	6	111
Quartzite	11–13	200
Sandstone	11–12	105
Basalt	6–8	74

During the cooling of hot-poured crack sealant on substrate, stresses develop at the interface due to the difference in the respective coefficients of thermal expansion. Hence, to be selected as a standard substrate, a material must have coefficients of thermal expansion close to that of aggregate. Considering all mentioned above, aluminum was conservatively selected as the substrate.

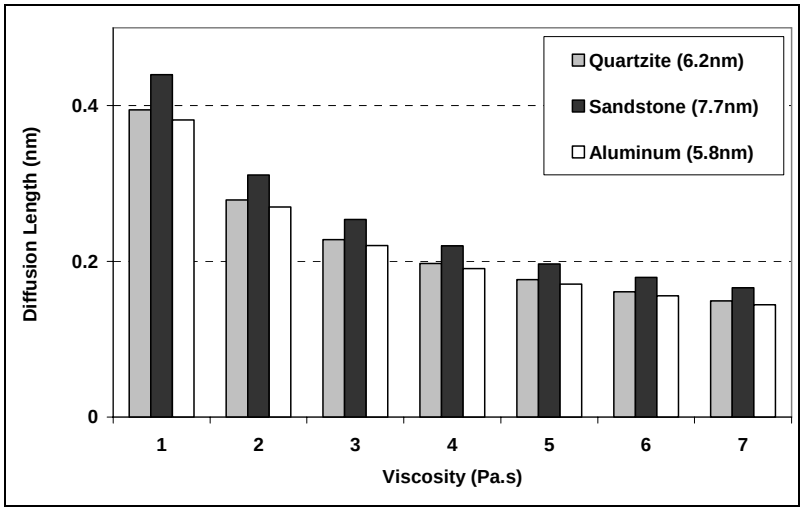

Figure 35. Diffusion distance for sealant vs. viscosity for various pore sizes

Optimum Cooling Time

Cooling time should be considered to allow the specimen to reach thermal equilibrium; this can be calculated knowing the thermal conductivity of the sealant and the aluminum plate. In addition, due to the difference in coefficient of thermal expansion between sealant and aluminum, residual stress may develop at the interface during specimen preparation. Since sealant is a viscoelastic material, it can release this stress with time. Hence, cooling time should be long enough to allow eliminate residual stresses prior to testing. In addition, sufficient cooling time is needed to prevent sealant hardening.

Because of the hardening effect of cold temperatures on hot-poured crack sealant, the shortest time to thermal equilibrium needs to be sought. The required time for the substrate (aluminum plate) and adhesive (sealant) to reach thermal equilibrium is calculated using thermodynamic principles. Having properties of the bath liquid, aluminum, and bitumen, the Biot number is calculated using Equation 18:

$$Bi = \frac{hL}{K} \tag{18}$$

where,
Bi is Biot Number;
h is heat transfer coefficient (W/m^2.ºK);
K is thermal conductivity (J/m.s.ºK); and
L is mid-plane distance (m).

The Biot number relates the heat transfer resistance inside and at the surface of the object. Then the critical time is calculated using Equations 19 or 20, depending on the Biot number calculated in the first step:

If $Bi > 1 \rightarrow$ $$t = 10\frac{L^2 \rho C_P}{K} \tag{19}$$

If $Bi < 1 \rightarrow$ $$t = 10\frac{L \rho C_P}{h} \tag{20}$$

where,
ρ is density (kg/m^3);
C_p is specific heat (J/kg.ºK); and
t is equilibrium time (s).

It was found that the specimen reaches thermal equilibrium within 13min, the maximum of the respective times for aluminum and sealant (Table 20). However, potential residual stress development should be considered. The residual (mismatch) strain due to rapid temperature changes, which causes the stress development, can be calculated using Equation 21 (Shirani and Liechti, 1998):

$$\varepsilon = (\alpha_s - \alpha_f).(T_2 - T_1) \tag{21}$$

where,

 is strain developed during cooling;
α_s is coefficient of thermal expansion of the substrate;
α_f is coefficient of thermal expansion of the adhesive (sealant);
T_1 is blister test temperature; and
T_2 is sealant temperature when it contacts the substrate (not pouring temperature).

Table 20. Minimum Required Cooling Time

Substrate material	Heat transfer of alcohol ($W/m^2.^oK$)	Mid-plane distance (m)	Thermal conductivity (J/m.s.ºK)	Specific heat (J/kg.ºK)	Density, □ (kg/m^3)	Bi* (Biot Number)	Cooling time (min)
Aluminum	300	0.006	237.00	900	2770	0.008	9
Bitumen	300	0.005	0.17	600	1000	8.294	13

* Biot number is a dimensionless number that relates the heat transfer resistance inside and at the surface of the object.

Temperature measurements indicated that T_2 was 50°C below the sealant pouring temperature. This finding is in agreement with other data presented elsewhere (Collins et al., 2006). For instance, when pouring temperature was 185ºC, T_2 was 135ºC. At a test temperature T_1 of -34ºC, a typical sealant has α_f of 235 x 10-6m/m/ºC, measured by TMA; an aluminum substrate has α_s of 23 x 10-6m/m/ºC; and the calculated residual strain is 0.036. Allen and Senturia (1988) showed that neglecting the residual strain for elastic material led to overestimating IFE.

In the case of hot-poured bituminous crack sealant, which is a viscoelastic material, it appeared that if the specimen is placed in a cooling bath for a sufficient period of time before running the test, the residual stress would diminish. To estimate the time required to release the residual stress, a creep compliance master curve, D (t_{red}), was generated using creep compliance data at various temperatures. The test was conducted using a Crack Sealant Bending Beam Rheometer (CSBBR), in accordance with the approach presented by Al-Qadi et al. (2006 b). The temperature superposition principle was implemented to construct a master curve of creep compliance D (t_{red}). Then a ten-parameter Voight-Kelvin model (Figure 36) was fitted to the value of D (t_{red}). The parameters of the model are in Equation 22 (Tschoegl, 1989).

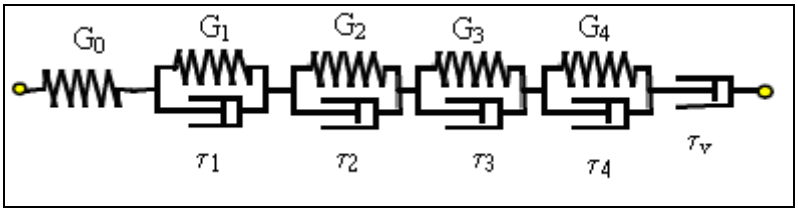

Figure 36. Ten-parameter Voight-Kelvin model

$$D(t_{red}) = G_0 + \sum_{n=1}^{4} G_n[1 - \exp(\frac{-t_{red}}{\tau_n})] + \frac{1}{\tau_v} \quad (22)$$

These parameters were used to calculate *D(s)* using Equation 23, where *s* = 1/*t*.

$$D(s) = \frac{G_0}{s} + \sum_{n=1}^{4} \frac{G_n}{s(1+\tau_n s)} + \frac{1}{\tau_v s^2} \tag{23}$$

Then, values of *E(s)* were determined from Equation 24.

$$E(s) = \frac{1}{s^2 D(s)} \tag{24}$$

Having values of *E(s)* and using regression, a ten-parameter equivalent Voight-Kelvin model, Equation 25 (Figure 37), was fitted to the *E(s)* data, and the model's parameters were determined.

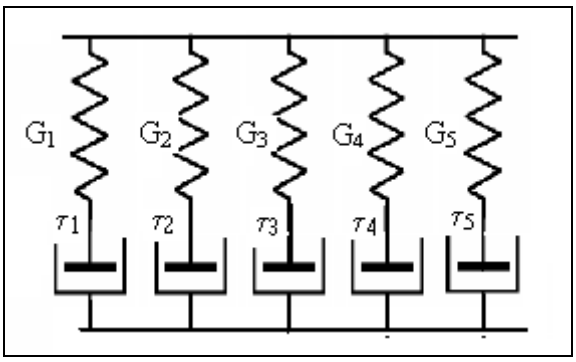

Figure 37. Ten-Parameter Equivalent Voight-Kelvin Model

$$E(s) = \sum_{n=1}^{5} \frac{E_n \tau_n}{1+\tau_n s} \tag{25}$$

Having these parameters, $\sigma(t)$ was calculated for the aforementioned step strain excitation, that developed due to unequal thermal contraction of the aluminum plate and sealant layer (Equation 26).

$$\sigma(t) = \varepsilon_0 \sum_{n=1}^{5} E_n \exp[\frac{-t}{\tau_n}] \tag{26}$$

The assumption of step strain excitation is overestimating the developed stress. In reality, the sealant experiences less stress, because the strain develops gradually as the sealant temperature drops. Figure 38 shows that the residual stress drops rapidly for sealant NN in the first 20min. Additionally, the specimen temperature decreases gradually to bath temperature, so the mismatch strain develops gradually, while stress continues to release at a faster rate than mismatch-strain development. To ensure the cooling time is sufficient if aggregates are used instead of aluminum, the thermal equilibrium times of limestone, granite, and sandstone were found to be 19min, 11.8min, and 20min, respectively. Therefore, to limit the physical hardening, to allow the specimen to reach thermal equilibrium, and to release most of the residual stress, a 20min cooling period was selected as the optimum cooling time.

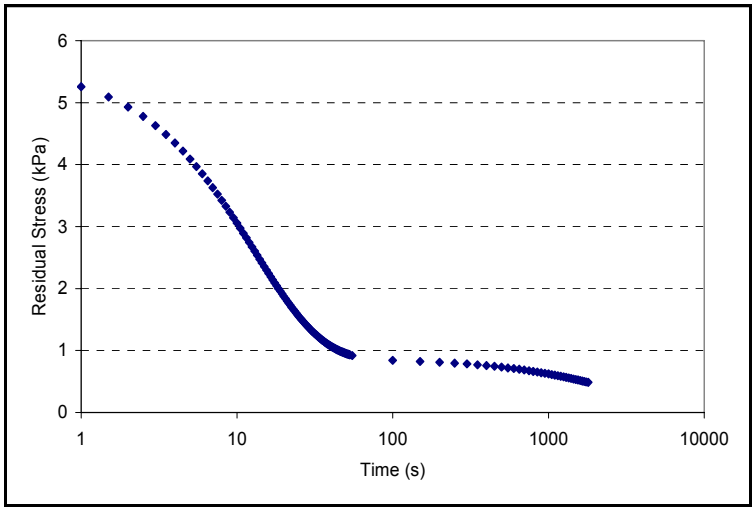

Figure 38. Residual stress versus time for sealant NN at -34ºC

Orifice Size

In 1987, Allen and coworkers showed that a larger orifice results in a larger dome, and the initial debonding would occur at lower pressure. Figure 39 shows the test results for two orifice sizes for the same sealant thickness. While some of the sealants tested using an orifice diameter of 50mm resulted in a relatively large dome with vague peak pressure, using an orifice diameter of 25mm resulted in an easily identified peak pressure. Therefore, the diameter of the orifice was selected to be 25mm.

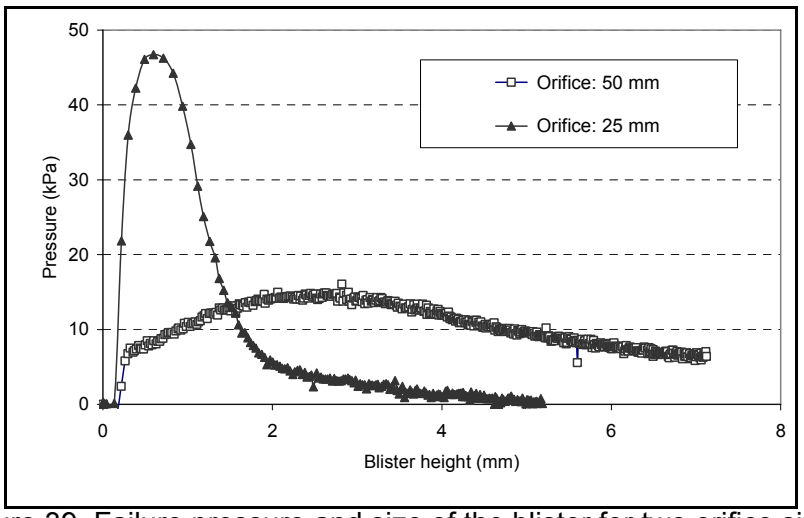

Figure 39. Failure pressure and size of the blister for two orifice sizes

Adhesive Thickness

A sealant thickness needs to be selected so that the bonding can be measured for a various sealant types having different range of characteristics. Tests conducted on a very thin sealant film resulted in either excessive deformation for a very soft sealant (sealant A in Figure 40), or cohesive failure for a relatively brittle sealant prior to debonding. In the case of a very thick sealant film, the deformation of the film was too small (sealant B in Figure 40),

and the resulting blister height could not be measured accurately. A film thickness of 4.7mm appeared to be appropriate for most of the sealants tested at various temperatures.

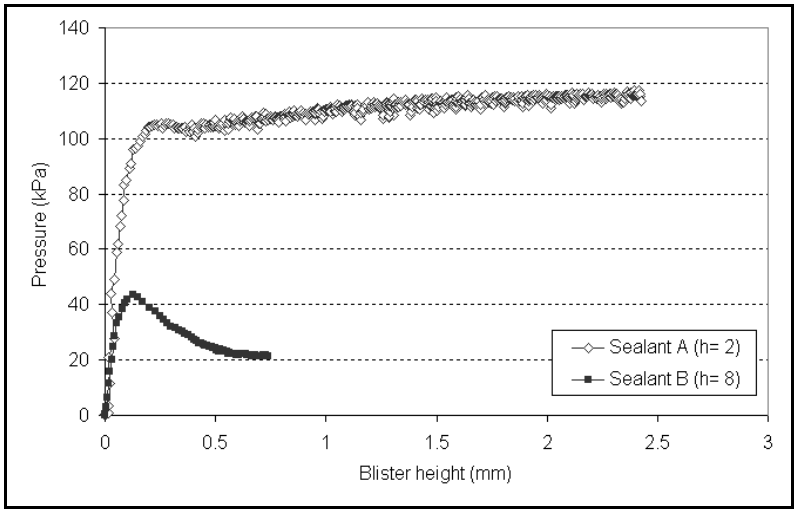

Figure 40. Debonding behaviour of relatively thin and thick sealants

Reversible Deformation

To study sealant behavior before and after debonding, the sealant specimen was unloaded at various times during the test progression. First, the specimen was unloaded before reaching the critical pressure at which debonding initiates. As can be seen in Figure 41, most of the deformation recovers quickly, and the blister almost disappears. The second specimen was unloaded right after critical pressure, so debonding had already initiated. In this case, although the blister size decreases after unloading, it does not recover completely.

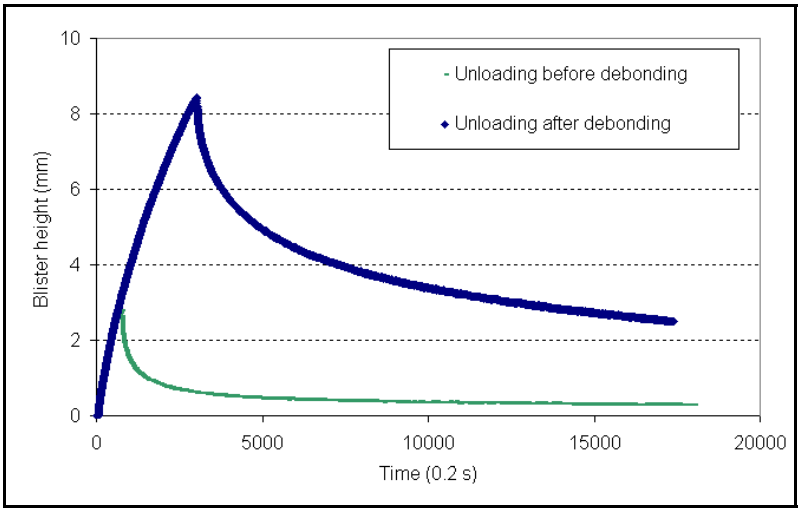

Figure 41. Unloading blister specimen before and after debonding initiates

.

Experimental Program

Upon identifying the experiment parameters, tests were conducted in accordance with the aforementioned testing procedures and presented in Appendix C. Figure 42 shows the IFE values calculated at peak pressure. It clearly shows that IFE parametric can differentiate among sealants at various temperatures. The average coefficient of variation for tested sealants was found to be 8.7 percent (Table 20). The variability in testing results is

mainly attributed to variation in tested sealants; especially sealants containing fillers and/or rubber.

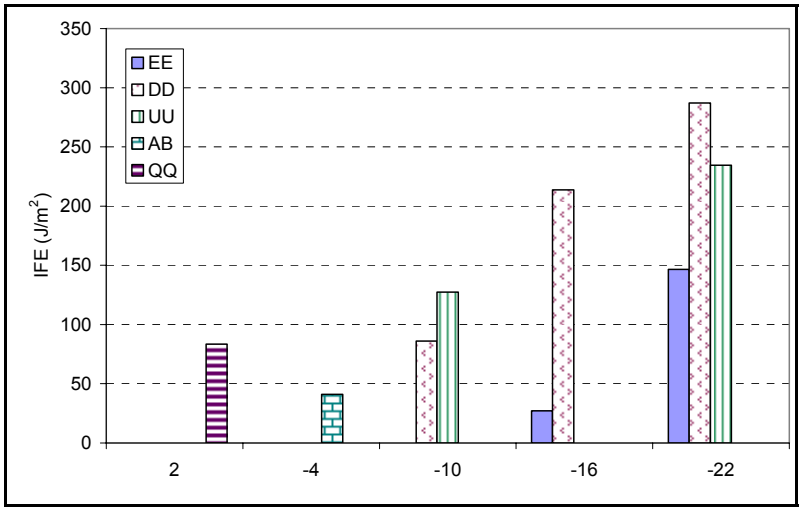

Figure 42-a. The IFE of five sealants at a temperature ranging from 2ºC to -22ºC

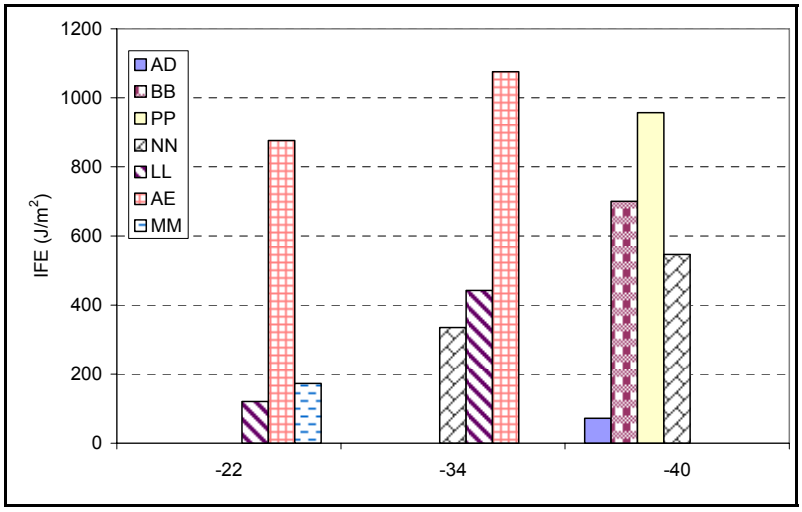

Figure 42-b. The IFE of seven sealants at a temperature ranging from -22ºC to -40ºC

EFFECT OF AGING

Sealant short-term aging occurs mainly inside the kettle. Therefore, sealant has been already aged before entering the crack and contacting crack walls (Masson and Al-Qadi, 2004). Because aging changes sealant's chemistry, sealant's rheological behavior and its interaction with any other material, such as crack wall's HMA, also varies. Some sealants degrade during aging and become softer while others get stiffer.

Table 20. Coefficient of Variation for Sealants Tested at Various Temperatures

Sealant	Temperature °C						
	2	-4	-10	-16	-22	-34	-40
AD							7.43
BB							0.29
PP							1.40
NN						4.99	25.81
LL					4.77	9.65	
AE					5.38	18.95	
MM					10.81		
EE				6.31	1.54		
DD			6.41	3.90	6.13		
UU			14.94		12.84		
AB		6.11					
QQ	18.98						
Average							8.77

Sealant aging is affected by crack sealant composition (polymer, ground rubber, and mineral filler). In order to examine the effect of aging on the IFE value, six aged sealants were tested using aluminum substrate. The resulting IFE values were compared to those of non-aged sealants, Figures 43. The IFE results were in agreement with P_{max} resulted from the ADT test; both tests show similar effect due to aging. For example, both tests indicate lower bonding for aged sealant NN at -34ºC than unaged sealant; however, higher bonding was indicated for aged sealant UU at -16ºC.

Given that sealant is already aged when entering a crack, aged sealant is recommended when conducting a blister test. To evaluate the most commonly used sealants in North America, eight various sealants were tested. These sealants have a wide range of rheological characteristics and are used in regions having low temperature varying from -4ºC to -40ºC. The IFE_{peak} and IFE_{avg} for each sealant-aluminum pair were calculated. Figures 44 and 45 present the IFE_{peak} and IFE_{avg} for aged sealants at a temperature range from +2ºC to -34ºC, respectively.

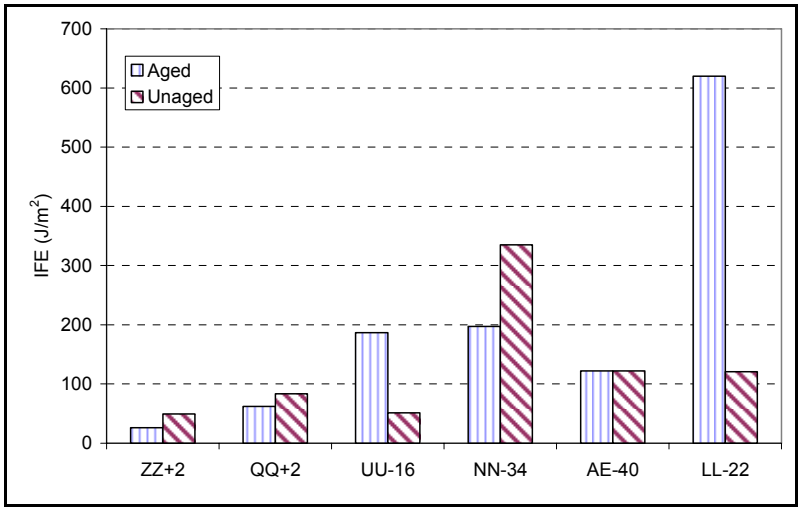

Figure 43. Effect of aging on sealant's IFE value

Statistical analysis using t paired was conducted on sealants tested at the same temperature. The Levene test was conducted to check the homogeneity of the groups (Tables 21-a and 22-a). A standard analysis of variance (ANOVA) was also performed at a significance level of 0.05 (Tables 21-b and 22-b).

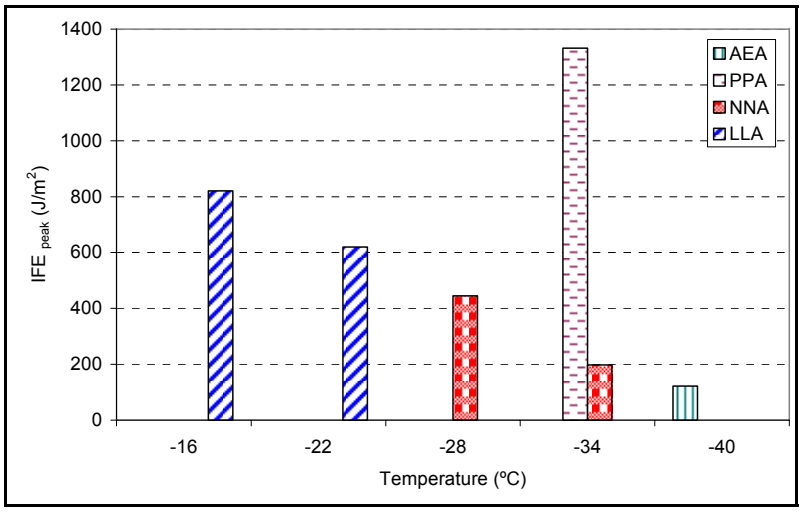

Figure 44-a. Effect of temperature on aged sealant's IFE_{peak} values

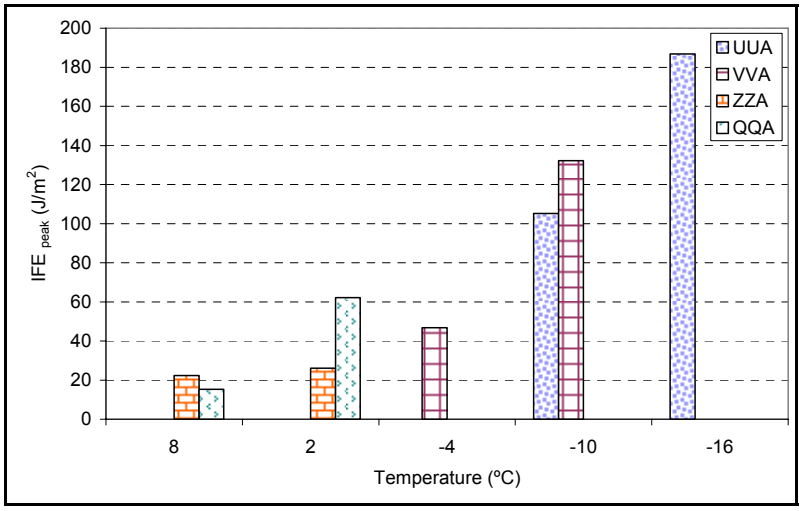

Figure 44-b. Effect of temperature on aged sealant's IFE_{peak} values

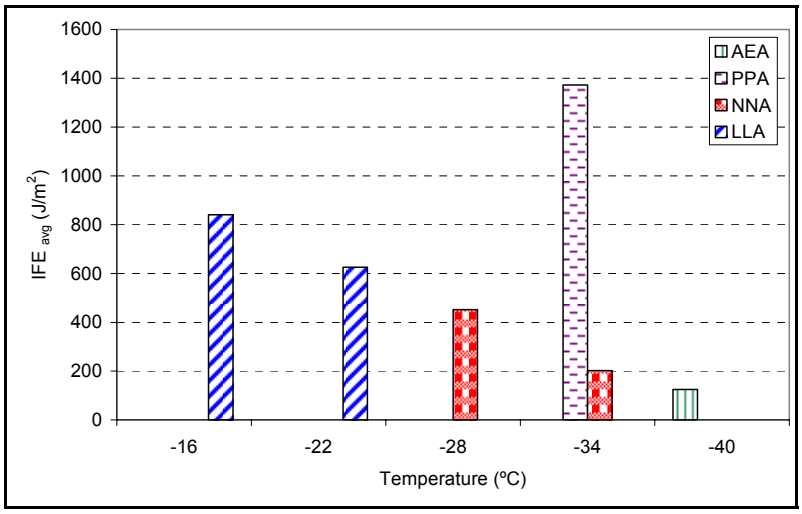

Figure 45-a. Effect of temperature on aged sealant's IFE_{avg} values

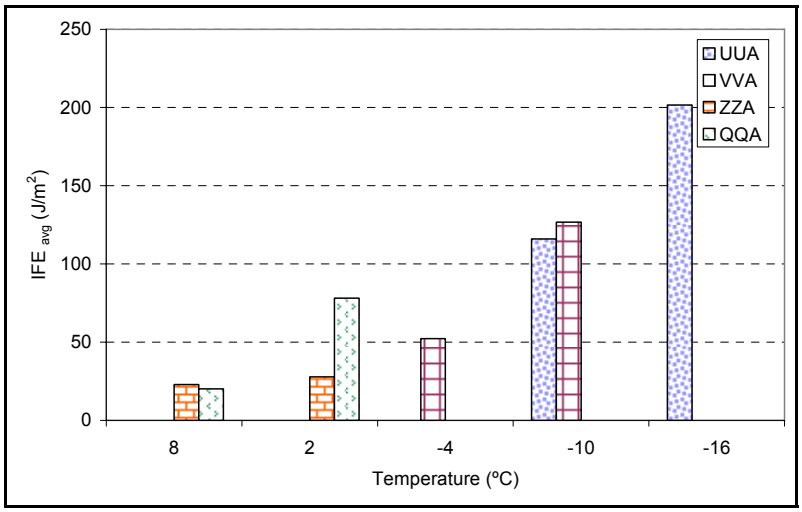

Figure 45-b. Effect of temperature on aged sealant's IFE_{avg} values

The null hypothesis was that the two sealants tested at the same temperature had the same mean value. The observed significance level at each temperature is below 0.05, which leads to rejection of the null hypothesis. Therefore, there is a significant difference between sealants tested at each temperature; hence, both IFE_{peak} and IFE_{avg} can differentiate between sealants appropriately.

Table 21-a. Levene Test Results on IFE_{peak} Values

Temperature (ºC)	Levene Statistic	Sig.
T-34	0.572	0.492
T-10	2.300	0.180
T+8	0.224	0.653
T+2	3.601	0.116

Table 21-b. ANOVA Results of IFE_{peak} of Two Sealants at One Temperature

	Sum of Squares	Mean Square	F	Sig.
T-10	5,108.741	5,108.741	20.398	0.011
T+8	313.907	313.907	6.855	0.040
T+2	4,407.896	4,407.896	32.153	0.001
T-34	1,898,616.045	1,898,616.045	89.269	0.000

Table 22-a. Test Results on IFE_{avg} Values

Temperature (ºC)	Levene Statistic	Sig.
T-34	0.041	0.849
T-10	0.000	0.991
T+8	0.210	0.663
T+2	4.845	0.079

Table 22-b. ANOVA Results of IFE_{avg} of Two Sealants at One Temperature

Temperature (ºC)	Sum of Squares	Mean Square	F	Sig.
T-10	6,077.837	6,077.837	31.468	0.005
T+8	3,793.067	3,793.067	94.370	0.001
T+2	7,270.877	7,270.877	55.492	0.000
T-34	1,992,110.930	1,992,110.930	64.211	0.000

Variation within Laboratories

Statistical analysis was used to check the variation within laboratory. The repeatability of blister test results for the same sealant was acceptable; the average coefficient of variation was 8.7 percent for two replicates and 19.3 percent for three replicates out of four. As with any test, to ensure test result consistency, testing procedures should be closely followed. Because temperature variation affects sealant viscosity, it is recommended to control temperature within ±1°C. In addition, tested sealants should be homogenized in accordance with ASTM D5167 (Standard Practice for Melting of Hot-Applied Joint and Crack Sealant and Filler for Evaluation). Using ASTM C670 standards, the acceptable variation should be established using precision of individual measurements. To define the maximum acceptable range for individual measurements, the standard deviation of measurements should be multiplied by a factor related to the number of replicates; 2.8 for two replicates, 3.3 for three replicates, and 3.6 for four replicates.

To evaluate data variability between operators, two operators tested sealants LL, NN, QQ, UU, VV, and ZZ independently. To check the homogeneity of the variances for each operator, the null hypothesis states that the groups come from populations with the same variance. The Levene test at a significance level of 0.05 was used to examine the significance of the hypothesis. The observed significance level for all sealants are greater than 0.05 (Table 23). Therefore, the null hypothesis would not be rejected, and variances of the groups are equal. The ANOVA was conducted to check whether the results of the two operators were statistically different. The significance level for all sealants was found to be

above 0.05. Therefore, no statistical evidence showed that the IFE value measured by two operators is different at a 5 percent level of significance (Table 24).

Table 23. Levene Test Results of the Six Sealants

Sealant	Levene Statistic	Sig.
LL	0.184	0.686
NN	1.005	0.362
QQ	5.404	0.081
UU	0.018	0.898
VV	2.143	0.203
ZZ	0.884	0.400

Table 24. ANOVA Results of IFE between Two Operators

Sealant	Sum of Squares	Mean Square	F	Sig.
LL	296856.31	362.177	0.006	0.941
NN	119758.75	20081.3	1.007	0.362
QQ	1106.5954	649.309	5.68	0.076
UU	4612.2779	2610.708	6.522	0.051
VV	6353.2435	2250.827	2.743	0.159
ZZ	151.96986	95.283	6.723	0.06

EFFECT OF SEALANT VISCOSITY ON BONDING

To investigate the effect of sealant viscosity on sealant bonding, seven sealants were tested at high and low viscosity using flawless nonporous aluminum substrate. The viscosity of each sealant was measured at several temperatures. Two of the testing temperatures were selected to ensure a corresponding variation in viscosity was 1Pa.s. The corresponding viscosities are referred to as high and low in following sections.

Variation of Viscosity with Temperature

Although it is important to control sealant temperature during installation, sealant temperature usually varies during installation due to several reasons: Kettle's temperature sometimes may not be accurately controlled; temperature variation within the kettle; and a drop of more than 50ºC as sealant enters a crack (Collins et al., 2006). In addition, there is a variation among producers in recommended heating temperature and its range: some suggest a range of 20ºC; while others set a specific heating temperature. Moreover, sealants show different sensitivity to temperature variation (Al-Qadi et al., 2006). To study the effect of viscosity on bonding, specimens were cast at two temperatures: 200ºC and at a closest temperature lower than 200ºC that corresponds to a viscosity differed by more than 1Pa.s than that of the sealant at 200ºC. Viscosity of each sealant at the corresponding temperature was measured following the test procedure recommended by Al-Qadi et al. (2006). The viscosity measurement is reported in Table 25 and Figure 47. It should be noted that 200ºC is above the installation temperature by 7 to 23ºC, with minimum overheating occurred for sealants QQ and DD, and maximum for sealant YY. Specimens were prepared and tested in accordance with the recommended blister testing procedure (Appendix D). Figure 48 presents the IFE value calculated for each pair of sealant-aluminum at low and high viscosities. It is clear that the sealant IFE values are greater for the relatively higher viscosity.

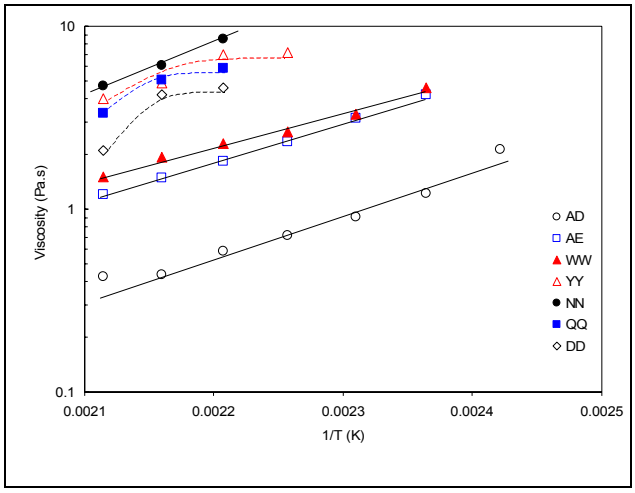

Figure 47. Arrhenius representation of temperature effect on sealant viscosity

Table 25. Sealant Viscosity Using the Brookfield Viscometer Model DV-III-RV

Sealant	Temperature (ºC)							
	130	140	150	160	170	180	190	200
	Viscosity (Pa.s)							
AD		2.11	1.22	0.91	0.72	0.59	0.44	0.43
AE			4.21	3.15	2.35	1.82	1.48	1.21
WW			4.58	3.31	2.64	2.29	1.91	1.51
DD						4.59	4.21	2.1
YY					7.18	6.96	4.87	4.01
NN						8.56	6.1	4.7
QQ						5.89	5.11	3.36

In general, high viscosity sealants are thought of resulting in incomplete coverage; hence, weak bonding. However, the aforementioned results showed that high viscosity sealants adhered better to substrate given that the substrate surface is covered adequately. Adequate coverage can be facilitated by modifying installation equipment to more effectively filling the crack. Although crack geometry effect is not considered, the study found that high viscosity sealants are desirable, provided they are installed appropriately and surface wetting is achieved. In the field application, a sealant flows into a narrow rough crack; the irregularity of the crack surface can disturb sealant flow. Consequently, a sealant may solidify before it has time to fill/wet the crack. This effect is accentuated by the drop in sealant temperature. Therefore, installation temperature is important to achieve optimum viscosity. The optimum viscosity should ensure ease of application and adequate crack surface wetting. In addition, controlling temperature in the kettle can help reduce the variation in field performance.

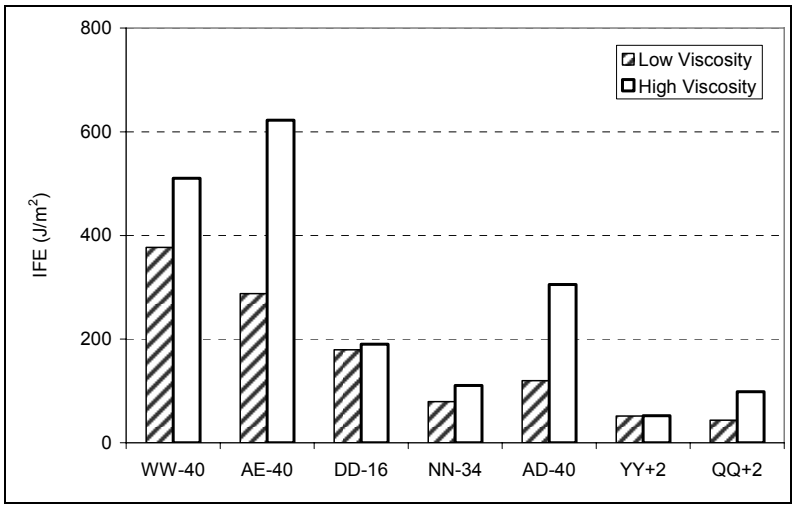

Figure 48. Interfacial fracture energy at 2°C to -40°C after pouring sealants at high and low Viscosities

To further investigate the aforementioned observations, the amounts of insoluble in four sealants were measured using FTIR method and are presented in Figure 49. Insoluble in sealants is composed of ground tire rubber (GTR) and mineral filler. The variation in bonding was calculated for the four sealants, Figure 50. It is evident that sealants having high mineral filler content are more susceptible to temperature and consequently to viscosity variation than those having ground tire rubber. However, since sealant viscosity, and consequently bonding, are affected by polymer content and molecular weight, further investigation is needed to interpret these findings. Gel Permeation Chromatography (GPC) or FTIR spectroscopy may be used to achieve that. The segregation of the mineral filler and the GTR may be evaluated using Thermo Gravimetric Analyzer, TGA (Al-Qadi et al., 2008).

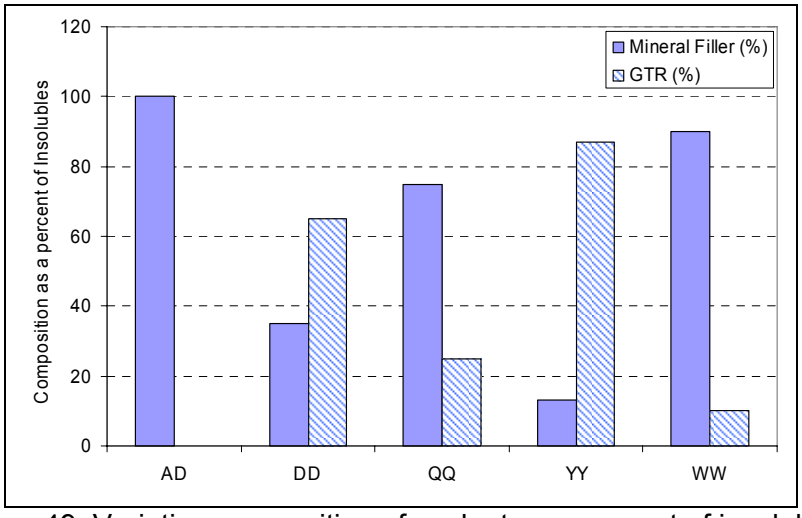

Figure 49. Variation composition of sealant as a percent of insolubles (Al-Qadi et al., 2008)

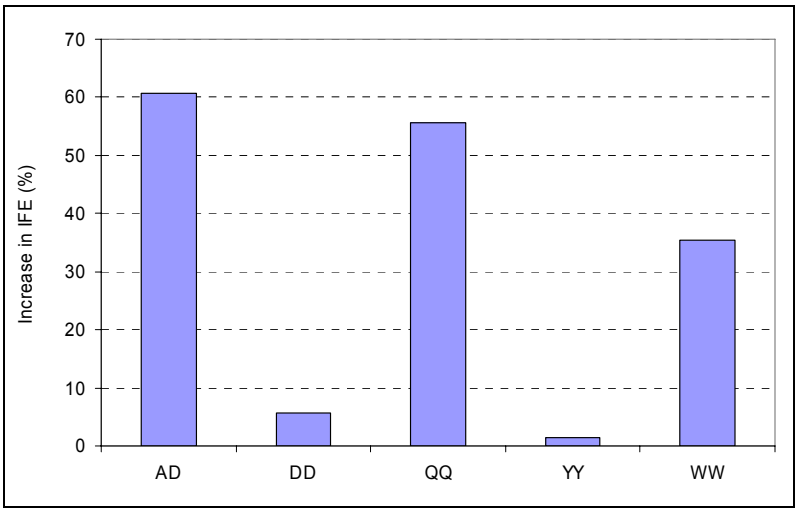

Figure 50. Increase in IFE at lower installation temperature

EFFECT OF ANNEALING TIME ON BONDING

Annealing time and conditioning are among the most important factors affecting adhesion and consequently sealant performance. Annealing time refers to the time period allowed for the cast specimen to set at room temperature. Initial bonding can play a significant role in sealant performance; stronger bonds are expected to last longer and to resist severe conditions better. While the optimum annealing time varies for different sealants, giving the sealant enough time to develop a strong bond with the crack walls can be as important as selecting the right sealant. If a potentially good sealant encounters traffic and severe conditions before it builds optimum adhesion, it won't be able to perform as expected. Although the issue of how the bond deteriorates under traffic and thermal loading is not known, it is believed that initial bonding conditions play a strong role in sealant performance (Masson et al., 2002).

Three sealants were cured for 1hr and 24hr at room temperature, conditioned for 20min in the cooling bath, and then tested using the blister test. Figure 51 shows that IFE increased significantly with increased annealing time. However, the amount of increase in adhesion varied among sealants. Statistical analysis was conducted to study if there is a significant difference between the results from the two annealing times. The significance levels are all below 0.05, which shows there is a significant difference in IFE value between specimens cured for 1hr and those cured for 24hrs before conditioning in the bath (Table 26). The difference can be due to ordering of asphaltenes during the annealing time at room temperature; this ordering also can be reflected in bitumen strain upon the application of a load; hence it has an effect on the interface bonding. Masson et al. (2005) showed that strain decreases with annealing time, and the strain reaches an asymptotic value within 16-24hrs. They also showed that not accounting for this phenomenon may lead to poor reproducibility in experiment data. Therefore, to maintain good reproducibility, they suggested that an annealing time of 24hrs be considered before conducting the test.

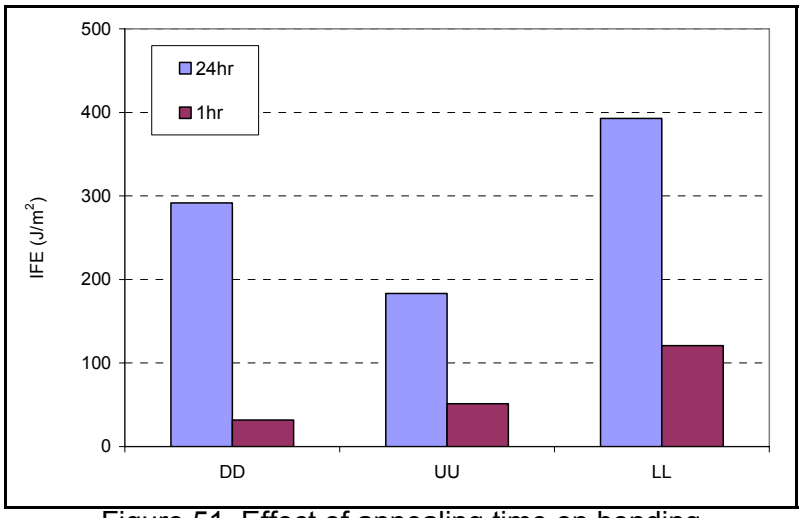

Figure 51. Effect of annealing time on bonding

Table 26. ANOVA Results to Compare IFE Values between Two Annealing Times (1and 24hrs)

Sealant	Sum of Squares	Mean Square	F	Sig.
DD	72,868.673	72,868.673	131.695	0.008
LL	86,829.544	86,829.544	3,781.133	0.000
UU	17,396.088	17,396.088	842.032	0.001

EFFECT OF LOADING RATE ON BONDING

The adhesion of bituminous material strongly depends on the rate of separation of the bonded surfaces and on the temperature. This section of the study investigates this dependence through laboratory experiments. Interfacial fracture energy was measured using the newly developed blister test method. Three binders and eight bituminous-based sealants were tested at various temperatures and loading rates. As presented earlier, the slope of the curve before peak pressure is related to the modulus, data at the peak pressure is related to IFE_{peak}, and data collected after the peak is related to IFE_{avg}. It was found that the modulus and both IFE_{peak} and IFE_{avg} vary significantly with temperature and rate of loading.

At certain temperature ranges, above glass transition temperature, T_g, bituminous material shows rubbery behavior in which material is defined as viscoelastic. At this status, IFE is highly affected by bituminous material characteristics including its deformation behavior. Therefore, the aforementioned time-temperature dependency of the IFE at rubbery status arises mainly from this feature of the adhesive. It was found at this stage that the IFE value increases as the temperature decreases/ loading rate increases. However, a reverse trend was observed when bituminous materials were tested at their glassy status. This transition occurs close to the glass transition temperature of the adhesive, below which a sharp decline in IFE measurement was observed. At glassy status, IFE values decrease as temperature decreases/ loading rate increases. It should be noted that applied laboratory loading rates are much higher than those in the field. In an attempt to relate the laboratory measurements to field observations, an IFE master curve covering a wide span of loading rates should be constructed, from which the IFE value corresponding to field condition can

be conferred. Using the blister test, the IFE values of sealant UU at six temperatures and three loading rates were determined, Figure 52.

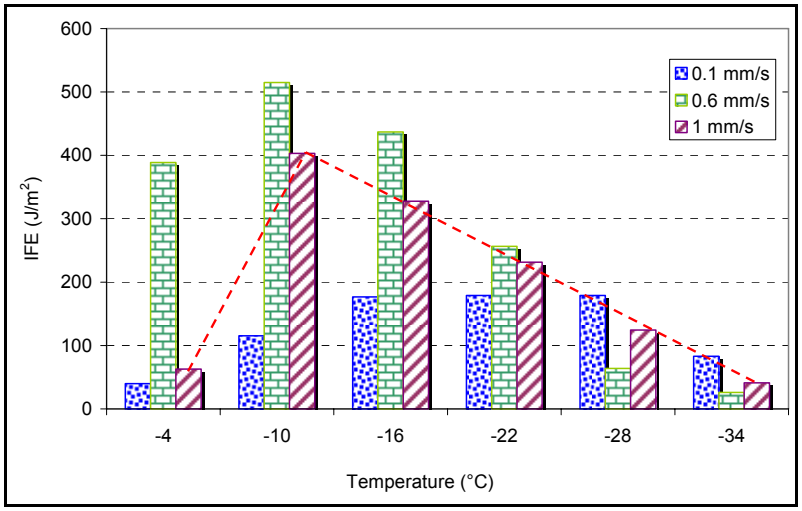

Figure 52. IFE value of sealant UU and aluminum at six temperatures and three loading rates

Figure 52 shows that the IFE of bituminous materials (sealant UU) varies with both temperature and loading rates. At all three rates, an increasing trend of IFE with decreasing temperature is followed by a decreasing trend. The transition point varies with the rate of loading. At the rate of 0.1mm/s, the transition occurs somewhere between -16°C and -28°C. At the other two rates, the transition occurs at a higher temperature of -10°C. This further confirms the fact that IFE is strongly dependent on rate/temperature. It is expected that if the tests were conducted at an extremely low loading rate, the transition would occur at the real glass transition temperature measured using Differential Scanning Calorimetry (DSC). The dashed line in Figure 52 shows the IFE values when tests were conducted at 0.1mm/s. To study this dependency, the Williams-Landel-Ferry (WLF) superposition principle (Williams et al., 1955) was applied to construct a master curve (Gent and Petrich, 1969; Lewandowski, 1988). To normalize the data with respect to the glass transition temperature, a shift factor, a_T, was calculated with the WLF equation (Equation 36).

$$Loga_T = 17.4(T - T_g)/51.6 + (T - T_g) \quad \textbf{(36)}$$

where,
T is the test temperature; and
T_g is the glass transition temperature of adhesive.

The WLF equation is restricted in its use to viscoelastic materials tested above their T_g, so it does not hold for glassy or crystalline materials. Since adhesives are polymers above their Tg, the WLF equation was applied to the study of polymer adhesion onto rigid substrates (Masson *et al.,* 2005). In order to apply the WLF equation, the glass transition temperature, T_g, of the sealant UU was measured, using DSC (Figure 53).

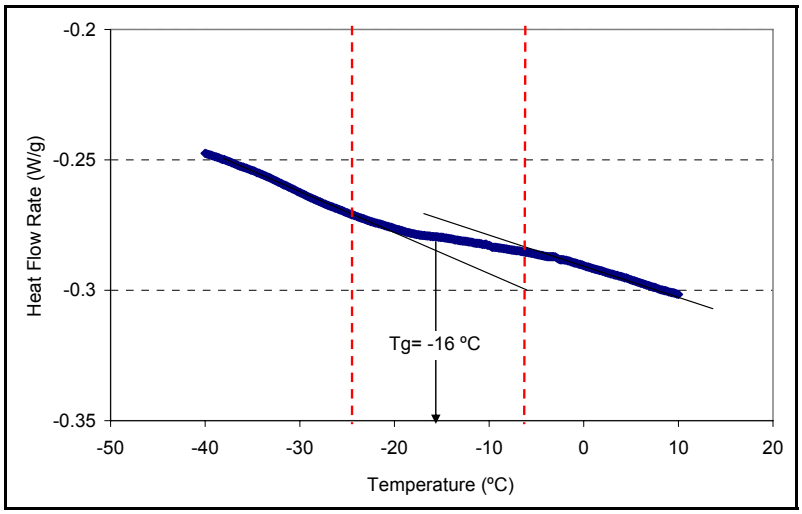

Figure 53. Sealant UU glass transition temperature determination using DSC

Knowing T_g value for this bituminous sealant (T_g = -16ºC), the shift factor was calculated at each temperature using Equation 36. Shift factors were used to develop master curves for modulus at critical pressure and IFE. The modulus value is plotted versus logarithm of the shift factor, a_T, multiplied by loading rates, R, Figure 54. As can be seen, the adhesive modulus increases with loading rate regardless of the material's glassy or rubbery stage. At higher loading rates (lower temperatures), material becomes stiffer and its modulus increases.

Bituminous materials are viscoelastic adhesives, so the WLF equation is also of interest to normalize the IFE in Figure 52 with respect to T_g. The result of this normalization is a master curve as shown in Figure 55, where Ra_T is the effective test rate. As can be seen, higher rates result in higher IFE up to certain rate, above which, as the loading rate increases, the IFE decreases. This transition is attributed to material rubbery/ glassy behavior which occurs above and below its T_g, respectively. This confirms that interface bonding is affected by the coupling effect of the bulk material and the interface. While at relatively low equivalent loading rates (rubbery stage), the bulk characteristics greatly contribute to the IFE value, at high rates (glassy stage), IFE is mainly controlled by the interface property.

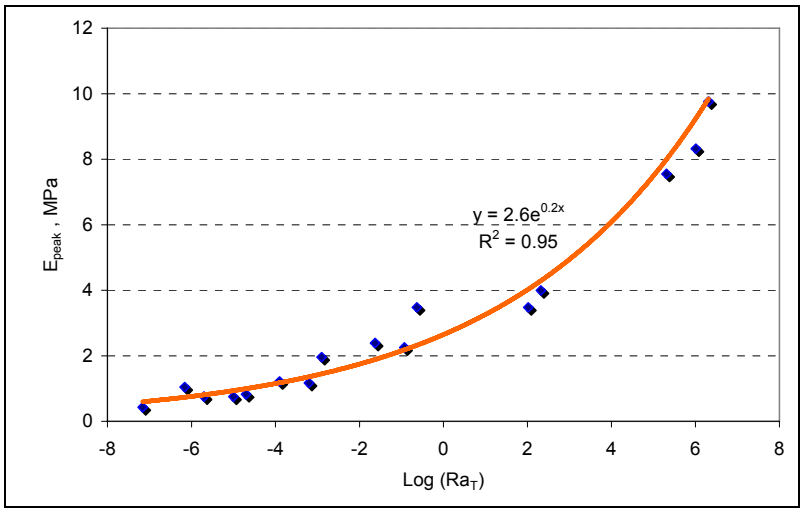

Figure 54. Modulus at peak pressure versus reduced rate for Sealant UU adhered to aluminum

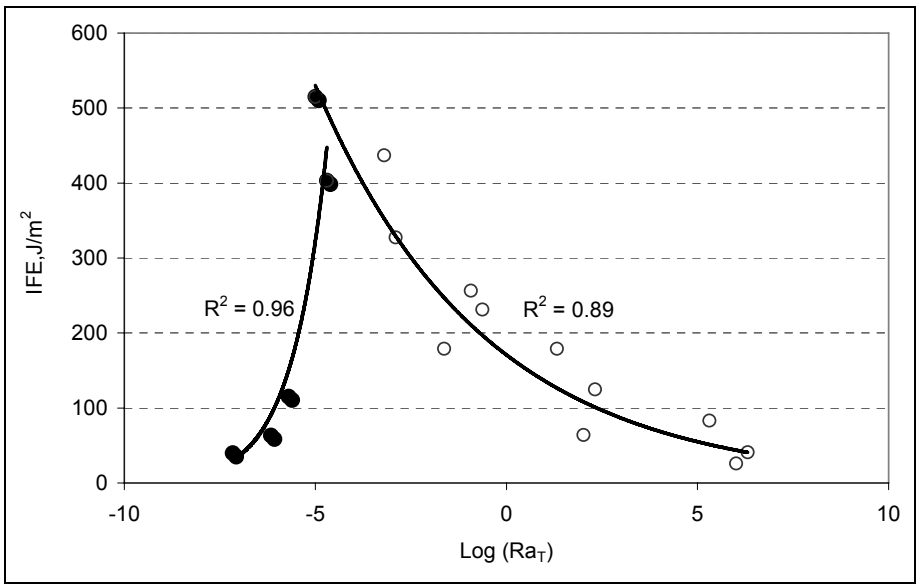

Figure 55. IFE value versus reduced rate for sealant UU bonded to aluminum

Summary of the Blister Test

Bituminous materials often fail in adhesion during winter. This is especially true of bituminous sealants applied to roadway cracks and joints. In an effort to better understand the nature of this failure, the effect of viscosity, aging, annealing time, temperature, and loading rate on the interfacial fracture energy (IFE) of bituminous sealants were measured by means of a blister test. The substrate was a normalized model aggregate, smooth aluminum.

When sealants were poured at a high and a low viscosity, the higher viscosity always led to a stronger bond. This indicated that in the absence of interfacial defects, the sealant bulk properties play a key role in the interfacial adhesion. Of particular importance in this respect was the content of rubbery material (ground-tire rubber -- GTR) and SB copolymer. Aging, which modifies viscosity, also affected the bonding, but since aging was material

specific, no trend emerged between bonding characteristics and aging. It was found that an optimum annealing time can improve sealant interface bonding.

After the measure of IFE at various temperatures and loading rates, and the time-temperature superposition of the results presented in a master curve, the effective viscoelastic properties of the sealants were found to play an important role in bonding and the mechanism of interfacial failure. In conditions where the material is in a liquid-rubbery state, above the glass transition temperature (T_g), IFE shows an increasing trend with loading rate, which shows that the bulk property is dominant. At a very low loading rate, failure tends to be cohesive. However, failure tends to be adhesive when the material is stiff, below the T_g. Sealants with a T_g below -60°C (because of high polymer content) were found to have the highest IFE when tested in sub-zero temperatures.

The benefit of this study is in being able to predict sealant bonding under realistic field conditions. With the combination of loading rates and temperatures expected in service, sealant users could determine and compare the IFE of various products. Alternatively, sealant producers could generate IFE master curves to better identify the conditions under which a particular sealant would perform well.

FIELD COMPARISON

There have been many attempts to evaluate the field performance of crack sealants installed in different configurations (Belangie and Anderson, 1985; Cook et al., 1990; Masson et al., 1999; Ward, 2001). Among those, studies conducted by Masson and his coworkers were used to conduct a limited validation of the laboratory test results and to determine a threshold for adhesion.

Masson et al. (1999) monitored the debonding and pull-out lengths of 12 hot-poured bituminous crack sealants installed in the city of Montreal, Canada. These sealants were installed in a HMA overlay over a PCC pavement; they were exposed to temperatures ranging from -40°C to 40°C. All sealed cracks were routed, cleaned, and heat treated. Cracks smaller than 4mm in width were routed to 12x12mm2; medium cracks were routed to 19x19mm2; larger cracks, 10 to15mm in width, were routed to 40x10mm2. Debonding and pull-out lengths were periodically surveyed using a measuring wheel. The percent failure lengths were calculated per rout size and per crack orientation. For each sealant, a performance index was calculated (Equation 37).

$$PI = 100 - (D + nP) \tag{37}$$

where,
PI is the performance index;
D is the percent debonded length of the sealant;
P is the percent pull-out length; and
n was taken as 4 (pull-out) or 1 (debonding).

The study showed that sealant performance varied significantly among sealants, and the performance index was found to be between 8 (very poor performance) and 75 (good performance), Table 26. 12mm routs showed the best performance among three configurations, with 40mm routs being the worst. The sealants' performance was classified in three stages. In the first stage, the number of failures increased rapidly; in the second stage, little failure occurred; while in the last stage, the number of failures again increased rapidly; but at a slower rate than that of stage one.

To simulate field conditions, an aging procedure was needed. The analysis of the sealants helped determine the aging mechanism in the field (Masson and Al-Qadi, 2004). Aging was found to include bitumen oxidation, polymer degradation and cross-linking, and a loss of light oils. The rate and the extent of the aging provided guidelines for the development of an accelerated-aging laboratory method that simulates in-service aging (Masson and Al-Qadi, 2004). Following this aging procedure, four sealants from Montreal and two sealants from the U.S. were aged in the laboratory, and the interface bonding of these sealants to aluminum was evaluated using the direct adhesion test and blister test methods (Figures 56 and 57). In addition, sealants at original status and those collected from the field (short-term < 5yr and long-term > 5yr) were tested in the laboratory. Also, kettle-aged sealants (which were only available for the U.S. samples) were tested. The W_a (surface energy test), P_{max} (direct adhesion test), and the IFE (blister test) of the bond between the tested sealants and aluminum are shown in Figures 56a, b and c. Sealant PP showed the highest work of adhesion, followed by LL, B, A, and G, with G having the lowest value among all. In the direct adhesion test, P_{max} at oven-aged status was found to be the highest for sealant LL, followed by PP, B, and A, while G failed cohesively and the results were discarded. In the blister test, the IFE of oven-aged sealant was found to be the highest for sealant PP followed by B and LL, with sealant A being relatively low, and sealant G found to be the lowest. Using test results from each approach, sealants were ranked and reported in Table 27. The field survey for Montreal sealant is reported in Table 26, and Sealants PP and LL were monitored separately in U.S. test sections and reported as having good performance. As can be seen, the laboratory results show similar ranking as those from the field study.

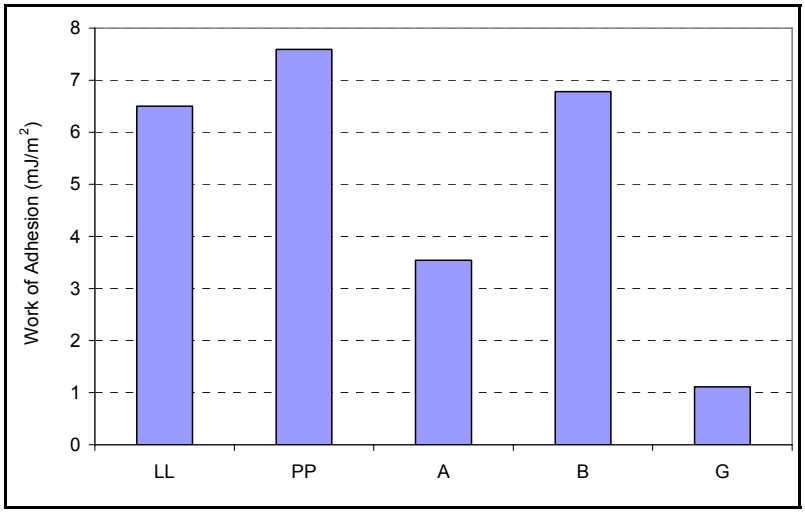

Figure 56-a. Work of adhesion of the sealant-aluminum bond at various aging status

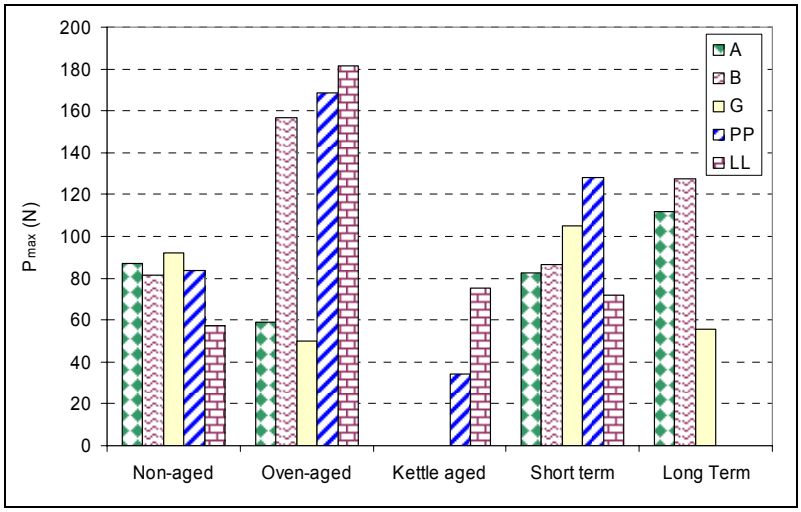

Figure 56-b. P_{max} value of the sealant-aluminum bond at various aging status

Figure 66-c. IFE value of the sealant-aluminum bond at various aging status

Table 26. Field Performance of Montreal Sealant (Masson *et al.*, 1999)

Sealant	De-bonding	Pull-out	Performance
A	11	14	Poor
B	22	1	Good
E	20	2	Good
G	36	14	Poor

Table 27. Laboratory Ranking Using Second Test (P_{max} Threshold)

Sealant	W (mJ/m^2)	P_{max} (N)	IFE (J/m^2)	Laboratory ranking
A	3.54	58.99	211.54	Fair
B	6.78	156.99	638.95	Good
G	1.11	50.11	100.67	Poor
PP	7.59	168.62	1331.7	Good
LL	6.50	181.38	619.68	Good
E	NA	pass	pass	Excellent

RESULTS AND CONCLUSION

A major cause of bituminous crack sealant failure in the field is debonding of the sealant from the crack walls. Therefore, a reliable test method that is based on rheology of the sealant and can correlate with field performance is urgently needed to predict interfacial bonding. Three laboratory tests were developed in this study: the work of adhesion, the direct adhesion, and the blister test, which respectively address the needs of producers, engineers, and researchers.

The first test uses a surface energy approach. Work of adhesion can be used to define the compatibility between sealant and substrate. Work of adhesion for each of several sealants with aggregates and aluminum was calculated through measuring the surface energy of the sealant and the contact angle between the sealant and aggregate/aluminum.

The second test is a mechanical test. The direct tension test (DTT) is modified for sealant application. A notch is introduced at the sealant-substrate to set the failure path. In this method, direct tensile force is applied to the assembly of sealant-aggregate to bring it to a failure point. The maximum load, P_{max}, and energy, E, to failure are calculated and reported as an indication of adhesion. It was evident that the maximum load can be easily differentiated among sealants. Identifying lower limits for the parameters allows for the selection of an appropriate sealant, which can develop an adequate bond with the crack wall.

The third test is the blister test where test results allow calculating two fundamental parameters: tensile modulus and the interfacial fracture energy (IFE). This test is more suited for research studies.

In an attempt to develop the aforementioned approaches into standard tests, aluminum was identified as an appropriate standard substrate replacement for aggregate because of its compatibility with sealant, low diffusion, controllable roughness, high resistance to extreme temperatures, and availability. It also has a similar thermal coefficient to that of aggregates. Each method was developed using an aluminum substrate. However, using local aggregate will provide further insight into the expected field performance. In this study, to investigate the effect of substrate variation on bond characteristics, tests were repeated with granite, limestone, and quartzite.

This study resulted in the following findings:

- Aluminum is an appropriate substrate for the developed adhesion tests.
- Work of adhesion is an appropriate parameter to examine sealant-aggregate compatibility.
- Aging affects adhesion significantly.

- Adhesion between aged sealant and aluminum is sealant specific. Depending on sealant composition, adhesion may increase or decrease after aging.
- Interface bonding is significantly affected by loading rate and temperature variations.
- Sealant viscosity at installation affects interface bonding.
- P_{max} obtained from direct adhesion test can be used to rank sealant-aggregate pairs.
- IFE measured using the blister test is a fundamental property of the interface and can be used to characterize sealant-aggregate interface.
- Annealing time affects interface bonding. Longer annealing time results in greater IFE value.

This study concluded that the direct adhesion test is best suited (of the three adhesion tests that were developed) for use in a practical performance-based guideline. Based on laboratory testing and limited field data, a maximum load of 50N (minimum) at graded temperature coincides with good field performance for sealant adhesion. The surface energy test may be used by manufacturers to measure the sealants-substrate compatibility, while the blister test may be used by researchers to better understand the sealant-substrate interface characteristics.

RECOMMENDATIONS

This study introduced three laboratory test methods, based on bituminous sealant rheology, which can predict sealant adhesion to aggregate. It is recommended to use the direct adhesion test as part of the developed performance-based guidelines for the selection of hot-poured crack sealants. The recommended threshold is a maximum load of 50N (minimum) at graded temperature. The surface energy test is recommended for use by manufacturers to identify the compatibility of sealant with local aggregates. Due to training requirements and equipment cost, the blister test may only be used by researchers at this time.

It is recommended that a field validation of the outcome this study be conducted.

REFERENCES

Allen, M.G. Measurement of Polyimide Interlayer Adhesion Using Micro-Fabricated Structures. *Journal of Polymeric Materials, Science and Engineering*, Proceedings of the ACS Division of Polymeric Materials, Science and Engineering, Vol. 59, 1988, pp. 352-356.

Allen, M.G., Mehregany, M., Howe, T.R.T., and Senturia, S.D. Microfabricated Structures for the in Situ Measurement of Residual Stress, Young's Modulus, and Ultimate Strain of Thin Films. *Applied Physics Letters*, Vol. 51, No. 4, 1987, pp. 241-243.

Allen, M.G., and Senturia, S.D. Analysis of Critical Debonding Pressures of Stressed Thin Films in the Blister Test. *Journal of Adhesion*, Vol. 25, 1988, pp. 303-315.

Al-Qadi, I.L., Fini, E., Elseifi, M.A., and Masson J-F. Procedure for Viscosity Determination of Hot-Poured Bituminous Sealants. In *Transportation Research Record 1958.* Transportation Research Board, Washington, DC, 2006, pp. 74-81.

Al-Qadi, I.L., Fini, E., and Masson, J-F. Effect of Bituminous Material Rheology on Its Adhesion. In *Proceedings of the 87th Transportation Research Board Annual Meeting 08-2331*, Washington, DC, 2008.

Al-Qadi, I.L., Yang, S., Elseifi, M., Masson, J-F., and McGhee, K. *Specifications of Bituminous-Based Crack Sealants Using Modified Bending Beam Rheometer*. 85th Transportation Research Board Annual Meeting, Washington, DC, 2006.

Anderson, D.A., Christensen, H.U., Bahia, R., Dongre, R., Sharma, M.G., and Button, J.J. *Binder Characterization and Evaluation*. Vol. 3: Physical Characterization, SHRP-A-369, Strategic Highway Research Program, Washington, DC, 1994.

ASTM C670-03. *Standard Practice for Preparing Precision and Bias Statements for Test Methods for Construction Materials*. American Society of Testing and Material, Philadelphia, Pennsylvania, www.astm.org.

ASTM D3405. *Joint Sealants, Hot Poured for Concrete and Asphalt Pavement.* American Society of Testing and Material, Philadelphia, Pennsylvania, www.astm.org.

ASTM D6690. *Standard Specification for Joint and Crack Sealants, Hot Applied, for Concrete and Asphalt Pavements*. American Society of Testing and Material, Philadelphia, Pennsylvania, 2006.

ASTM D5167-03. *Standard Practice for Melting of Hot-Applied Joint and Crack Sealant and Filler for Evaluation.* American Society of Testing and Material, Philadelphia, Pennsylvania, www.astm.org.

Bayomy, F.M., Mull-Aglan, M.A., Abdo, A.A., and Santi, M.J. *Evaluation of Hot Mix Asphalt (HMA) Fracture Resistance Using the Critical Strain Energy Release Rate*. 85th Transportation Research Board Annual Meeting, Washington, DC, 2006.

Beams, J.W. *Mechanical Properties of Thin Films of Gold and Silver, in Structure and Properties of Thin Films*. C.A. Neugebauer, J.B. Newkirk, D.A. Vermilyea, (Eds). Wiley, New York, 1959, pp. 183-192.

Belangie, M.C., and Anderson, D.I. *Crack Sealing Methods and Materials for Flexible Pavements.* Final Report, No. FHWA-UT-85-1. 74 p., Utah Department of Transportation, Salt Lake City, Utah, 1985.

Bennett, S.J., Devries, K.L., and Williams, M.L. Adhesion Fracture Mechanics. *International Journal of Fracture*, Vol. 10, No. 1, 1974, pp. 33-43.

Bhasin, A., Masad, E., Little, D., and Lytton, R. *Limits on Adhesive Bond Energy for Improved Resistance of Hot Mix Asphalt to Moisture Damage*. 85th Transportation Research Board Annual Meetings, Washington, DC, 2006.

Burton, J.D., Jones, W.B., and Williams, M.L. Theoretical and Experimental Treatment of Fracture in an Adhesive Interlayer. *Transaction of the Society of Rheology*, 5:1, 1971, pp. 39-50.

Cheng, D.X., Little, D., Lytton, R., and Holste, J.C. *Surface Free Energy Measurement of Aggregates and Its Application to Adhesion and Moisture Damage of Asphalt Aggregate Systems*. International Center for Aggregates Research, 9th Annual Symposium, Austin, Texas, 2001.

Chu, Y.Z., and Durning, C.J. Application of the Blister Test to the Study of Polymer-Polymer Adhesion. *Journal of Applied Polymer Science*, Vol. 45, 1992, pp. 1151-1164.

Collins, P., Masson, J-F., and Al-Qadi, I.L. *Cooling Rates in Hot-Poured Bituminous Sealants*. 85th Transportation Research Board Annual Meeting, Washington, DC, 2006.

Cotterell, B., and Chen, Z. The Blister Test — Transition from Plate to Membrane Behavior for an Elastic Material. *International Journal of Fracture*, Vol. 86, 1997, pp.191-198.

Cook, J.P., Weisgerber, F.E., and Minkarah, I.A. *Evaluation of Joint and Crack Sealants*. FHWA/OH-91/007. University of Cincinnati, Cincinnati, Ohio, 1990.

Curtis, C.W. Investigation of Asphalt-Aggregate Interaction in Asphalt Pavements. *American Chemical Society* (Fuel section), Vol. 37, 1992, pp. 1292-1297.

Curtis, C.W., Clapp, D.J., Jeon, Y.W., and Kiggundu, B.M. Adsorption of Model Asphalt Functionalities, AC-20, and Oxidized Asphalts on Aggregate Surfaces. In *Transportation Research Record 1228.* Transportation Research Board, Washington, DC, 1989, pp. 112-127.

Dannenberg, H. Measurement of Adhesion by a Blister Method. *Journal of Applied Polymer Science*, Vol. 5, 1961, pp. 125-134.

Despain, R.R., DeVries, K.L., Luntz, R.D., and William, M.L. *A Strength Comparison of Barnacle and Commercial Dental Cements*. 49th International Association for Dental Research General Meeting, UTEC DO 70-195, 1970.

Dundurs, J. *Mathematical Theory of Dislocations*. American Society of Mechanical Engineers, New York, 1969, pp. 70-115.

Einstein, A. *Investigations of the Theory of Brownian Movement*. Dover, New York, 1956.

Evans, A.G., Rilhle, M., Dalgleish, B.J., and Charalambides, P.G. *The Fracture Energy of Bimaterial Interfaces*, UCSB Materials Department Report, Santa Barbara, California, 1989.

Fowkes, F.M. Attractive Forces at Interfaces. *Industrial and Engineering Chemistry*, Vol. 56, No. 12, 1964, pp. 40-52.

Galerie, A., Toscan, F., N'Dah, E., Przybylski, K., Wouters, Y., and Dupeux, M. Measuring Adhesion of Cr2O3 and AL2O3 Scales on Fe-based Alloys, *Material Science Forum*, Vols. 461-464, 2004, pp. 631-638.

Gent, A.N., and Petrich, R.P. Adhesion of Viscoelastic Material to Rigid Substrates. *Proceeding of Royal Society*, A. 310, 1969, pp. 433-448.

Lewandowski, L.H. *Blister Test for Adhesion of Thin Films*. PhD Dissertation, The University of Akron, 1988, AAT 8816754.

Gent, A.N., and Lewandowski, L.H. Blowoff Pressures for Adhering Layers. *Journal of Applied Polymer Science*, Vol. 33, 1987, pp. 1567-1577.

Green, H., and Lamattina, T.P. Measurement of Adherence of Organic Coating to Metal Surfaces. *Analytical Chemistry*, Vol. 20, 1948, pp. 523.

Griffith, A.A. The Phenomena of Rupture and Flow in Solids. *Philosophical Transactions of the Royal Society of London*, 221, 1921, pp. 163-198.

Hbaieb, K., and Zhang, Y.W. A Parametric Study of a Pressurized Blister Test for an Elasto-Plastic, Film-Rigid Substrate System. *Material Science and Engineering*, A390, 2005, pp. 385-392.

Hefer, A.W. *Adhesion in Bitumin-Aggregate System and Quantification of the Effects of Water on the Adhesive Bond*. PhD dissertation, Texas A&M University, Texas, 2004.

Hinkley, J.A. A Blister Test for Adhesion of Polymer Films to SiO2. *Journal of Adhesion*, Vol. 16, 1983, pp. 115-126.

Hutchinson, J.W., Thouless, M.D., and Liniger, E.G. Growth and Configurational Stability of Circular, Buckling-Driven Film Delaminations. *Acta Metall. Mater*., Vol. 40, No. 2, 1992, pp. 295-308.

Jensen, H.M. The Blister Test for Interface Toughness Measurement. *Engineering Fracture Mechanics*, Vol. 40, No. 3, 1991, pp. 475-486.

Jensen, H.M., and Thouless, M.D. Effects of Residual Stresses in the Blister Test. *International Journal of Solids and Structures*, Vol. 30, 1993, pp. 779-795.

Jiang, K.R., and Penn, L.S. Use of the Blister Test to Study the Adhesion of Brittle Materials, Test Modification and Validation. *Journal of Adhesion*, Vol. 32, 1990, pp. 203-216.

Jones, W.B. *A Simple Test for Certain Cases of Adhesion*. UTEC DO 69-088. College of Engineering, University of Utah, Salt Lake City, 1969.

Kendall, K. Adhesion: Molecules and Mechanics. *Science*, Vol. 263, No. 5154, pp. 1720-1725.

Kim, K.S., and Kim, J. Elasto-Plastic Analysis of the Peel Test for Thin film Adhesion. *Journal of Engineering Material Technology*, Vol. 110, 1988, pp. 266-273.

Lin, P., and Senturia, S.D. The In Situ Measurement of Biaxial Modulus and Residual Stress of Multi-Layer Polymeric Thin Films. In *Materials Research Society Symposium Proceedings*, Vol. 188, 1990, pp. 41-46.

Malyshev, B.M., and Salganik, R.L. The Strength of Adhesive Joints Using the Theory of Cracks. *International Journal of Fracture Mechanics*, Vol. 1, 1965, pp. 114-128.

Masson, J-F., and Veitch, M. *Quantification of Filler and Ground Tire Rubber in Bituminous Sealants* (To be submitted).

Masson, J-F., Collins, P., Wood, J.R., and Bundalo-Perc, S. *Degradation of Bituminous Sealants Due to Extended Heating before Installation*. 85th Transportation Research Board Annual Meeting, Washington, DC, 2006.

Masson, J-F., and Al-Qadi, I.L. *Long-Term Accelerated Aging and Low Temperature BBR Testing of Sealants*. Internal Report, National Research Council of Canada, No. B5508.5, 2004.

Masson, J-F., and Lacasse, M.A. A Review of Adhesion Mechanisms at the Crack Sealant/Asphalt Concrete Interface. In *Proceedings of the 3rd International Symposium on Durability of Building and Construction Sealants*, Fort Lauderdale, Florida, 2000.

Masson, J. F., Collins, P., and Légaré, P.P. Performance of Pavement Crack Sealants in Cold Urban Conditions. *Canadian Journal of Civil Engineering*, Vol. 26, No. 4, 1999, pp. 395-401.

Masson, J-F., and Lacasse, M.A. Effect of the Hot-Aired Lance on Crack Sealant Adhesion, *Journal of Transportation Engineering*, Vol. 125, 1999.

Masson, J-F., Polomark, G., and Collins, P. Glass Transitions and Amorphous Phases in SBS-Bitumen Blends. *Thermochimica Acta*, Vol. 435, 2005, pp. 96-100.

Penn, L.S., and Defex, E. Relation between Work of Adhesion and Work of Fracture for Simple Interfaces. *Journal of Material Science*, Vol. 37, 2002, pp. 505-513.

Reddy, J. N. *Theory and Analysis of Elastic Plates*. Taylor and Francis, Philadelphia, Pennsylvania, 1998.

Sheplak, M., and Dugundji, J. Large Deflections of Clamped Circular Plates Under Initial Tension and Transitions to Membrane Behavior. *ASME Journal of Applied Mechanics*, Vol. 65, 1998, pp.107-115.

Shirani, A., and Liechti, K.L. A Calibrated Fracture Process Zone Model for Thin Film Blistering. *International Journal of Fracture*, Vol. 93, 1998, pp. 281-314.

Sneddon, I.N. The Distribution of Stress in the Neighborhood of a Crack in an Elastic Solid. *Proceedings of the Royal Society of London*, A. 187, 1946, pp. 229.

Sue, Z., and Hutchinson, J.W. Interface Crack Between Two Elastic Layers. *International Journal of Fracture*, Vol. 43, 1990, pp. 1-18.

Thelen, E. *Surface Energy and Adhesion Properties in Asphalt-Aggregate Systems*. 37th Annual Meeting of the Highway Research Board; Rheological and Adhesion Characteristics of Asphalt, Bulletin 192, 1958.

Thouless, M.D., Hutchinson, J.W., and Liniger, E.G. Plane-Strain Buckling-Driven Delamination of Thin Films, Model Experiments and Mode-II Fracture. *Acta Metall. Mater.,* Vol. 40, No. 10, 1992, pp. 2639-2649.

Tschoegl, N.W. *The Phenomenological Theory of Linear Viscoelastic Behavior*. Springer-Verlag, 1989, New York.

Van Oss, C.J., Chaudhury, M.K., and Good, R.J. Interfacial Lifshitz-van der Waals and Polar Interactions in Macroscopic Systems. *Chemical Reviews*, Vol. 88, No. 6, 1988, pp. 927-941.

Wan, K-T., and Mai, Y-W. Fracture Mechanics of a New Blister Test with Stable Crack Growth. *Acta Metall. Mater.*, Vol. 43, No 22, 1995, pp. 4109-4115.

Wang, C.M., Reddy, J.N., and Lee, K.H. *Shear Deformable Beams and Plates*. Amsterdam: Elsevier, 2000.

Ward, D.R. *Evaluation of the Implementation of Hot-Pour Sealants and Equipment for Crack Sealing in Indiana*. Final Report, No. FHWA/IN/JTRP-2000/27, 189 p., 2001.

William, J.G. Energy Release Rate for the Peeling of Flexible Membrane and the Analysis of Blister Tests. *International Journal of Fracture*, Vol. 87, 1997, pp. 265-288.

Williams, M.L. The Continuum Interpretation for Fracture and Adhesion. *Journal of Applied Polymer Science*, Vol. 13, 1969, pp. 20-40.

Williams, M.L., and Kelley, F.N. *The Interaction between Polymeric Structure, Deformation and Fracture, in Polymer Networks: Structural and Mechanical Properties*. A.J. Chompff, (Ed), New York: Plenum Press, 1971, pp. 193-218.

Zanzotto, L. *Laboratory Testing of Crack Sealing Materials for Flexible Pavement*. Transportation Association of Canada, Ottawa, Canada, 1996.

Zollinger, C.J. *Application of Surface Energy Measurements to Evaluate Moisture Susceptibility of Asphalt and Aggregates*. MSc dissertation, Texas A&M University, Texas, 2005.

APPENDIX (A)

Coefficient of Thermal Expansion

The coefficient of thermal expansion of the sealant was measured using TMA. About 60mg of the sample was placed in the small aluminum pan (diameter of the pan ~6mm, thickness of the sample ~1.5mm) and heated in the convection oven at 110°C for 30 minutes in order to make the sealant pliable. Three samples of each sealant were tested two days after preparation. The test was performed on the 2940 TMA instrument (TA Instruments Inc.). The instrument was calibrated by following the TMA instrument calibration procedure from the manual. Four calibrations were performed: for the probe, for force, for cell constant with the Aluminum calibration standard, and for temperature with the Indium calibration standard. The same test conditions were used for the calibrations and for the sample testing.

The probe was cooled to a temperature of -100°C before being placed on the sealant surface to keep it from sticking to the surface. Then sample thickness was measured, and the test was started. To reach the sub-ambient temperature for the probe, a liquid nitrogen cooling system was used.

For the data analysis, the Universal Analysis 2000 software (version 4.1 d) from TA instruments was used.

Glass Transition Temperature

Because crack sealant is a viscoelastic material, its behavior at low temperature can be either rubbery or glassy, depending on its glass transition temperature (Tg). Glass transition temperature is a temperature at which molecular mobility is reduced dramatically from the mobility of a liquid state to that of a glassy state. In order to determine the temperature ranges in which a crack sealant shows rubbery behavior (above its Tg) or glassy behavior (below its Tg), the Tg was measured using a Differential Scanning Calorimetry (DSC) machine. In DSC experiments, a small sample is heated and cooled at a predetermined rate while exothermic or endothermic heat flows are measured. The measurements in this study were conducted with a Mettler Toledo DSC821e, connected to a computer equipped with STARe for the manipulation and transfer of data. About 20mg of each sample was sealed in an aluminum pan. The sample was then cooled from 25°C to -150°C at a rate of 10°C/min, held at -150°C for 3min, then heated to 150°C at a rate of 10°C/min. The DSC cell was swept by a constant flow of nitrogen at 80mL/min, and liquid nitrogen was used to cool the sample. The heat flow curves for the third segment, in which the sample was heated from -150°C to 150°C, were separated from the other two segments and analyzed. Figure B-1 illustrates the determination of Tg from the endothermic shift in the DSC curve corresponding to an increase in the specific heat for sealant UU. The temperatures at which the slope of the curve changes are recorded; the average of the two is reported as Tg.

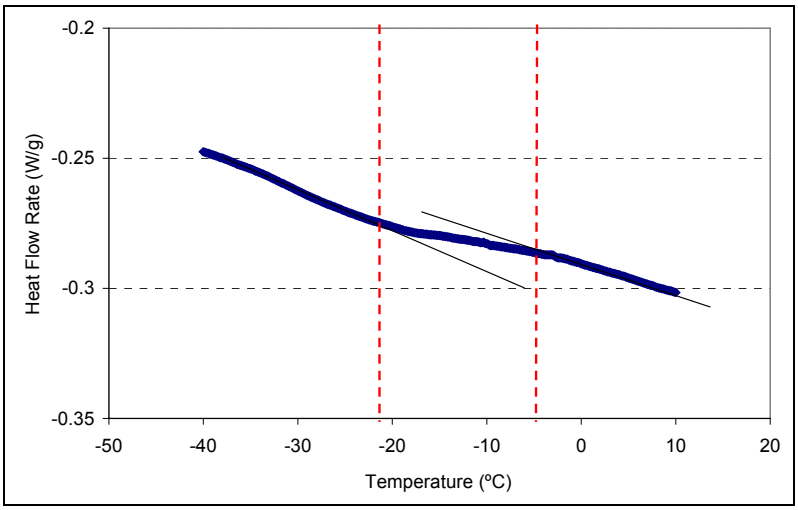

Figure A-1. Determining glass transition temperature using DSC machine for Sealant UU

APPENDIX (B)

Guidelines for Measuring Adhesion of Hot-Poured Crack Sealant Using a Direct Adhesion Test (DAT)

1. Purpose

The direct adhesion test is used to determine the adhesion of hot-poured crack sealant at the application temperatures.

2. Scope

2.1. The adhesion test is a test of fracture. The object of the test is to apply tensile forces to the interface between sealant and aggregate. Sealant is confined between two half cylindrical aggregate (aluminum can be used for standard test). The applied force and displacement can be recorded as functions of time. Energy required to break the bond can be calculated by measuring the area under the load-displacement curve. This energy can be considered a measure of bonding. In addition, the maximum force to failure can be reported as adhesion.

2.2. These guidelines do not purport to address all of the safety concerns, if any, associated with their use. It is the responsibility of the user of this standard to establish and follow appropriate health and safety practices and to determine the applicability of regulatory limitations prior to use.

3. Terminology

3.1. Bituminous sealants and fillers are hot-poured modified asphaltic materials used in pavement cracks and joints.

4. Summary

4.1. Crack sealant material is homogenized, following the procedure given in ASTM D5176. For each test including four replicates, 40g of sealant will be cut and heated to the manufacturer's recommended pouring temperature. Sealant will be poured in the mold placed between the two half cylindrical aggregate samples. The mold confines the sealant at the bottom and between the two aggregate samples at the sides.

5. Significance and Use

5.1. This procedure is designed to measure the adhesion of hot-poured sealant to aggregate.

5.2. Sealants must be rehomogenized (ASTM D5176) before measuring the adhesion by this method.

6. Apparatus

6.1. Modified DTT machine.

6.2. Chiller which can reach -40°C± 0.5°C.

6.3. Laboratory oven — any standard laboratory oven capable of producing and maintaining temperature ranging from 170°C to 193°C ± 0.5°C.

6.4. Release agent.

6.5. Four test setups, four molds and rubber band.

7. Calibration and Standardization

7.1. Temperature of the ovens should be calibrated according to each user's quality assurance program.

7.2. Temperature of the chiller should be calibrated according to each user's quality assurance program.

7.3. Thermometer (temperature detector) — verify the calibration of the temperature sensing device to +/-0.1°C every six months.

8. Procedure

8.1. All adhesion measurements must be performed on rehomogenized sealant. Follow the procedure for homogenization given in ASTM D5176, Melting of Hot-Applied Joint and Crack Sealant and Filler for Evaluation. It is recommended that a minimum of 400g of sealant be homogenized.

8.2. Once homogenized, hot sealant should be molded, cooled, and stored for later usage. To store the sealant, it is recommended that a can or plastic-lined box be used. The mold must be of sufficient size that the sealant depth is no greater than 100mm, to allow for rapid cooling.

8.3. Adjust the oven's temperature to recommended pouring temperature for sealant being tested.

8.4. Turn on the DTT machine, load the program and cool the chiller to test temperature.

8.5. Place a half cylinder of aggregate in each grip and tighten it.

8.6. Assemble the setup which is composed of an aggregate sample on each side and an aluminum mold in between. Wrap a rubber band around the setup to keep all the components in place.

8.7. Place the notch on the edge of one of the aggregates/ aluminum.

8.8. Prepare a can of sealant by cutting 40g of homogenized sealant for each set of four samples.

8.9. Place the can in the oven for 15 minutes, remove it from the oven, stir the sealant thoroughly, and place it back in the oven for another 15 minutes.

8.10. Remove the can from the oven, stir the sealant thoroughly, and pour into all the assembled setups.

8.11. Use four replicates for each sealant; care should be taken in filling up the molds to prevent any trapped air bubbles in the sample.

8.12. Let samples sit one hour at room temperature.

8.13. Trim the excessive sealant away with a hot spatula.

8.13.1. Move spatula once over and parallel to the interface of the sample; trimming direction shall not be changed during trimming

8.13.2. Use well-heated spatula to prevent any shearing of the sealant.

Use two tanks to grab the plate underneath the specimen, and place the specimens in the cooling bath.

Remove the plates underneath each specimen and leave specimens in the bath for 15 minutes.

Remove one specimen at a time from the bath; place it on a flat surface.

Flip the specimen, keep the two end pieces still using point fingers and remove the mold with your thumb.

Place the specimen back in the bath.

Repeat 8.16 until all specimens are demolded.

Leave the samples for 45 minutes in the bath prior to testing.

Turn on the DTT's test builder, adjust the machine so the sample can sit freely on the posts, and place the specimen on the posts. Care should be taken not to disturb the specimen.
Tare the load to zero.
Run the test and record the data.

9. Reporting

9.1. Report the following information: sealant name and supplier, lot number, date received, date of adhesion measurement, recommended pouring temperature, safe heating temperature, any deviations from test temperature.

10. Description of Equipment

10.1. The modified DTT apparatus is used for this test method. Tensile force is applied at the interface of hot-poured crack sealant and aggregate (or aluminum pieces). The Load cell and the LVDT imbedded in the equipment record the load applied to the specimen and the displacement of the two end pieces while test is running.

11. Points of Caution

11.1. The DAT test was developed to measure the adhesion of hot-poured crack sealant to aggregate. This test applies to an interface; if any of the aggregate pieces become contaminated with any release agent, water, dust, or other contaminant, this will distort the test data and nullify the test results.

11.2. The notch should be placed carefully on the edge of the aggregate, in close contact with aggregate. If there is a gap between notch and aggregate, liquid sealant can seep under the notch. In such cases, specimen should be discarded.

11.3. Avoid excessive heating. Excessive heating may cause volatiles to be lost from the sample or polymer chains to be degraded, leading to decreased viscosity of the sealant and inaccurate results.

Figure B-1. Heat 35 gram of homogenized sealant at recommended pouring temperature for 30 minutes

Figure B-2. Placing each end pieced in one grip and tighten it

Figure B-3. Spray release agent on the mold

Figure B-4. Place two end pieces on the mold

Figure B-5. Hold the assembly in place using a rubber band

Figure B-6. Remove the sealant from the oven and mix thoroughly and pour it in the mold from one corner

Figure B-7. Let sealant set for one hour at room temperature

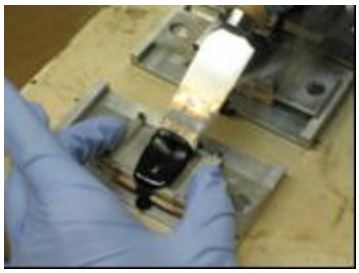

Figure B-8. Trim the extra sealant away using a heated spatula

Figure B-9. Grab the base plate with two tangs and place it in cooling bath

Figure B-10. Remove the base plates

Figure B-11. Leave the specimens in cooling bath for 15 minutes

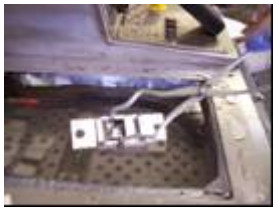

Figure B-12. Remove one specimen at a time holding its center using a tang

Figure B-13. Flip the specimen on a flat surface

Figure B-14. Remove the rubber band

Figure B-15. Remove the mold while keeping the two end pieces in place

Figure B-16. Flip back the specimen and push the notch horizontally until it comes off

Figure B-17. Grab the specimen from two corners and place it back in the bath

Figure B-18. Leave the specimens for 45 minutes in the bath

Figure B-19. Turn on the DTT machine, load adhesion program, mount the specimen, tare the load to zero, run the test and record the data

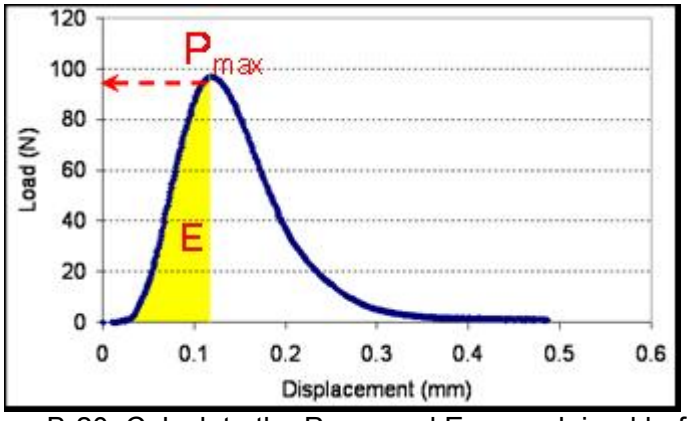

Figure B-20. Calculate the Pmax and E as explained before

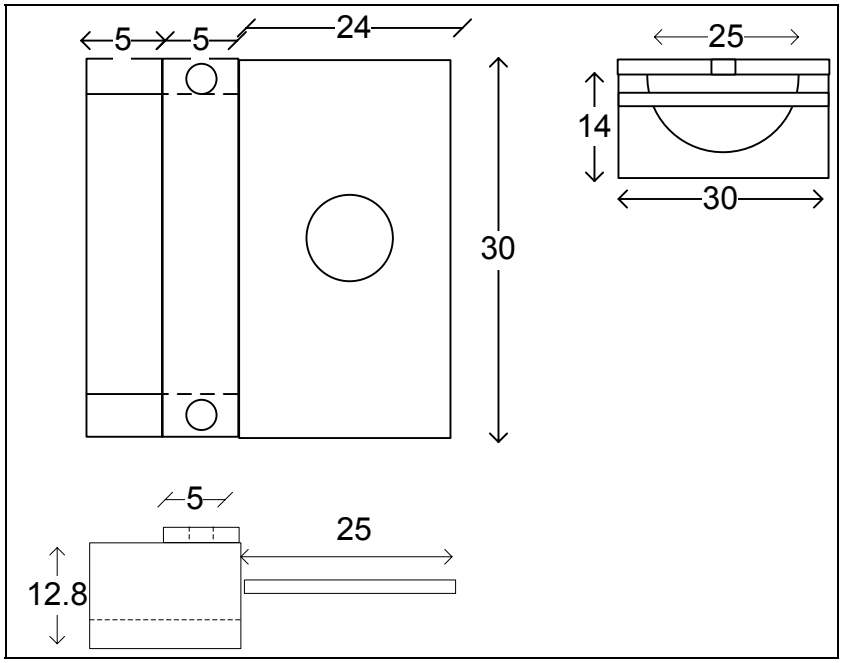

Figure B-21. Schematic of the setup

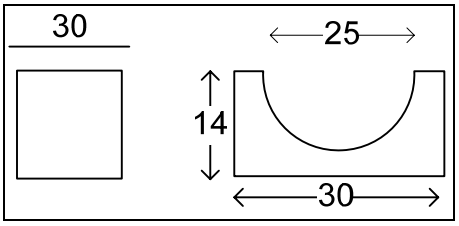

Figure B-22. Schematic of the mold

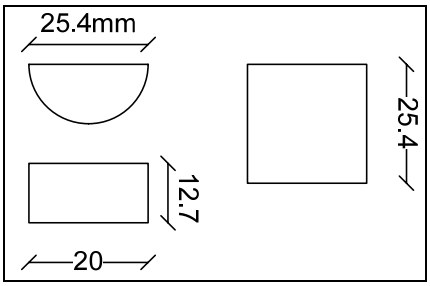

Figure B-23. Schematic of the aluminum end piece

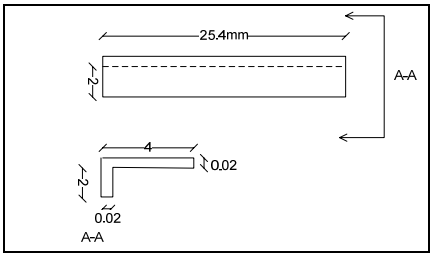

Figure B-24. Schematic of the shim

APPENDIX (C)

Guidelines for Measuring Adhesion of Hot-Poured Crack Sealant Using a Blister Test

1. Purpose

1.1. The blister test is used to determine the adhesion of hot-poured crack sealant at the application temperatures.

2. Scope

2.1. The blister test is a test of fracture. The objective of the test is to inject alcohol between a substrate (aluminum plate) and hot-poured crack sealant in such a way that the sealant is detached from the substrate in the form of a blister. The energy balance principle is used to calculate the adhesive fracture energy, which is a fundamental and unique property of each individual interface. Pressure of the injected alcohol is measured using a pressure transducer, while the height of the blister in the center of the dome will be measured through an LVDT. Using the data collected from the test period and the energy balance principle, one can calculate the adhesive fracture energy.

2.2. These guidelines do not purport to address all of the safety concerns, if any, associated with their use. It is the responsibility of the user of this standard to establish and follow appropriate health and safety practices and to determine the applicability of regulatory limitations prior to use.

3. Terminology

3.1. Bituminous sealants and fillers are hot-poured modified asphaltic materials used in pavement cracks and joints.

4. Summary

4.1. Crack sealant material is homogenized, following the procedure given in ASTM D5176. For each specimen, 80g of sealant will be cut and heated to the manufacturer's recommended pouring temperature. To prepare the specimen an aluminum mold is assembled on top of the annular-shaped substrate. An aluminum plug is inserted to close the orifice. Sealant will be poured on top of the aluminum plate to provide a film of 4.6mm thickness. After cooling and conditioning the specimen, the test will be conducted using a servo-hydraulic machine.

5. Significance and Use

5.1. This procedure is designed to measure the adhesion of hot-poured sealant to aggregate.

5.2. Sealants must be rehomogenized (ASTM D5176) before measuring adhesion by this method.

6. Apparatus

6.1. Servo-hydraulic machine.

6.2. Chiller which can reach -40°C± 0.5°C.

6.3. Blister test software.

6.4. Laboratory oven — any standard laboratory oven capable of producing and maintaining a temperature ranging from 170°C to 193°C ± 0.5°C.

6.5. Silicon-based release agent.
6.7. Adhesive-backed fluoropolymer (FEP) film.
6.8. Sitting plate for cooling period

7. Calibration and Standardization

7.1 Temperature of the ovens should be calibrated according to each user's quality assurance program.
7.2. Temperature of the chiller should be calibrated according to each user's quality assurance program.
7.3. Thermometer (temperature detector) — verify the calibration of the temperature sensing device to +/-0.1°C every six months.
7.4. Blister machine needs to be calibrated using the steel plate.
7.4.1. For calibration of the equipment, follow the specifications defined by the manufacturer.

8. Procedure

8.1. All adhesion measurements must be performed on rehomogenized sealant. Follow the procedure for homogenization given in ASTM D5176, Melting of Hot-Applied Joint and Crack Sealant and Filler for Evaluation. It is recommended that a minimum of 400g of sealant be homogenized.
8.2. Once homogenized, hot sealant should be molded, cooled, and stored for later usage. To store the sealant, it is recommended that a can or plastic-lined box be used. The mold must be of sufficient size that the sealant depth is no greater than 100mm, to allow for rapid cooling.
8.3. Prepare 4 cans of sealant by cutting 80g of homogenized sealant for each.
8.4. Heat the sealant to the recommended pouring temperature for 15 minutes.
8.5. Remove the can from the oven, stir the sealant thoroughly, and place it back in the oven for another 15 minutes.
8.6. Use a compass to draw a circle on fluoropolymer (FEP) film.
8.7. Punch out the circle using a sharp manual punch.
8.8. Peel FEP film and place it on a level surface, adhesive side up.
8.9. Place the needle on the center of the FEP film.
8.10. Place the flat side of the plug on top of the needle and let the needle go through the plug.
8.11. Press the plug on the film gently to make sure it has adhered to the film.
8.12. Spray release agent on the plug while keeping it inclined.
8.13. Place the plug on top of annular disk; care should be taken not to contaminate the surface of the disk.
8.14. Place the disk and the plug on the sitting plate.
8.15. Assemble the mold on top of the disk.
8.15.1. Stack two molds on top of each other to achieve double the thickness.
8.16. Wrap the mold with a rubber band stretched through the groove around the mold, to keep the components in place.
8.17. Pour the sealant on the top-center of the plate to fill the mold.
8.18. Let the specimen sit at room temperature for one hour (annealing time).
8.19. Trim the extra sealant away using a heated potty knife.
8.20. Place the specimen in the cooling bath.
8.21. Wait for 15 minutes before demolding the specimen.

8.22. Remove the rubber band, pull out the plug, dissemble the mold, and place the specimen back in the bath.
8.23. Wait for 45 minutes before running the test.
8.24. Open the outlet valve to prevent any pressure being applied to the sample while assembling.
8.25. Lower the piston.
8.26. Plug the sample in the setup, and clamp/screw it tightly.
8.27. Adjust the moving rate of the piston to 0.12mm/s.
8.28. Start running the test; record the data until any of the three conditions below is achieved.
8.28.1. The sample fails suddenly and pressure drops to zero.
8.28.1.1. Find the peak pressure and the corresponding height of the blister.
8.28.1.2. Calculate interfacial fracture energy using the following equation:
$IFE = 0.5 p_c d_c$, where p_c and d_c are the peak pressure and blister height respectively, and report IFE as bonding.
8.28.2. The height of the blister is more than 1"; Stop the test, refer to 8.15.1.
8.28.3. Pressure drops slowly.
8.28.3.1. Stop the test when pressure drops to 40% of the peak pressure. And calculate the interfacial fracture energy using following equation:
$IFE(t) = 0.5 p(t)\ d\ (t)$, where p and d are pressure and blister height, respectively, which are recorded while pressure is decreasing.
8.28.3.2. Average all interfacial fracture energy values calculated at previous step and report it as bonding.
8.29. Regardless of the type of failure, run four specimens for each sealant, average the values of interfacial fracture energy, and report the average of the best three out of four results as the bond energy.
8.30. It is recommended that specimens be examined after the tests are completed, to make sure failure is between sealant and substrate. Refer to 8.15.1 if the failure is within sealant.

9. Reporting

9.1. Report the following information: sealant name and supplier, lot number, date received, date of adhesion measurement, recommended pouring temperature, safe heating temperature, any deviations from test temperature.

10. Data Acquisition

10.1. The blister test setup contains a servo-hydraulic system that moves the piston at a specific speed. The travel distance of the piston is 150mm, through which 0.043 liter of alcohol can be injected. The rate of the movement (0.01v/s, which is equivalent to 0.12mm/s) can be input to the software. An interface is used to send the signal from the instrument to a personal computer. The data acquisition system records the pressure and the height of the blister in the center, with a frequency of 100 H.

11. Description of Equipment

11.1. The blister test setup is used for this test method. Adhesive measurement is obtained by injecting alcohol between a substrate (Aluminum plate) and hot-

poured crack sealant in such a way that the sealant is delaminated from the substrate in the form of a blister. The equipment includes the blister test setup accompanied by a servo-hydraulic machine and a chiller. Pressure of the injected alcohol is measured using a pressure transducer, while the height of the blister in the center of the dome will be measured using an LVDT. The setup is equipped with software to control the piston movement and a data acquisition system to record the data.

12. Points of Caution

12.1. Since test result is strongly affected by surface property of interface components, if the substrate becomes contaminated with any release agent, water, dust, or other contamination, this will distort the test data and nullify the test results.

12.2. Film thickness strongly affects the test results. The required thickness should be achieved with ±0.01mm tolerance.

12.3. Leveling the sitting plate is critical. To achieve this goal, care should be taken in preparing the sample so that it always stays level. Any tilting in the sample plate will cause the sealant to flow to one side, changing the thickness. Without uniform film thickness, the debonding might not proceed symmetrically.

12.4. Avoid excessive heating. Excessive heating may cause volatiles to be lost from the sample or polymer chains to be degraded, leading to decreased viscosity of the sealant and inaccurate results. During the test, the sample should not be heated to temperatures greater than the pouring temperature recommended by the company.

Figure C-1. Heat four cans of 80g homogenized sealant for 15 minutes at the recommended pouring temperature

Figure C-2. Remove the can, mix the sealant thoroughly and place it back in the oven for another 15 minutes

Figure C-3. Peel the transparent film, and place it on a flat surface with adhesive side up, place the pin on its center and let the plug slide through the pin to the film

Figure C-4. Spray release agent on the plugs and the molds


Figure C-5. Place the plug on the annular plate, and pull it from underneath the plate until it fits in the orifice and the film edges sits on the plate

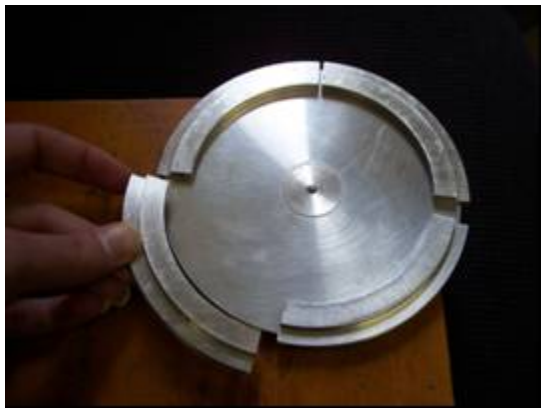

Figure C-6. Assemble the molds on top of the plate

Figure C-7. Use rubber band to keep the mold together

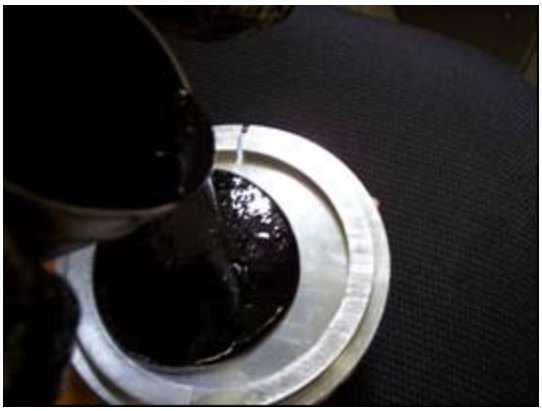

Figure C-8. Mix sealant thoroughly and pour on center top of the plug and let it flow to fill the mold

Figure C-9. Let the sealant set for one hour at room temperature

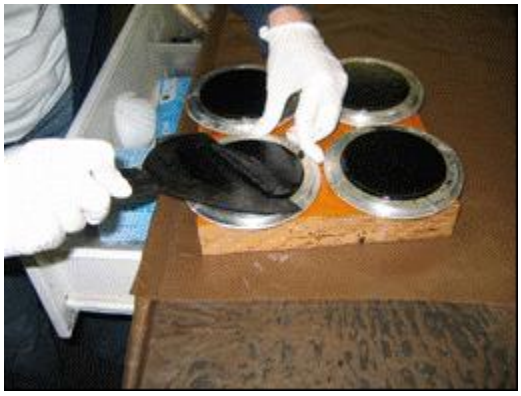

Figure C-10. Trim the extra sealant away with a heated potty knife

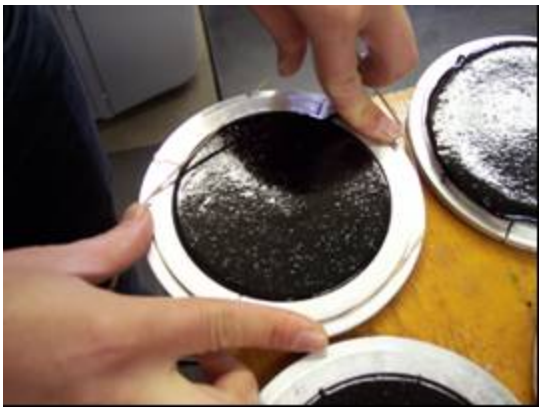

Figure C-11. Remove the rubber band

Figure C-12. Remove the molds gently

Figure C-13. Place the plated on the rack; allow enough clearance between each two specimens

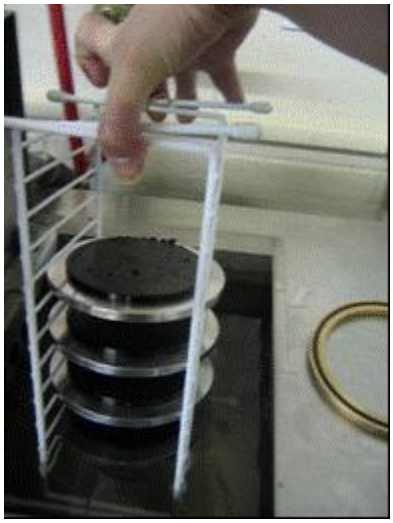

Figure C-14. Place the rack in the bath for 15 minutes

Figure C-15. Deplug the specimen and place them back on the rack

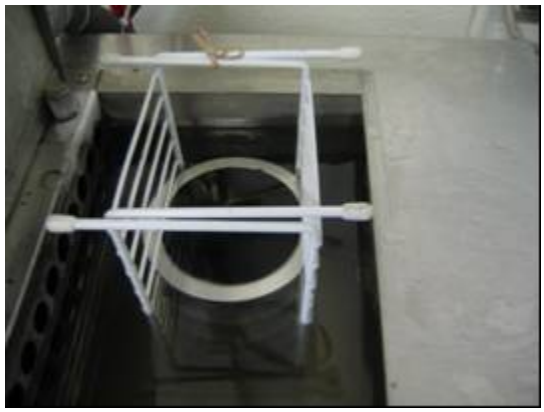

Figure C-16. Condition the specimens in the bath for 20 minutes

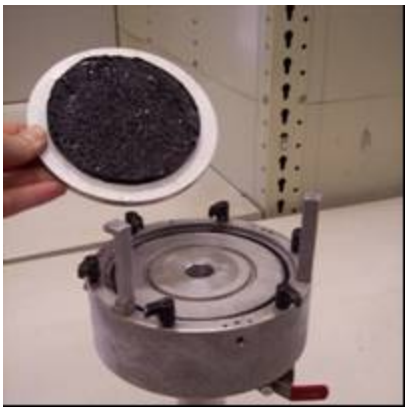

Figure C-17. Place the first specimen on the base setup

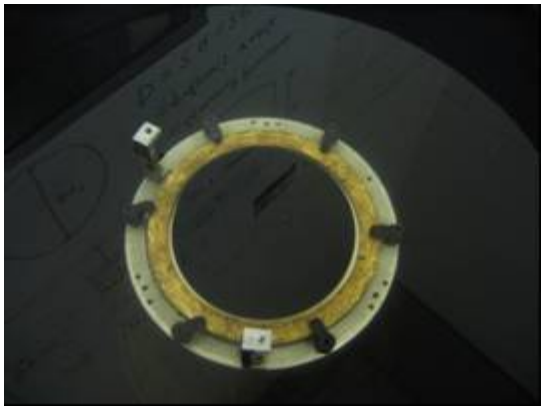

Figure C-18. Place the supporting ring on top and tighten the screws

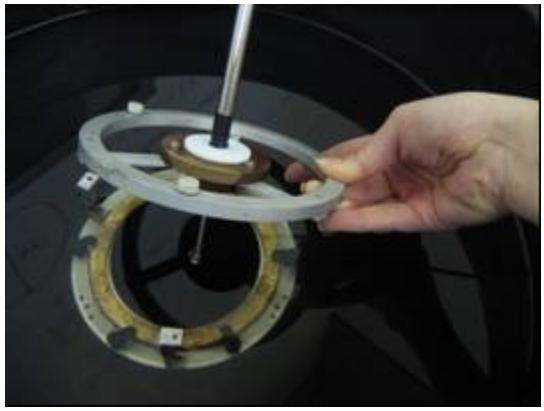

Figure C-19. Assemble the LVDT

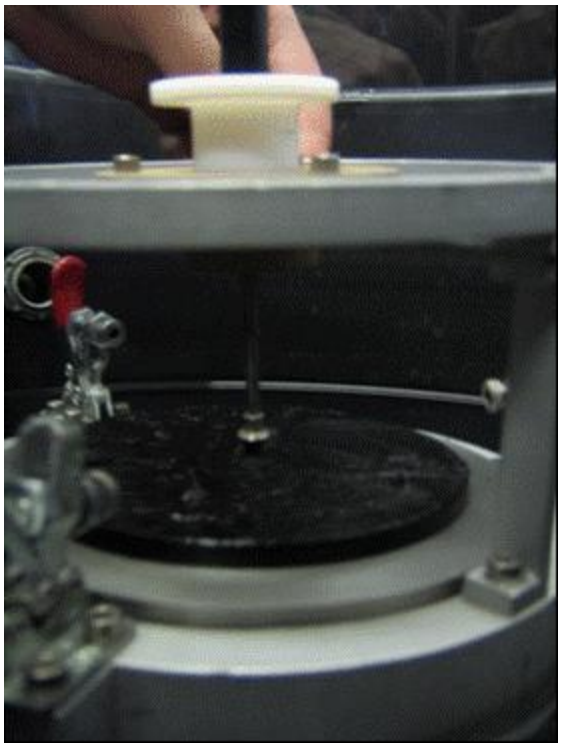

Figure C-20. Close the outlet valve and start the test

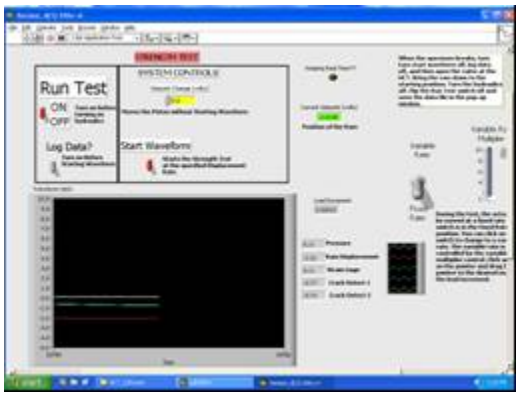

Figure C-21. Run the test

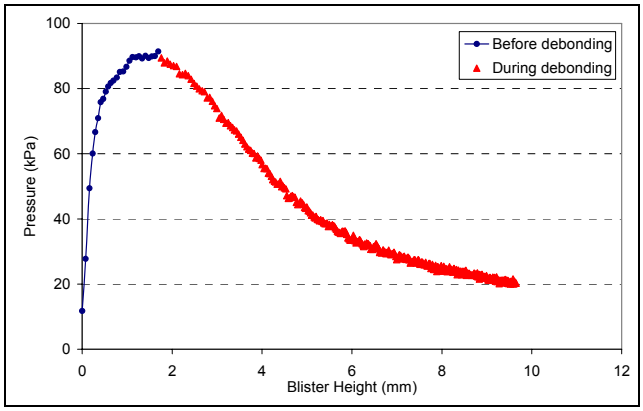

Figure C-22. Record the pressure and displacement of the blister as functions of time

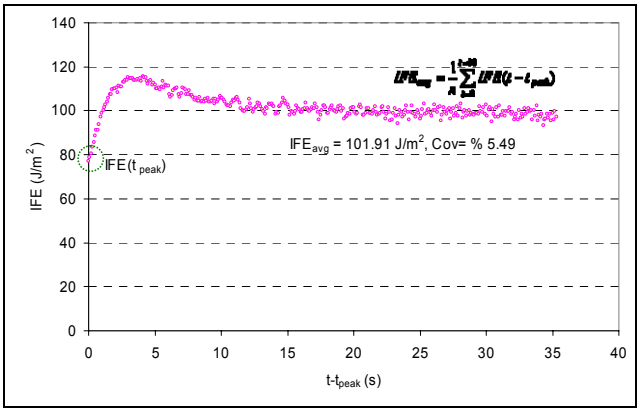

Figure C-23. Calculate the IFE $_{peak}$ (at peak pressure) and IFE $_{avg}$. (for 40 seconds of debonding period)

Figure C-24. Remove the sample and examine if the failure type was adhesive in which sealant film separates from the plate

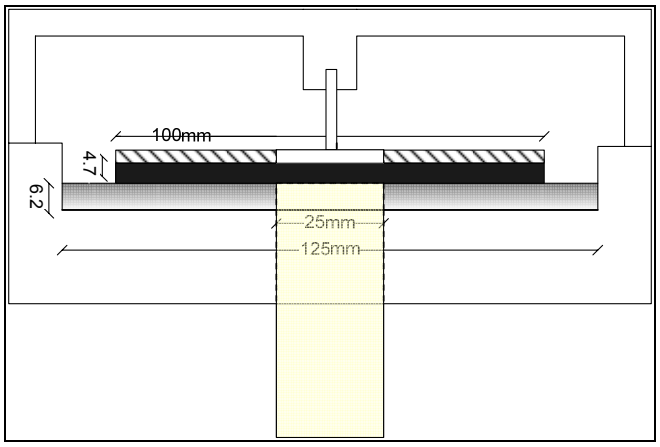

Figure C-25. Schematic of the blister setup

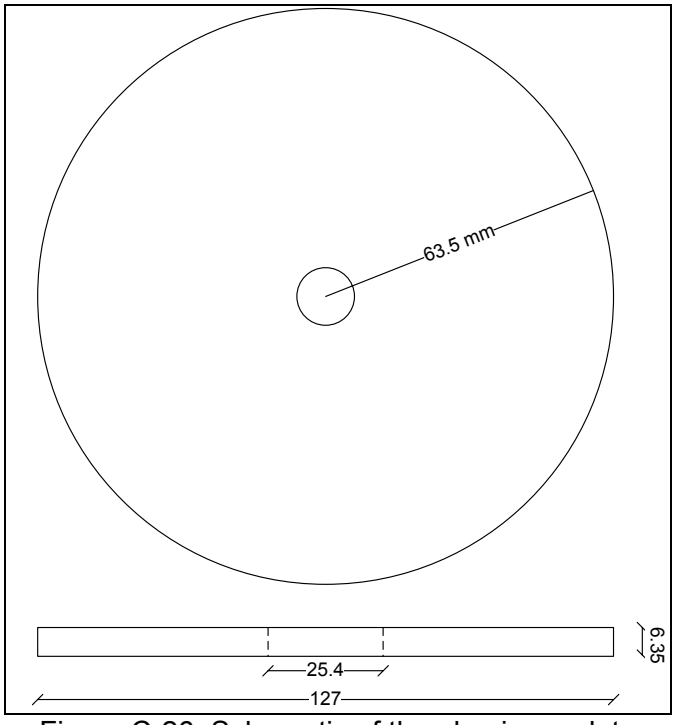

Figure C-26. Schematic of the aluminum plate

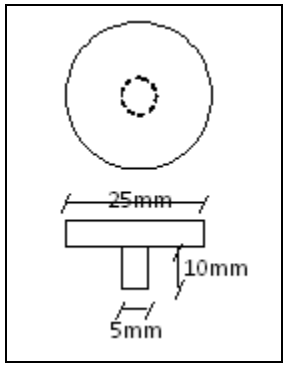

Figure C-27. Schematic of the plug

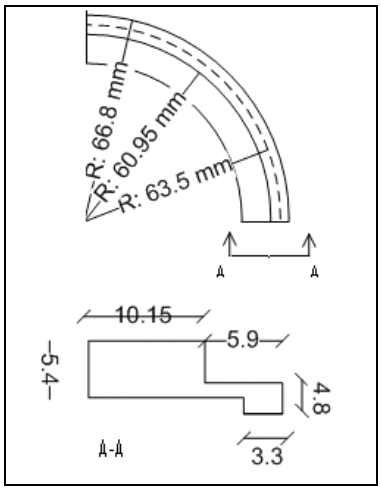

Figure C-28. Schematic of one section of the four-piece-mold


Illinois Department
of Transportation


ILLINOIS
UNIVERSITY OF ILLINOIS AT URBANA-CHAMPAIGN